

AD A122556

NPS-69-82-010

NAVAL POSTGRADUATE SCHOOL
Monterey, California



DTIC
ELECTE
DEC 17 1982
S D D

**EFFECT OF CORE SIZE ON THE RISE AND DEMISE
OF TRAILING VORTICES**

by

T. SARPKAYA

December 1982

Approved for public release; distribution unlimited.

Prepared for: Defense Advanced Research Projects Agency
1400 Wilson Blvd., Arlington, VA 22209

DTIC FILE COPY

82 12 17 057

NAVAL POSTGRADUATE SCHOOL
Monterey, California

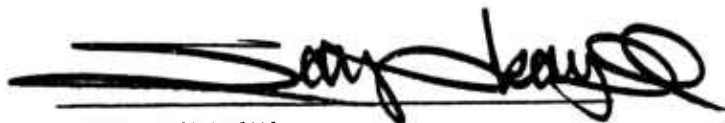
J. J. Ekelund, RADM, USN
Superintendent

D. A. Schradly
Provost

The work reported herein was supported by the Defense Advanced Research Projects Agency (DARPA).

Reproduction of all or part of this report is authorized.

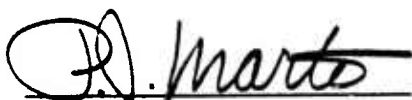
This report was prepared by:



TURGUT SARPKAYA
Distinguished Professor of Mechanical
Engineering

Reviewed by:

Released by:



Paul J. Marto, Chairman
Department of Mechanical
Engineering



William M. Tolles
Dean of Research

UNCLASSIFIED

SECURITY CLASSIFICATION OF THIS PAGE (When Data Entered)

REPORT DOCUMENTATION PAGE		READ INSTRUCTIONS BEFORE COMPLETING FORM
1. REPORT NUMBER NPS-69-82-010	2. GOVT ACCESSION NO. AD-722	3. RECIPIENT'S CATALOG NUMBER 556
4. TITLE (and Subtitle) EFFECT OF CORE SIZE ON THE RISE AND DEMISE OF TRAILING VORTICES	5. TYPE OF REPORT & PERIOD COVERED Progress Report	
7. AUTHOR(s) Professor Turgut Sarpkaya Mechanical Engineering Code 69SL	6. PERFORMING ORG. REPORT NUMBER	
9. PERFORMING ORGANIZATION NAME AND ADDRESS Naval Postgraduate School Monterey, California 93940	8. CONTRACT OR GRANT NUMBER(s) ARPA Order 3925	
11. CONTROLLING OFFICE NAME AND ADDRESS Defense Advanced Research Projects Agency (DARPA) 1400 Wilson Blvd., Arlington, VA 22209 (Attn: Dr. Arthur J. Bruckheim)	10. PROGRAM ELEMENT, PROJECT, TASK AREA & WORK UNIT NUMBERS	
14. MONITORING AGENCY NAME & ADDRESS (if different from Controlling Office)	12. REPORT DATE December 1982	
	13. NUMBER OF PAGES 109	
	15. SECURITY CLASS. (of this report)	
	15a. DECLASSIFICATION/DOWNGRADING SCHEDULE	
16. DISTRIBUTION STATEMENT (of this Report) Approved for public release; distribution unlimited.		
17. DISTRIBUTION STATEMENT (of the abstract entered in Block 20, if different from Report)		
18. SUPPLEMENTARY NOTES		
19. KEY WORDS (Continue on reverse side if necessary and identify by block number) Trailing Vortices; Vortex Core; Stratified Flow; Demise of Vortices		
20. ABSTRACT (Continue on reverse side if necessary and identify by block number) Experiments were conducted with five lifting surfaces to investigate the evolution of trailing vortices in stratified and unstratified water. The vortex trajectories were determined as a function of the relative depth D/b_0 , normalized time $V_0 t/b_0$, stratification parameter Nb_0/V_0 , and the relative vortex core size r_0/b_0 . The results have shown that the vortices rise only to a finite height as they gradually demise under the influence of turbulence, sinusoidal instability, and the vortex breakdown. The effect		

UNCLASSIFIED

SECURITY CLASSIFICATION OF THIS PAGE/When Data Entered

of stratification is to reduce the lifespan of vortices and the maximum height attained by them. Various approximate analyses have been examined and new ones have been proposed to determine the lifespan of the trailing vortices.

UNCLASSIFIED

SECURITY CLASSIFICATION OF THIS PAGE/When Data Entered

ABSTRACT

Experiments were conducted with five lifting surfaces to investigate the evolution of trailing vortices in stratified and unstratified water. The vortex trajectories were determined as a function of the relative depth D/b_0 , normalized time $V_0 t/b_0$, stratification parameter Nb_0/V_0 , and the relative vortex core size r_0/b_0 . The results have shown that the vortices rise only to a finite height as they gradually demise under the influence of turbulence, sinusoidal instability, and the vortex breakdown. The effect of stratification is to reduce the lifespan of vortices and the maximum height attained by them. Various approximate analyses have been examined and new ones have been proposed to determine the lifespan of the trailing vortices.

Accession For	
NTIS GRA&I	<input checked="" type="checkbox"/>
DTIC TAB	<input type="checkbox"/>
Unannounced	<input type="checkbox"/>
Justification	
By	
Distribution/	
Availability Codes	
Dist	Avail and/or Special
A	



PREFACE

The work reported herein is part of a basic research on trailing vortices in stratified and unstratified fluids and was performed during the period 30 June 1982 to 30 December 1982. The principal investigator is Dr. T. Sarpkaya, Distinguished Professor of Mechanical Engineering. Sponsorship was provided by the Defense Advanced Research Projects Agency (DARPA) under ARPA Order 3925. The contract technical monitor was Dr. Arthur J. Bruckheim, Program Manager, Tactical Technology Office, DARPA.

The writer wishes to acknowledge the generous support of DARPA and the constructive comments and recommendations of Dr. Arthur J. Bruckheim. A special note of thanks is extended to Mr. Jack McKay for his most skillful work in the construction of the test models.

TABLE OF CONTENTS

I.	INTRODUCTION-----	12
II.	EXPERIMENTAL EQUIPMENT AND PROCEDURES-----	18
	A. WATER BASIN-----	18
	B. STRATIFICATION SYSTEM-----	23
	C. MODELS-----	24
	D. TEST PROCEDURES-----	25
III.	RESULTS-----	34
	A. DIMENSIONAL ANALYSIS-----	34
	B. BODY AND SAIL-PLANE GENERATED VORTICES IN UNSTRATIFIED WATER-----	36
	C. SAIL-PLANE GENERATED VORTICES-----	37
	D. DELTA AND RECTANGULAR-WING GENERATED VORTICES-----	43
	E. NUMERICAL MODEL OF LAMINAR VORTEX PAIR-----	58
IV.	CONCLUSIONS-----	87
	LIST OF REFERENCES-----	88
	APPENDIX A: BODY AND SAIL-PLANE TABULATED DATA-----	89
	APPENDIX B: SAIL-PLANE TABULATED DATA-----	91
	APPENDIX C: RECTANGULAR PLATE TABULATED DATA-----	96
	APPENDIX D: ROUNDED DELTA 2 TABULATED DATA-----	101
	APPENDIX E: SMALL RECTANGULAR PLATE TABULATED DATA-----	105
	INITIAL DISTRIBUTION LIST-----	107

LIST OF FIGURES

1.	Water Basin-----	19
2.	Central Window and the Horizontal and Vertical Scales-----	20
3.	Top View of Stratification System-----	21
4.	Towing Mechanism-----	22
5.	Turbulence Management System-----	28
6.	Stratification System Auxiliary Tanks-----	29
7.	Delta-Wing Models-----	30
8.	Motion Generation Mechanism-----	31
9.	Front View of the Basin-----	32
10.	Side View of the Trailing Vortices-----	33
11.	The Rise of the Body-Sail-Plane Generated Vortices as a Function of $V_0 t/b_0$ for $\alpha = 10$ deg.-----	38
12.	Comparison of the Rise History of the Vortices Generated by the Body-Sail-Plane Combination, ($\alpha = 10$ deg.)-----	39
13.	The Rise of the Body-Sail-Plane Generated Vortices as a Function of $V_0 t/b_0$ for $\alpha = 12$ deg.-----	40
14.	Comparison of the Rise History of the Vortices Generated by the Body-Sail-Plane Combination, ($\alpha = 12$ deg.)-----	41
15.	Comparison of the Vortex Rise History for $\alpha = 10$ deg. and $\alpha = 12$ deg., (Body-Sail-Plane Combination)-----	42
16.	The Rise of Sail-Plane Generated Vortices for $\alpha = 8$ deg.-----	44
17.	Comparison of the Rise of Sail-Plane Generated Vortices for $\alpha = 8$ deg.-----	45
18.	The Rise of Sail-Plane Generated Vortices for $\alpha = 10$ deg.-----	46
19.	Comparison of the Rise of Sail-Plane Generated Vortices for $\alpha = 10$ deg.-----	47

20.	The Rise of the Sail-Plane Generated Vortices for $\alpha = 12$ deg.-----	48
21.	Comparison of the Rise of Sail-Plane Generated Vortices for $\alpha = 12$ deg.-----	49
22.	Comparison of the Rise of Vortices Generated by the Body-Sail-Plane Combination and the Sail-Plane-----	50
23.	The Rise of Vortices Generated by the Rounded Delta 2 Model, ($\alpha = 8$ deg.)-----	52
24.	Comparison of the Rise of Vortices Generated by the Rounded Delta 2 Model, ($\alpha = 8$ deg.)-----	53
25.	The Rise of Vortices Generated by the Rounded Delta 2 Model, ($\alpha = 10$ deg.)-----	54
26.	Comparison of the Rise of Vortices Generated by the Rounded Delta 2 Model, ($\alpha = 10$ deg.)-----	55
27.	Comparison of the Rise of Vortices Generated by Rounded and Sharp-Edge Delta 2 Models-----	56
28.	Effect of Stratification on the Rise of Vortices Generated by a Rounded Delta 2 Model, (SP = 0.375)-----	59
29.	Comparison of the Rise of Vortices in a Stratified Fluid (Rounded Delta 2 and Sharp-Edge Delta 2, SP = 0.375)-----	60
30.	Effect of Stratification on the Rise of Vortices Generated by a Rounded Delta 2 Model, (SP = 0.625)-----	61
31.	Comparison of the Rise of Vortices in a Stratified Fluid (Rounded Delta 2 and Sharp-Edge Delta 2, SP = 0.625)-----	62
32.	Rise of Vortices Generated by a Rectangular Wing ($\alpha = 12$ deg.)-----	63
33.	Comparison of the Rise of Vortices Generated by a Rectangular Wing, ($\alpha = 12$ deg.)-----	64
34.	Comparison of the Rise of Vortices Generated by the Rounded Delta 2 and Rectangular Wing-----	65
35.	Comparison of Experimental Data with that Predicted by Hecht et al. [Ref. 3]-----	67
36.	Comparison of Experimental Data with that Predicted by Hecht et al. [Ref. 4]-----	68

37.	Computational Field and Boundary Conditions for the Numerical Model-----	73
38.	Streamlines of the Numerical Model for $H/b_0 = 0.00$ -----	76
39.	Streamlines of the Numerical Model for $H/b_0 = 0.69$ -----	77
40.	Streamlines of the Numerical Model for $H/b_0 = 1.29$ -----	78
41.	Streamlines of the Numerical Model for $H/b_0 = 1.88$ -----	79
42.	Streamlines of the Numerical Model for $H/b_0 = 2.35$ -----	80
43.	Streamlines of the Numerical Model for $H/b_0 = 2.69$ -----	81
44.	Streamlines of the Numerical Model for $H/b_0 = 3.16$ -----	82
45.	Streamlines of the Numerical Model for $H/b_0 = 3.57$ -----	83
46.	Streamlines of the Numerical Model for $H/b_0 = 3.90$ -----	84
47.	Streamlines of the Numerical Model for $H/b_0 = 4.23$ -----	85
48.	Comparison of Experimental Data with the Predictions of the Numerical Model for $SP = 0$.-----	86

TABLE OF SYMBOLS AND ABBREVIATIONS

AR	-	The aspect ratio
B	-	The model base chord length
b_0	-	Vortex separation distance
D	-	Initial depth of the vortices
g	-	Acceleration of gravity
H	-	The height of the vortices above the original position
N	-	Brunt-Vaisala frequency for gravity
p	-	Pressure
r_0	-	Initial vortex core radius
SP	-	Stratification parameter (Nb_0/V_0)
t	-	Time
U	-	Speed of the model
u,v	-	Fluid velocity in the x and y directions
V_0	-	The vortex rise velocity at the moment of its generation
Y	-	Vertical distance from the streamlined body
α	-	Angle of attack of the model
Γ	-	Vortex strength
γ	-	Angular vortex separation
ϵ	-	Angle of the vertex of the model
ζ	-	Vorticity
ν	-	Kinematic viscosity
ρ	-	Density

σ - Spread parameter

ψ - Stream-function

1. INTRODUCTION

Trailing vortices formed by a lifting surface traveling through a stratified or unstratified fluid medium have been the subject of recent interest primarily because of their importance in the determination of safe aircraft separation distances for terminal areas. In recent years this interest has extended to a better understanding of the role played by turbulence, sinusoidal instability, and vortex breakdown on the rise and demise of vortices.

The trailing vortices may be generated by any number of lifting surfaces such as an airplane wing, single or double Delta wings, etc. The initial organization or roll-up of a trailing vortex from the vorticity generated by the lifting surface is very rapid and is generally complete within the space of several lifting-surface spans.

Whereas a single vortex is extremely stable, one or more vortices in close proximity exhibit a number of complex interactions and give rise to new phenomena which tend to accelerate the demise of the vortices involved. When a lifting surface starts from rest, a starting-vortex or a Horseshoe vortex is formed since a vortex must be connected either to itself or to a rigid boundary. A Horseshoe vortex is also formed when a lifting surface accelerates or decelerates rapidly, or undergoes a radical change in the angle of attack. After an interval of time, the starting vortex is so far removed from the lifting line that its influence in the vicinity of the latter is negligible and the flow field is no longer a function of time. Finite-wing analysis presumes that the motion has continued long enough so that the flow field is steady. When a lifting surface (e.g.,

a Delta wing) starts from rest and moves with a constant velocity, the Horseshoe vortex closes on itself, breaks away from the rest of the trailing vortex, links rapidly, and forms a vortex ring. While the first vortex ring undergoes highly complex deformations, a second vortex ring is formed from the Horseshoe vortex connecting the tail end of the trailing vortex. This process does not continue forever for a number of reasons. The speed of the generating surface is much greater than the speed of advance of the vortex rings. Thus, the length of the vortex trail increases rapidly and the motion of the vortices becomes dominated by the mutual interactions of the vortices rather than by the horseshoe vortices at their tail end. The motion of each new vortex ring differs from the one shed previously partly because of the continued aging or diffusion of vorticity (i.e., a weaker ring is formed at succeeding steps) and partly because the motion of each new ring is controlled by all the rings shed previously and by the ever-increasing vortex trail. These phenomena lead to the rapid demise of vortex rings. In fact, shortly after the start of the motion of the lifting surface the horseshoe vortex and the vortex rings play a very minor role on the evolution of the trailing vortex.

The trailing vortices are subjected to three known decay mechanisms: (i) Aging of vortices due to eddy viscosity; (ii) sinusoidal instability leading to the linking of vortices (known as the Crow instability); and (iii) vortex breakdown.

These mechanisms can act independently or in combination. The viscous and turbulent diffusion of vorticity lead to the gradual dissipation of the trailing vortices. Clearly, this phenomenon is strongly influenced by the initial vorticity distribution and the ambient turbulence.

Furthermore, the proximity of other vortices, free surface, rigid surfaces (e.g., the submerged body, ground, etc.), ambient shear, stratification of the fluid medium, etc., affect the demise of the vortices. Clearly, the aging of the vortices is ever present and affects the evolution of the trailing vortices regardless of whether the Crow instability and/or vortex bursting take place or not.

Breaking up by linking or sinusoidal instability involves the growth of a rather regular sinusoidal pattern, usually symmetrical for the trailing vortex pair. This is commonly referred to as Crow linking. The time to link (the formation of a series of vortex rings and Horseshoe vortices) has been found to depend, statistically, on atmospheric turbulence within the inertial subrange of eddy sizes (a size range from a few cm to some hundreds of meters). The scale of linking varies around nine times the vortex spacing. Thus, it is the eddy sizes in the range of one to ten times the span or vortex spacing which has the main effect on linking. The formation of vortex rings by linking (distinctly different from those generated at the start of motion) lead to the rapid demise of the vortex trail. Consequently, one would want to accelerate the formation of links (e.g., by periodically changing the angle of attack of the control surfaces) if one is interested in decreasing the hazard posed by the trailing vortices to other aircraft or in decreasing the energy transferred to the fluid medium.

The vortex breakdown is essentially a single-vortex phenomenon, in the sense that it is not necessarily connected with the induced flows associated with the other vortex of the pair. There are, however, frequent occurrences of core bursting in conjunction with the sinuous

instability, in which case the sinuous vortex deformation appears to induce core bursting. The effect of vortex breakdown is to flatten the velocity profile by significantly reducing the peak velocity (or the velocity of numerous peaks of several smaller vortices) under the center of the vortex, but without major effect on the speeds away from the vortex center. A definite vortex flow remains in all cases, indicating that core bursting does not totally eliminate the vortex. In fact, the persistence of the outer flow circulation suggests that vortex breakdown may not significantly alleviate the vortex hazard and the energy transfer to the surrounding medium. The understanding of the vortex-breakdown and the determination of how much circulation remains after breakdown remain as critical and vexing questions.

The trailing vortices move downward (downwash) when generated by a lifting surface with a positive angle of attack, as in the case of an airplane, or upward (upwash) when generated by a sail plane with a negative angle of attack, as in the case of a submarine. In either case, the motion of the vortices is determined by the mutual induction, vorticity distribution, the three types of the instabilities or demise mechanisms cited above, stratification effects of the fluid medium, ambient flow turbulence, shear and currents present in the fluid medium, and the proximity effects (e.g., free surface, bottom, ground, other bodies, etc.). An inviscid flow analysis based on concentrated line vortices can help to predict the early stages of motion of the vortices. However, the later stages of the motion become increasingly dominated by the factors cited above and it is not possible to examine the evolution of the trailing vortices without taking into consideration the effect of viscosity,

turbulence, stratification, mutual induction, proximity, and all the other phenomena which arise as a consequence of these fundamental variables. It must also be pointed out that whereas the trailing vortices generated by an aircraft are under each other's influence (in addition to the external non-vortical influences), the trailing vortices generated by a large submerged body may also be under the influence of a complex system of image vortices imbedded in the body.

Density stratification within the fluid medium is of great importance in the migration and ultimate demise of trailing vortices. The atmosphere is less dense at higher altitude while the oceans exhibit various patterns of stratification due to local temperature, salinity, and depth. Generally, a vortex migrates with the fluid in which it was born, retaining most of the original fluid in a so-called recirculation cell. The upwash of the vortices in the ocean environment into a layer of lesser density gives rise to a buoyancy which is in the opposite direction to the velocity resulting from the mutual induction. Furthermore, the motion of the recirculation cell produces oppositely-signed vorticity in the surrounding medium. This, in turn, gives rise to the entrainment and detrainment of fluid from the recirculation cell. Altogether, these additional consequences of stratification help to reduce not only the life of vortices but also the height to which the vortices rise asymptotically. One may also surmise that the stratification will tend to change the occurrence and the resulting characteristics of eddy diffusion, Crow instability, and core bursting. It is evident from the foregoing that the phenomena associated with the generation, migration, interaction, and demise of trailing vortices are very complex. In fact, a comprehensive review of the previous investigations

by Sarpkaya and Johnson [Ref. 1] has revealed that it is not yet possible to devise mathematical models with which some or all of the characteristics of the phenomena can be predicted. As in many other flow situations, the role played by turbulence and the quantification of the turbulence stresses pose difficult questions. The gradual understanding of the behavior of trailing vortices must rely for the time being on carefully conducted experiments without losing sight of the fact that one must ultimately devise a model to acquire a power of prediction as well as a means to reduce the number of experiments for model verification.

It is clear from the foregoing that the reason for developing as much an understanding as possible of the behavior of trailing vortices is to permit design and improvement of an operational system which properly balances safety and efficiency in the motion of vortex-generating bodies and also to aid in the development of devices to enhance vortex decay, limit vortex upwash, and minimize energy transfer to the surrounding medium. The effort towards the understanding of some of the underlying phenomena forms the basis of the present investigation.

II. EXPERIMENTAL EQUIPMENT AND PROCEDURES

The experimental equipment consists of the water basin, the stratification system, and the models.

A. WATER BASIN

The basin is 36 feet long, 3 feet wide and 4 feet high and is made of 0.5-inch thick aluminum plates, welded appropriately (see Fig. 1). The back wall of the tank is reinforced to prevent bulging under hydrostatic pressure. The front wall is fitted with square windows of 1.0 inch thick plexiglass for flow visualization.

Vertical and horizontal scales of 0.5-inch increments are marked on the central window. The scales are used during the experiments to evaluate the position of the trailing vortices (see Fig. 2).

The aluminum interior of the tank is painted with marine epoxy to prevent corrosion. In addition, the inside part of the back wall is painted with flat white paint to provide better contrast and make the flow visualization easier with the dye used.

The filling pipes lie on the bottom of the tank. They are plastic pipes 2.0 inch diameter, perforated along their entire length with holes of 1/16-inch diameter (see Fig. 3).

Two drains are provided at the bottom at each end of the basin. Two parallel rails of 1.0 inch diameter are mounted along the bottom of the tank. A carriage rides smoothly on these rails and provides the test body with a constant velocity through the use of an endless cable and a 3/4 Hp DC motor (see Fig. 4). The velocity of the model is measured and

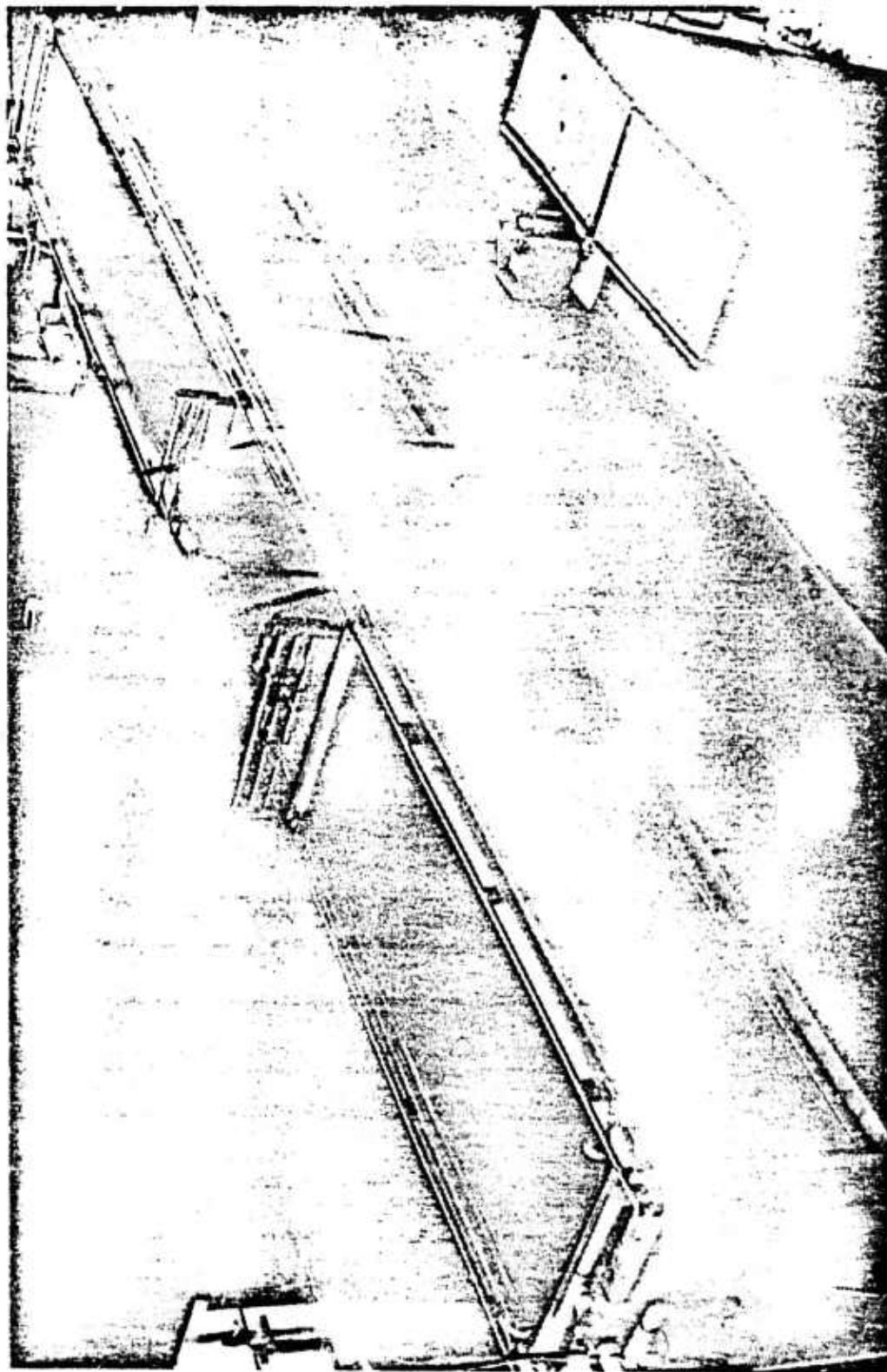


Figure 1. Water Basin.

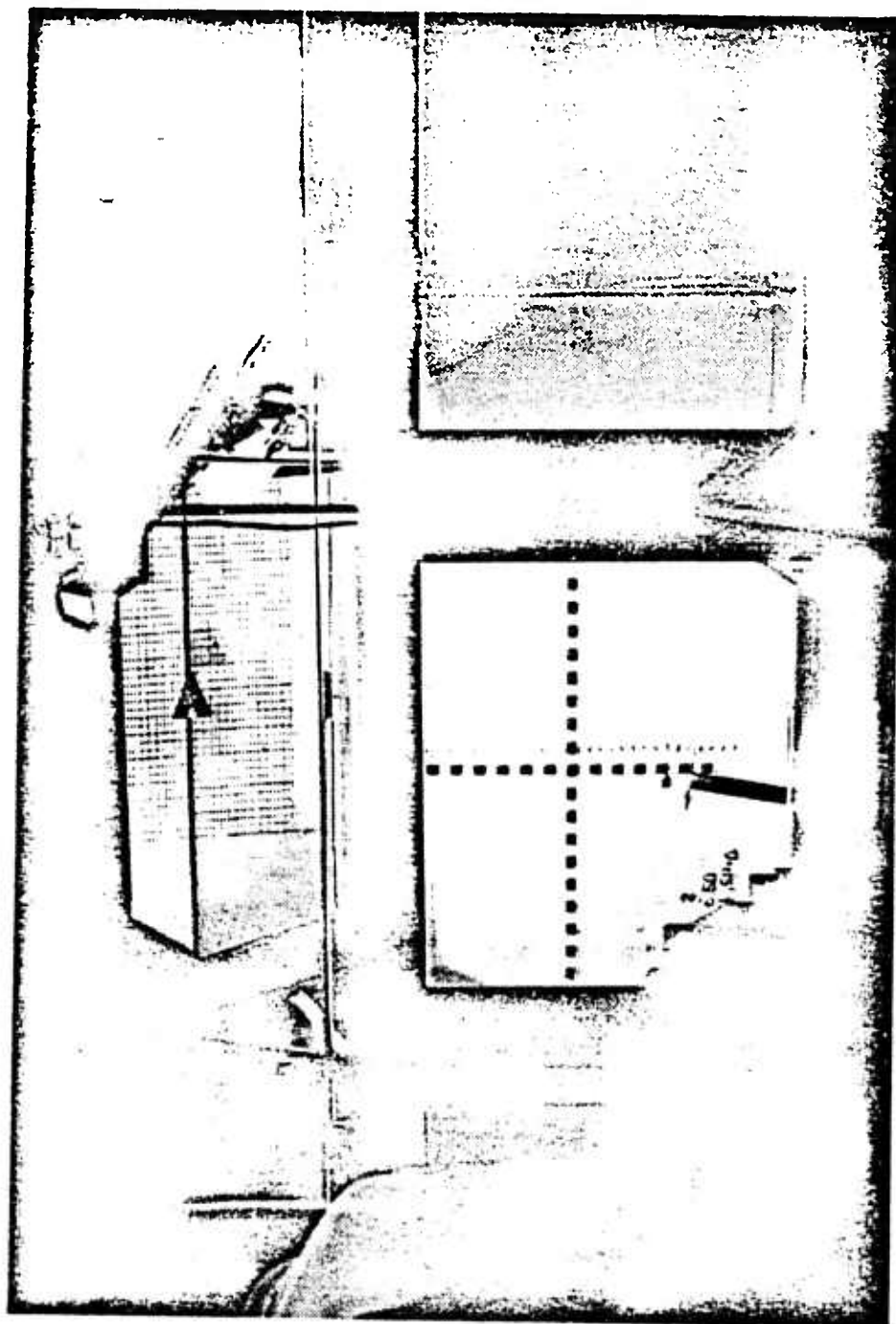


Figure 2. Central Window and the Horizontal and Vertical Scales.

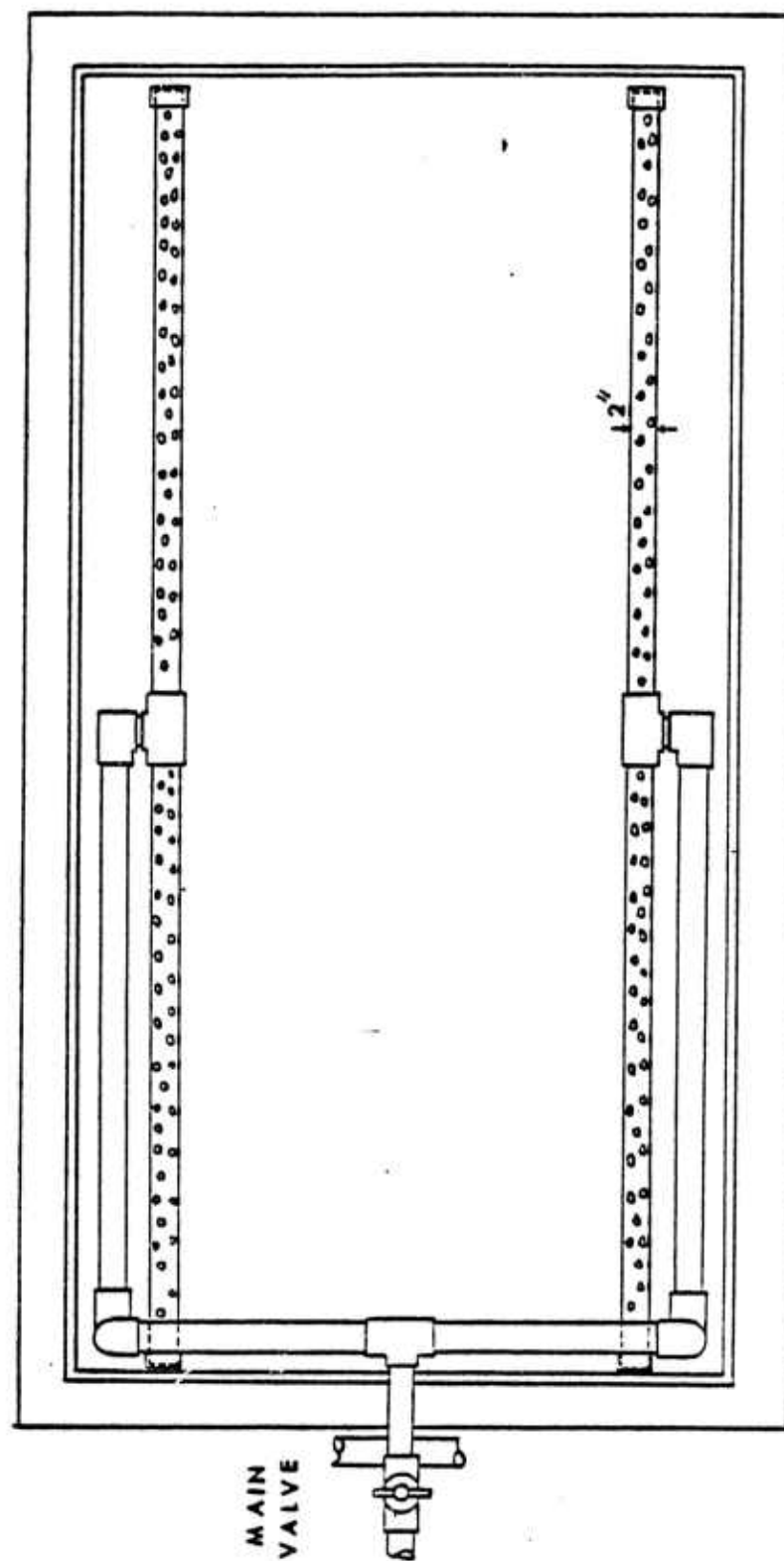


Figure 3. Top View of Stratification System.

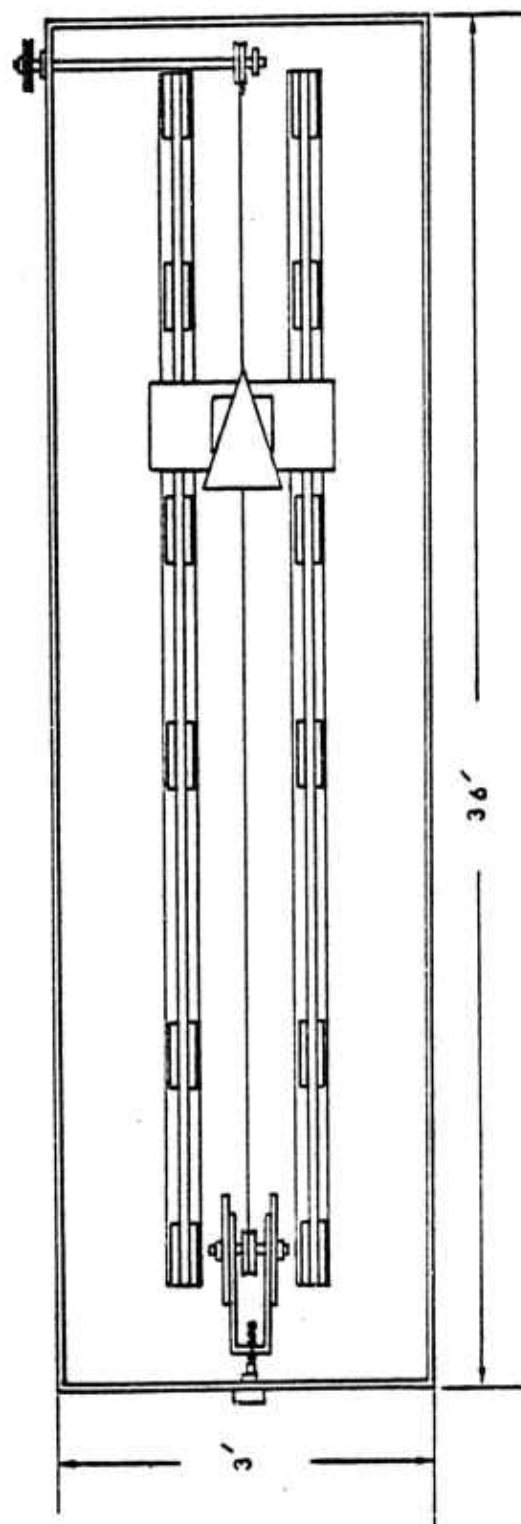


Figure 4. Towing Mechanisms.

continuously monitored through the use of a magnetic velocity sensor, mounted above a precision gear. The sensor counts the number of teeth and yields and instantaneous velocity proportional to the velocity of the model.

The two rails, the carriage and the filling pipes are located on or near the bottom of the basin and under a turbulence management system. This system consists of a one-inch-thick polyurethane foam, sandwiched between two perforated aluminum plates (see Fig. 6).

B. STRATIFICATION SYSTEM

The stratification system consists of four tanks (60-gallon capacity each) and the necessary tubes and valves.

First, brine water of certain salt concentration is prepared in one of these tanks. Then precalculated amounts of brine water are added to the other three tanks, depending on the desired density gradient and the number of the layers. The calculation of the amount of salt needed, for a certain density gradient or for a certain stratification parameter, has been described by Sarpkaya and Johnson [Ref. 1] and will not be repeated here.

The resulting solution is drained into the basin at a rate of 2.1 CFM. Necessary precautions have been taken to prevent air entrainment and subsequent bubble generation. Furthermore, two air-bubble traps have been installed, one just before the main valve of the filling system and one at the middle point of the delivery pipes.

This system can fill the water basin and establish a desired stratification in about three hours. There is no difficulty regarding the

desired density gradient, even for the lower gradients (e.g., $dp/dy = 5 \times 10^{-5}$ slug/ft³/inch). The density discontinuity between the 0.9-inch layers disappeared by diffusion after a short time for the stratification of interest. Smooth density gradients were obtained as verified by a salinity meter. The parts of the stratification system are shown in Figures 3 and 6.

C. MODELS

Five models were used in the experiments: A streamlined body and sail-plane combination; sail-plane alone; a rectangular foil; and a Delta-wing, all with hollow interiors. Each model cavity is filled with dye prior to the filling of the basin with water. The two holes at the rear edge of each model and the third hole in the middle of the upper surface are plugged prior to an experimental run to prevent dye leakage (see Fig. 7). The dye consisted of food coloring and proper amounts of alcohol. The density of the mixture was such that the dye was only slightly buoyant relative to its surroundings.

The rectangular and Delta wings are mounted on their bases by means of a streamlined thin aluminum bar (its cross section was a NACA 0006 foil) and set at the desired angle of attack. The models are placed at a level 9 inches above the foam.

The streamlined body is half of an axisymmetric body. Its bottom half was removed to allow testing at a greater depth with negligible hydrodynamic ground effects. The sail-plane, attached to the top of the streamlined body had a base length of 6.9 inches with an aspect ratio of

2.2 [Aspect ratio = (base length)²/Area]. The model is mounted to the carriage such that the plane bottom of the body is flush with the top of the aluminum plate above the foam.

A hollowed core within the supporting column of the planing surfaces is filled with dye. The dye is dispensed from the tips of the planing surfaces with small holes connected to the dye reservoir (i.e., the hollow core).

Finally, the sail-plane was tested alone in order to delineate the effect of the body from that of the sail-plane on the evolution of the vortices. For this purpose, the height of the sail was increased to 9 inches and the sail-planes were attached to it in exactly the same manner as before.

As noted earlier all models are pulled by means of a DC motor, pulley, and cable system at the desired speed (ranging from 1.0 to 5.0 ft/sec). The entire arrangement is shown in Figures 8 and 9.

D. TEST PROCEDURES

The model is initially filled with dye and all the fill and drain holes on the model are closed with wooden pegs. Then the basin is filled gradually either with fresh water (for unstratified flow experiments) or with salt water (for stratified flow experiments) to the desired level. After sufficient period of waiting for the elimination of any internal currents in the basin the model was set in motion at a desired speed.

The motion of the trailing vortices are recorded on high-speed Polaroid film at the test section (one of the plexiglass panels near the middle of the basin). Each picture included two clocks accurate to

0.01 second, the vertical and horizontal scales on the plexiglass window and, of course, the side view of the trailing vortices as they rose from the model after formation (see Fig. 10). The time interval between successive pictures is determined from the two clocks. The vertical rise of the vortices is determined from the vertical scale. Attention has been paid to the fact that the vortices are farther away from the scale on the plexiglass window and that the scale placed vertically in the middle of the test section does not exactly correspond to the scale marked on the plexiglass window due to refraction and parallax. The necessary correction was made by photographing a scale placed in water in the middle of the test section together with the scale marked on the plexiglass window. This resulted in a simple conversion table which enabled the determination of the actual position of the vortex from the scale reading on the photograph.

The results are non-dimensionalized and plotted in various forms and compared with those obtained in the previous runs. Each experiment was repeated at least twice to ascertain that the experiments were repeatable.

The experiments with the formation of Horseshoe vortices and vortex rings were conducted in the manner described above with the exception that the model was initially placed closer to the test section, rather than at one end of the basin, and that both the horizontal and vertical scales were used to determine the velocity components of the translation of the vortices.

All trailing vortices and vortex rings were recorded on film until the time they have completely dissipated either due to aging (diffusion of vorticity due to viscosity, turbulence, entrainment, and detrainment),

or due to Crow instability (sinusoidal instability and linking leading to the formation of vortex rings), and/or due to vortex breakdown (core bursting). It was thus possible to determine the life span of vortex cores from their formation to their final demise.

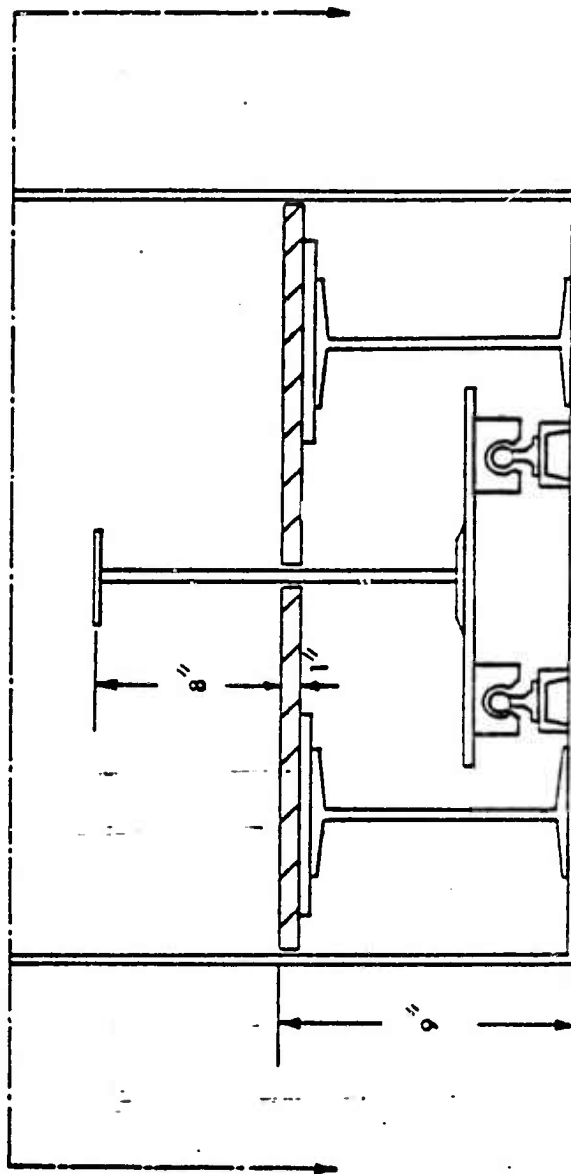


Figure 5. Turbulence Management System.

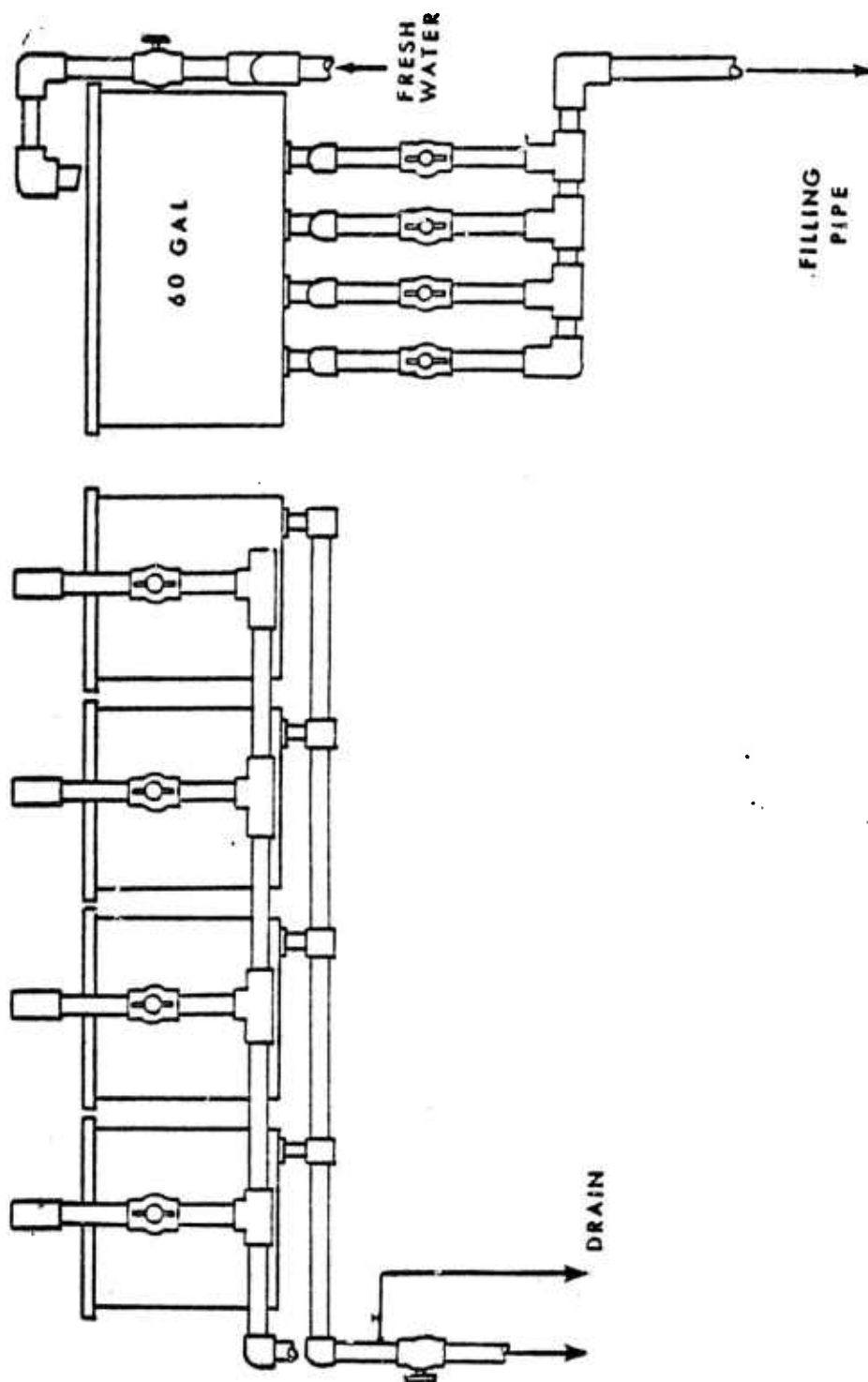
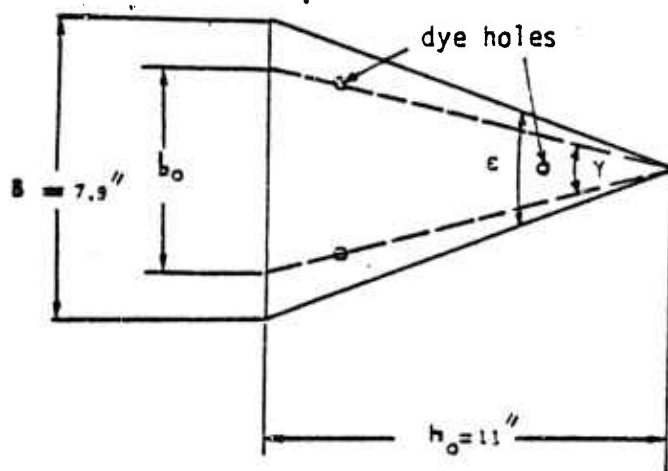


Figure 6. Stratification System Auxiliary Tanks.



Delta-wing Model No. 1

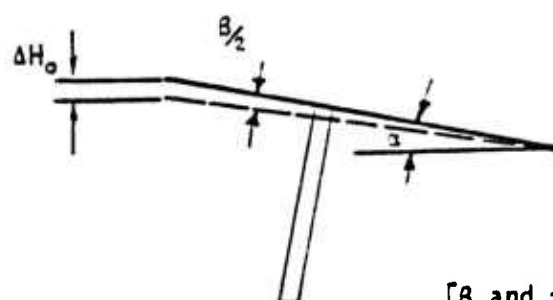
DIMENSIONS

Delta 1:

$B = 7.90"$
 $b_0 = 5.585"$
 $h_0 = 11.00"$
 $\epsilon = 39.5 \text{ deg.}$

Delta 2:

$B = 5.07"$
 $b_0 = 3.70"$
 $h_0 = 6.00"$
 $\epsilon = 50.0 \text{ deg.}$



[B and γ are from Ref. 2]

Figure 7. Delta-Wing Models.

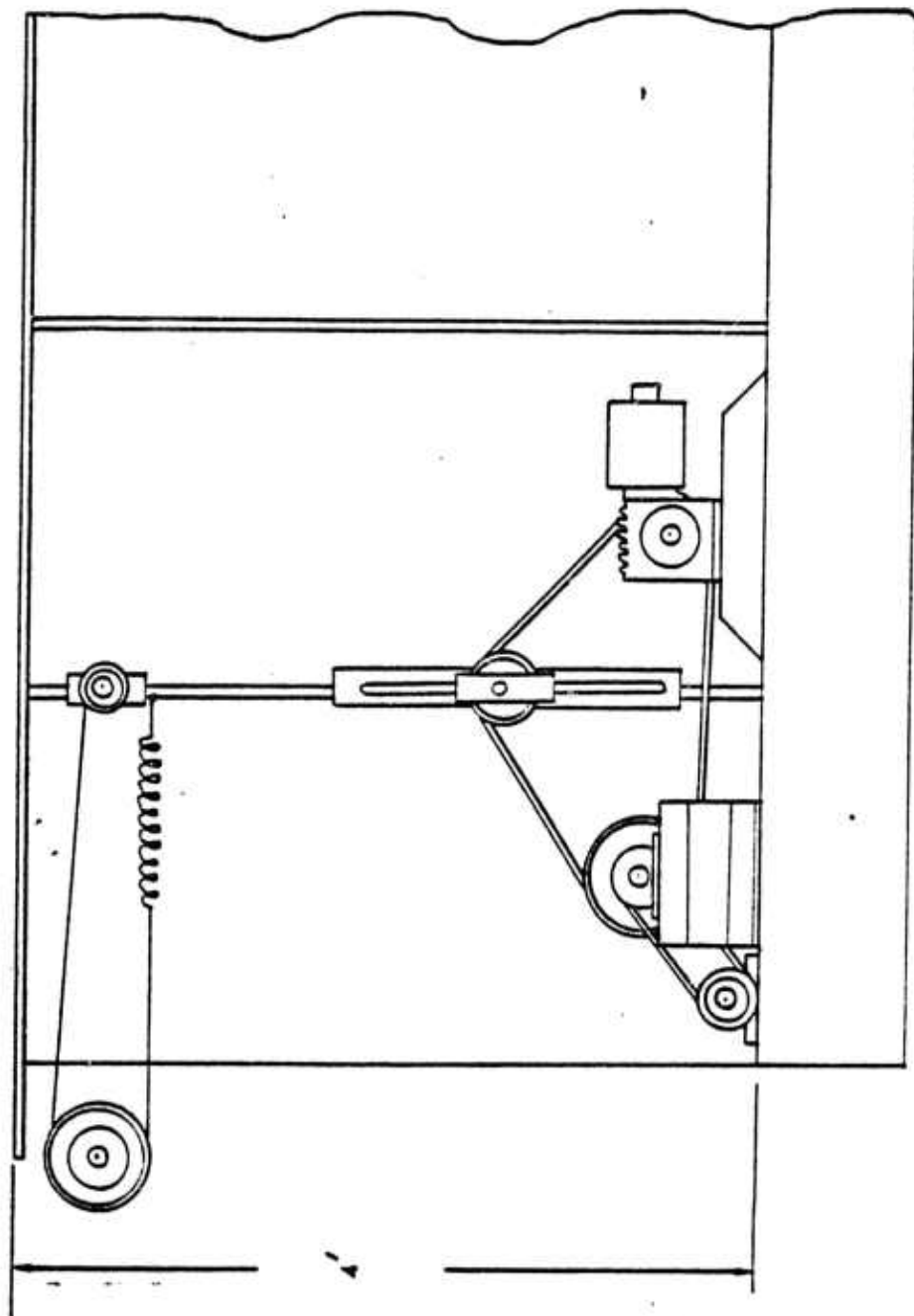


Figure 8. Motion Generation Mechanism.

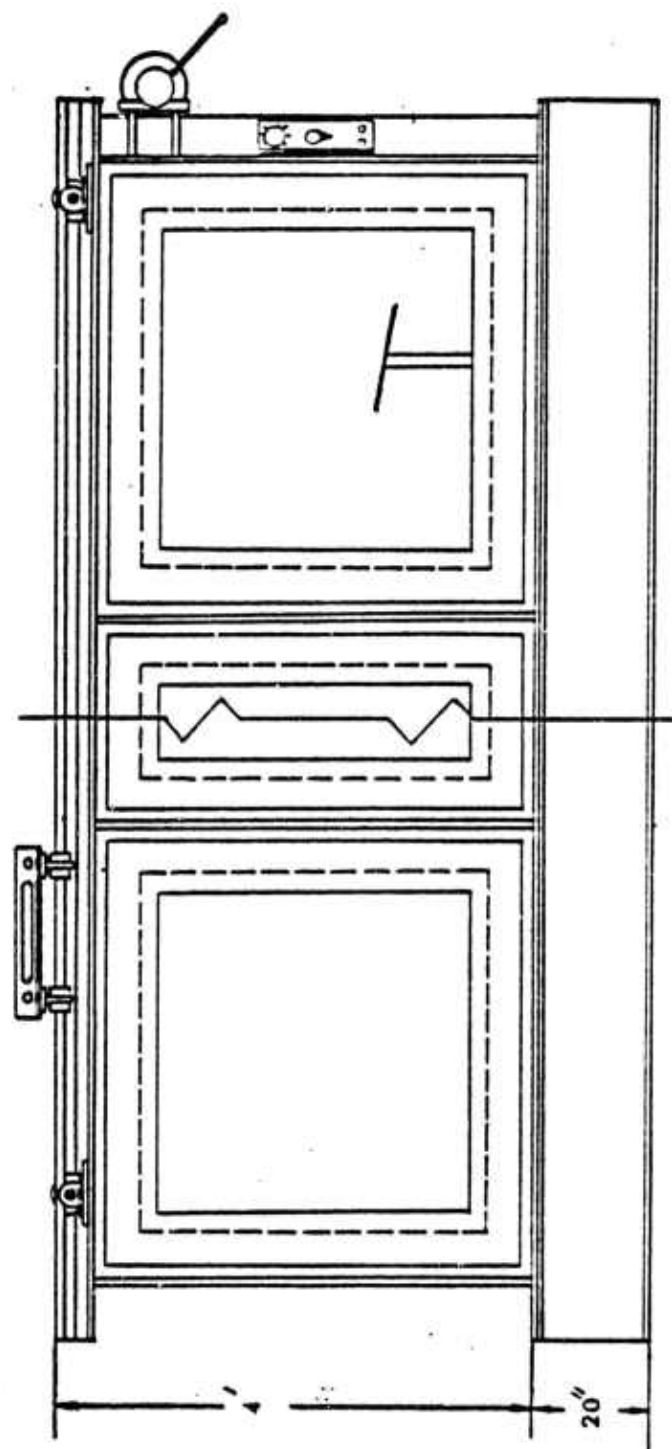


Figure 9. Front View of the Basin.

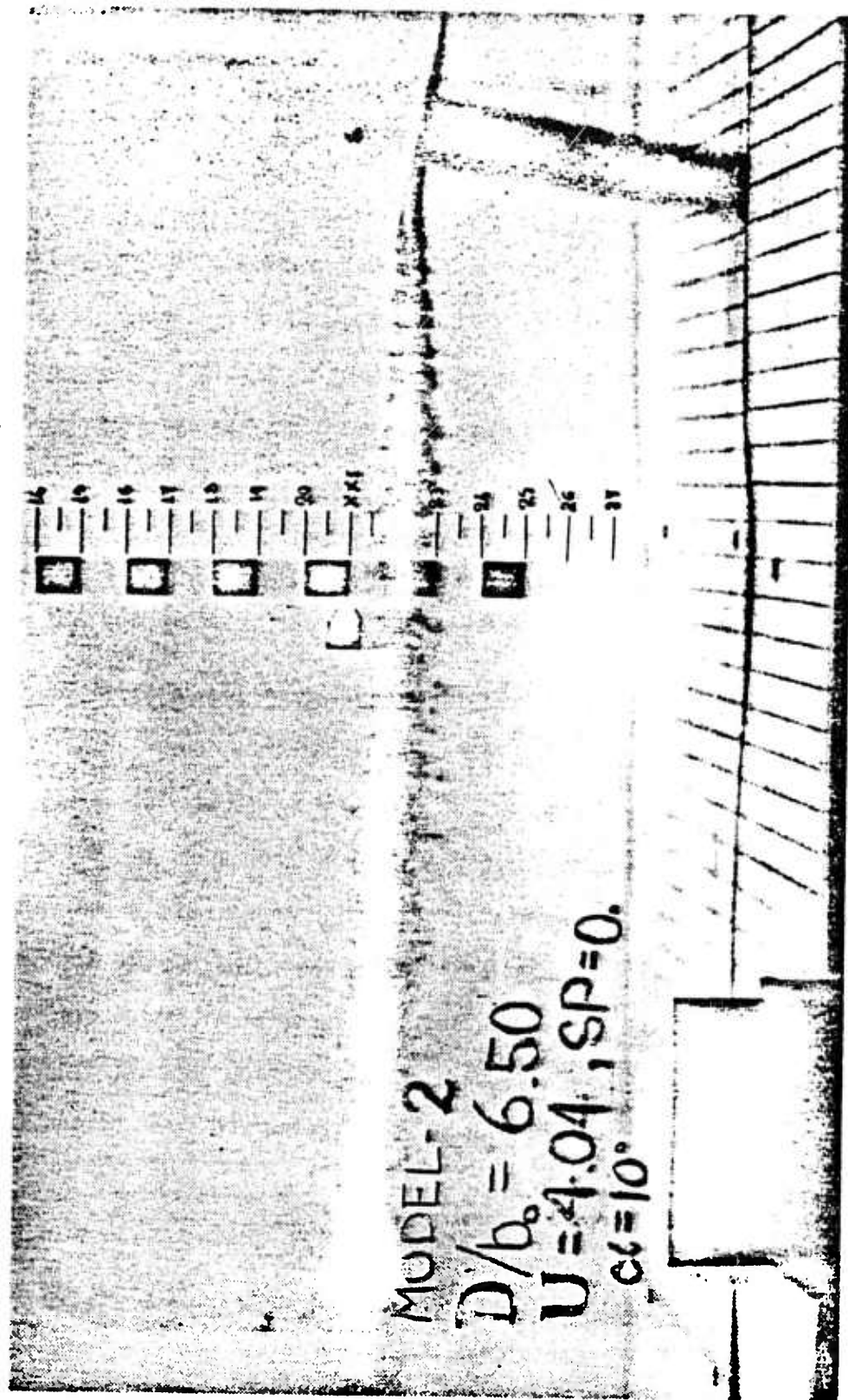


Figure 10. Side View of the Trailing Vortices.

III. RESULTS

A. DIMENSIONAL ANALYSIS

The experimental procedure is based on a careful dimensional analysis of the parameters entering into the phenomenon.

The dependent parameter of major importance is the displacement H of the vortex in the vertical direction and it may be expressed as a function of the following independent parameters for a given body shape:

$$H = f(t, U, D, \rho_0, \frac{\partial \rho}{\partial y}, \nu, B, AR, \alpha, g, r_0) \quad (1)$$

where t denotes the time; U , the forward velocity of the model; D , the initial depth of submergence of the vortex pair; ρ_0 , the fluid density; $\partial \rho / \partial y$, the density gradient; ν , the kinematic viscosity of water; B , the base width of the model (see Fig. 7); AR , the aspect ratio; α , the angle of attack; g , the gravitational acceleration; and r_0 , the vortex-core radius. The other parameters such as the vortex strength Γ , the vortex separation b_0 , and the velocity of vertical migration of vortices V_0 , are determined by the same parameters governing the variation of H . Furthermore, r_0 can be changed only by modifying the shape of the separation lines on the model.

A dimensional analysis of Eq. (1) yields

$$\frac{H}{B} = f\left(\frac{Ut}{B}, \frac{D}{B}, \frac{NB}{U}, \frac{U^2}{gB}, \frac{UB}{\nu}, AR, \alpha, \frac{r_0}{B}\right) \quad (2)$$

in which

$$N = \left(\frac{g}{\rho_0} \frac{\partial \rho}{\partial y} \right)^{1/2}$$

and is known as the Brunt-Vaisala frequency. The other dimensionless parameters appearing in Eq. (2) are self-explanatory.

In the present investigation B , AR , α , r_0 , and D were determined by the model being investigated. The velocity of the model was varied from 0.30 ft/s to 5.0 ft/s in experiments with fresh water ($N = 0$). The experiments with stratified water were carried out by varying N ($N = 0.0974 \text{ s}^{-1}$ to 0.2101 s^{-1}) at various velocities.

The dimensionless parameter NB/U is often replaced by another parameter Nb_0/V_0 , known as the stratification parameter. It should be noted that both b_0 and V_0 are dependent parameters. b_0 is determined by the shape of the body and its angle of attack. V_0 is determined by

$$\frac{V_0}{U} = f\left(\frac{D}{B}, \frac{NB}{U}, \frac{U^2}{gB}, \frac{UB}{V}, AR, \alpha, \frac{r_0}{B}\right) \quad (3)$$

Thus, Eq. (2) may be recast as

$$\frac{H}{b_0} = f\left(\frac{V_0 t}{b_0}, \frac{D}{b_0}, \frac{Nb_0}{V_0}, \frac{V_0^2}{gb_0}, \frac{V_0 b_0}{V}, AR, \alpha, \frac{r_0}{b_0}\right) \quad (4)$$

Of the parameters appearing in Eq. (4) only D , N , g , and ν are independent and may be varied irrespective of the shape of the body. However, the remaining parameters with the exception of α depend on the shape, aspect ratio, and the velocity of the body. The variations of AR and α are imbedded in the variation of V_0 and b_0 . Experiments were performed with a given body by varying the angle of attack and the speed of the body for a given Brunt-Vaisala frequency, N . Then V_0 and H were determined from the pictures. The parameters β and b_0 (see Fig. 7) were obtained from the existing experimental data [Ref. 2]. Subsequently, the data were plotted in terms of H/b_0 versus $V_0 t/b_0$ for specific values of D/b_0 , Nb_0/V_0 , and r_0/b_0 . The measurements have shown that the dimensionless parameters V_0^2/gb_0 and $V_0 b_0/\nu$ are not important within the range of the parameters encountered in the experiments. With the foregoing arguments, Eq. (4) may be written as

$$\frac{H}{b_0} = f\left(\frac{V_0 t}{b_0}, \frac{D}{b_0}, \frac{Nb_0}{V_0}, \frac{r_0}{b_0}\right) \quad (5)$$

This equation formed the basis for the analysis of the entire experimental data.

B. BODY AND SAIL-PLANE GENERATED VORTICES IN UNSTRATIFIED WATER

The results obtained with the streamlined body and its sail-plane are presented in the following.

Figure 11 shows the variation of H/b_0 as a function of $V_0 t/b_0$ for a representative model speed of $U = 3.59$ ft/sec and an angle of attack of

10 degrees. Figure 12 is a composite plot of all the data obtained at the angle of attack of 10 degrees. Plots similar to those discussed above are presented in Figures 13 and 14 for an angle of attack of 12 degrees. Finally, a comparison of the two sets of data for the two angles of attack is shown in Figure 15. In all these runs, the relative vortex-core size was estimated to be about $r_0/b_0 = 0.08$. In spite of the scatter, the data show that the rise of the vortices are not dependent on the angle of attack of the sail-plane. This is expected in view of the fact that the rise velocity V_0 is dictated by the angle of attack in addition to other parameters. In these tests the relative depth was kept constant at $D/b_0 = 4.45$. Furthermore, the edges of the sail-plane have not been modified so as to change the vortex core size. Consequently, it is not possible to ascertain the effects of D/b_0 and r_0/b_0 on the data shown in Figure 15.

Figure 15 shows that the maximum rise of vortices prior to their ultimate demise is limited to about $2.4b_0$. This is considerably lower than that obtained with Delta wings [Ref. 1]. The reason for this is that the vortices generated by the sail-plane undergo rapid vortex breakdown under the influence of the streamlined body. The vortex breakdown rapidly diffuses the vorticity of the vortices, indicating that the body proximity is an effective means of limiting the rise of the trailing vortices.

C. SAIL-PLANE GENERATED VORTICES

Experiments were conducted for three different angles of attack. Figure 16 shows the results for $\alpha = 8$ degrees. Figure 17 is a composite

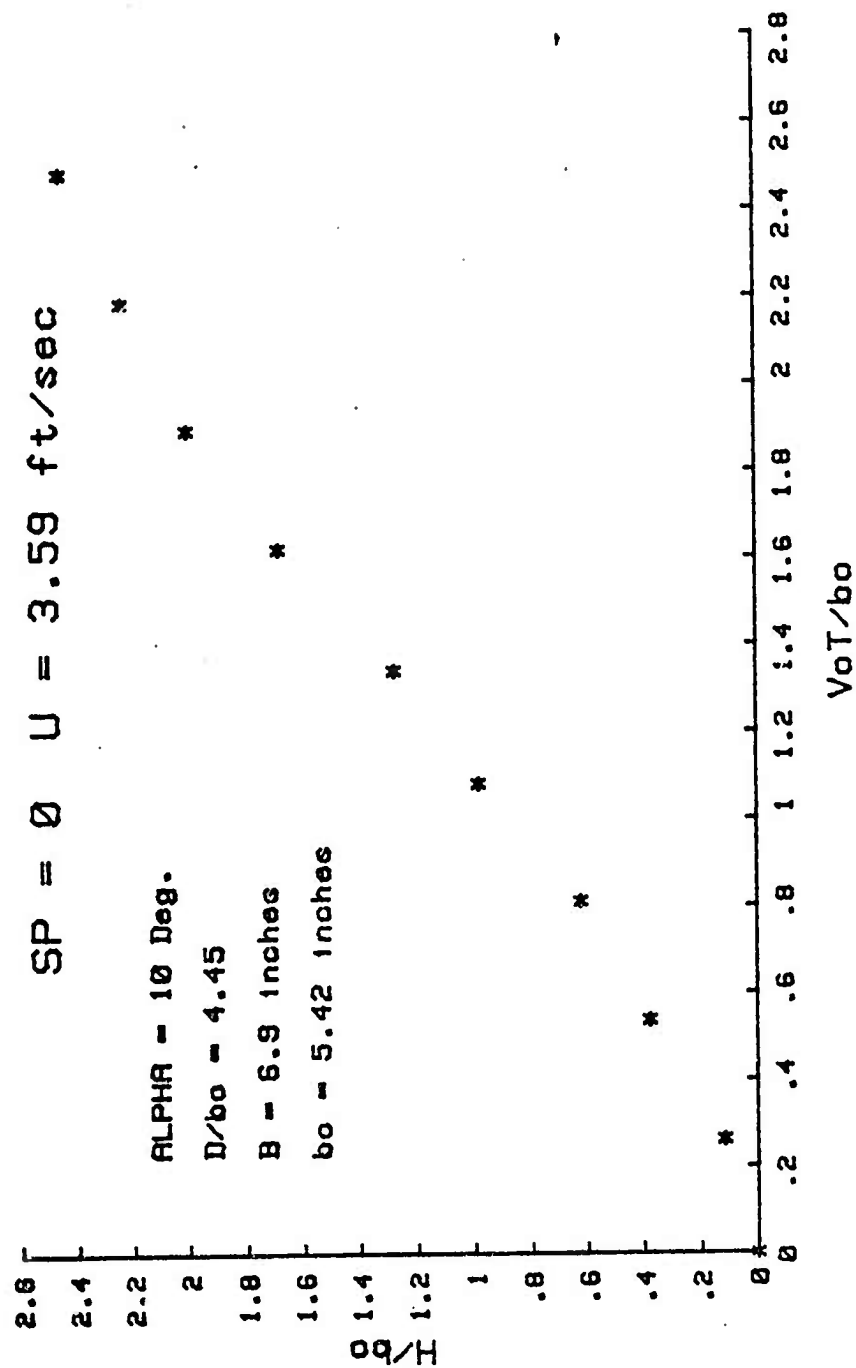


Figure 11. The Rise of the Body-Sail-Plane Generated Vortices
as a Function of $V_0 t / b_0$ for $\alpha = 10 \text{ deg.}$

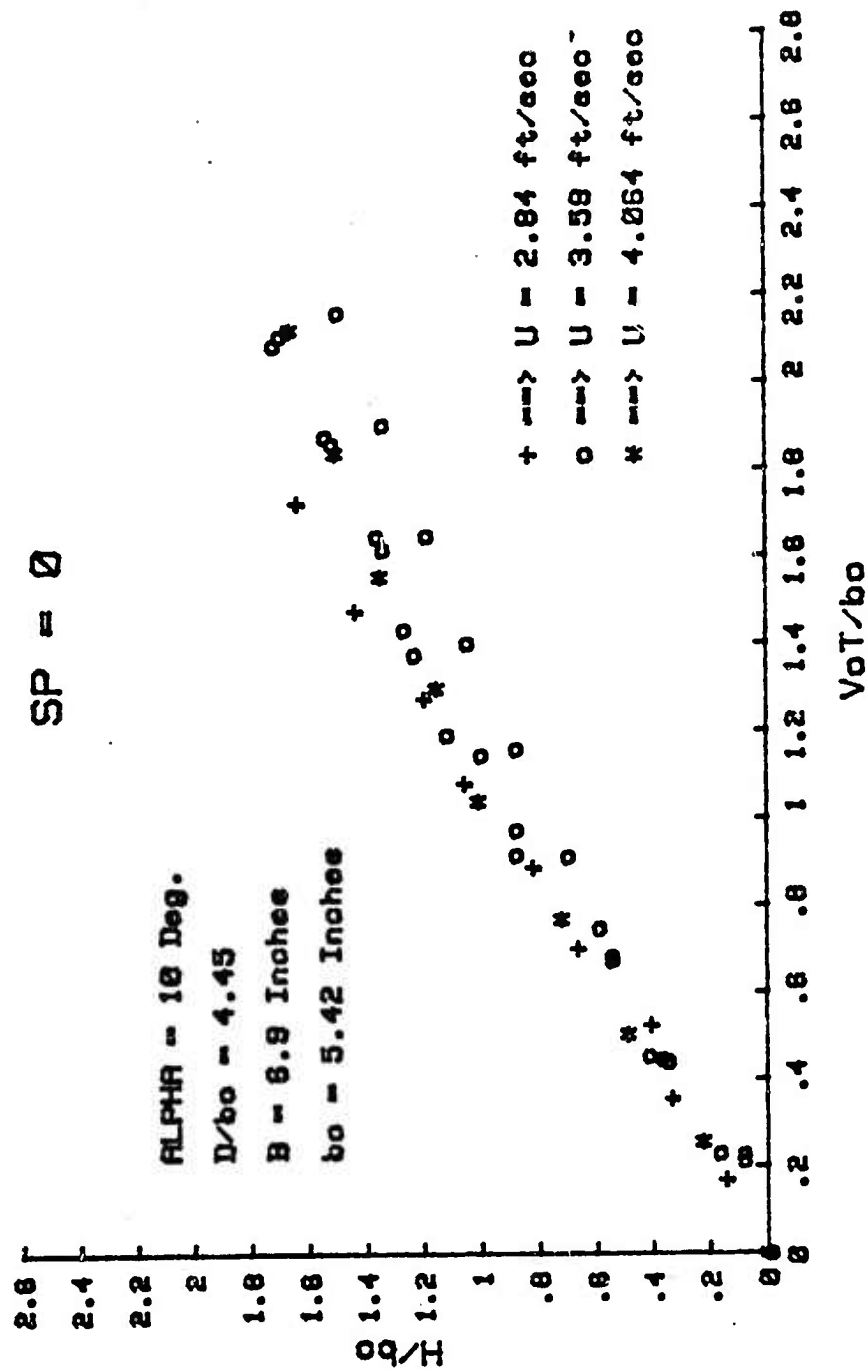


Figure 12. Comparison of the Rise History of the Vortices Generated by the Body-Sail-Plane Combination, ($\alpha = 10$ deg.).

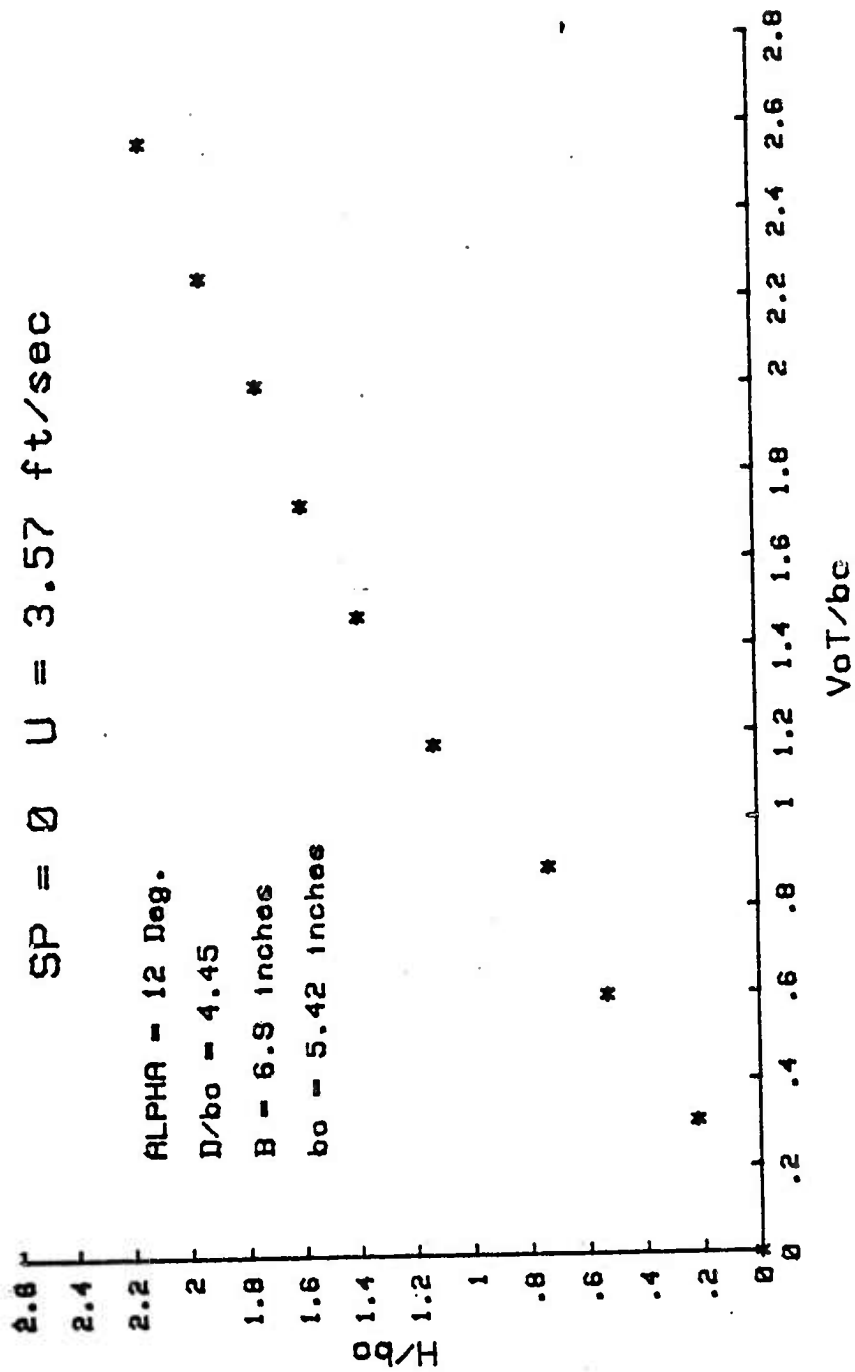


Figure 13. The Rise of the Body-Sail-Plane Generated Vortices as a Function of $V_0 t/b_0$ for $\alpha = 12 \text{ deg.}$

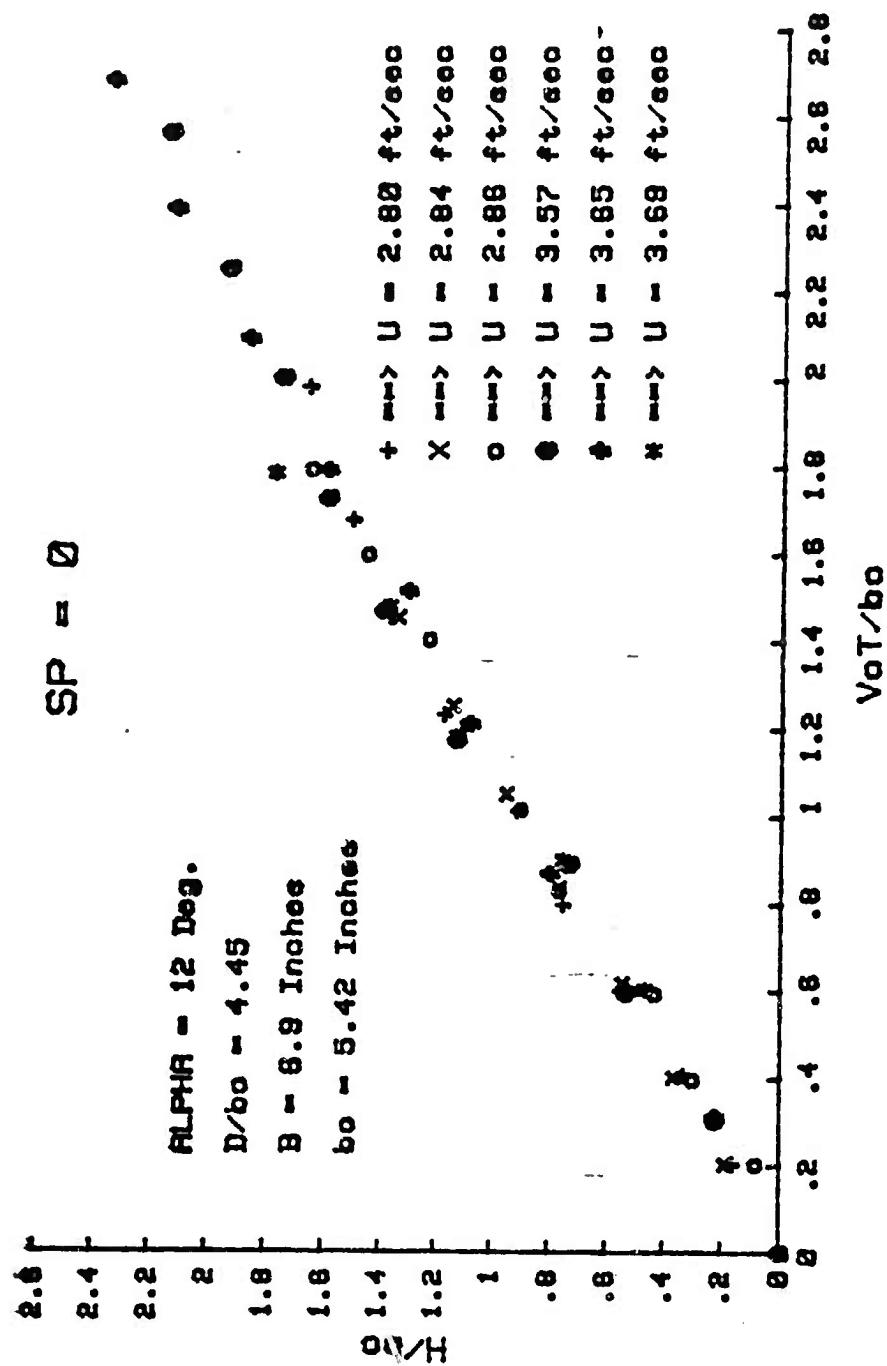


Figure 14. Comparison of the Rise History of the Vortices Generated by the Body-Sail-Plane Combination, ($\alpha = 12$ deg.).

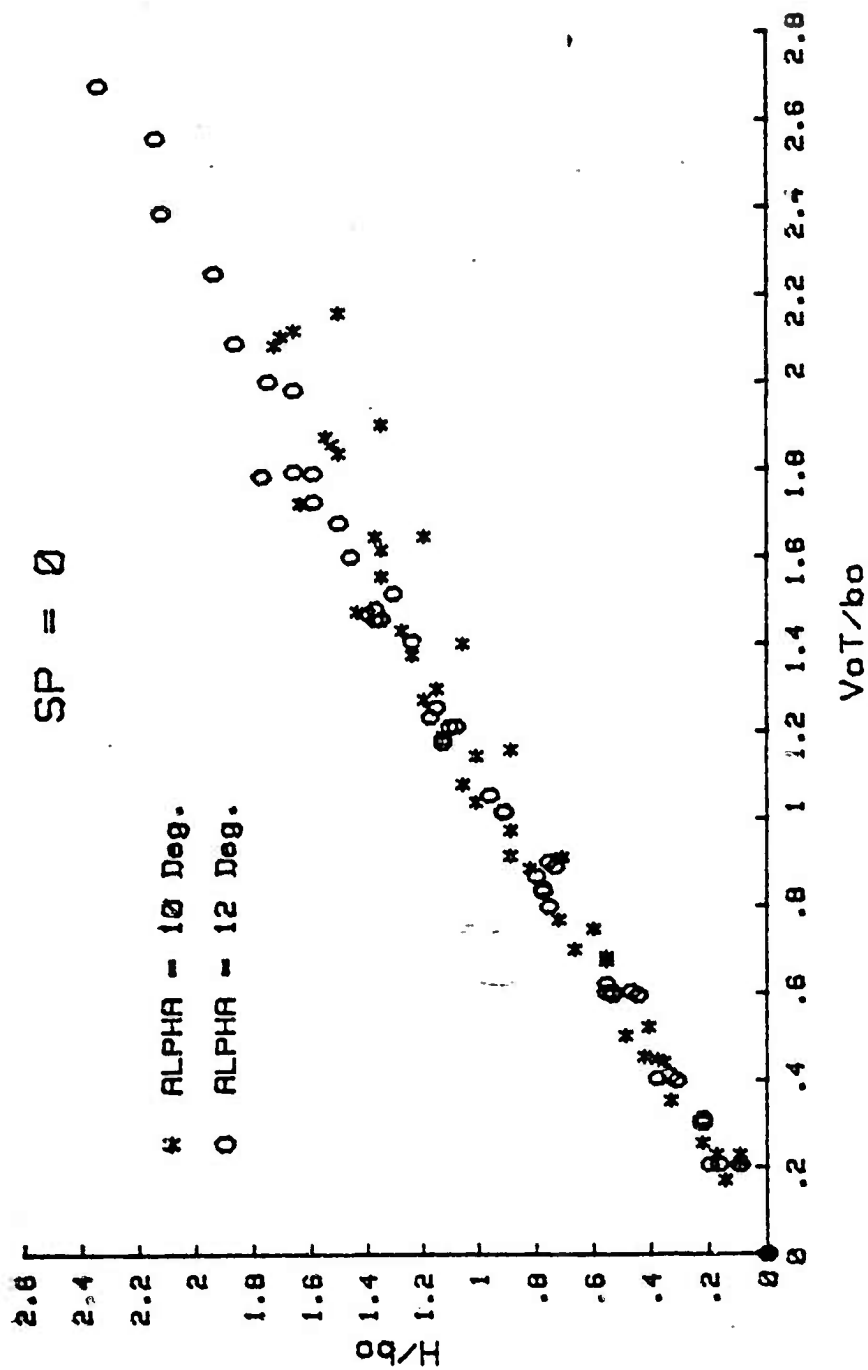


Figure 15. Comparison of the Vortex Rise History for $\alpha = 10$ deg. and $\alpha = 12$ deg., (Body-Sail-Plane Combination).

plot of all the data obtained at this angle of attack for various model velocities. Figures 18 and 19 show similar results for $\alpha = 10$ degrees and Figures 20 and 21 for $\alpha = 12$ degrees. Finally, the entire data obtained with the sail-plane are shown in Figure 22 together with those obtained with the body and sail-plane combination. It is clear that the vortices generated by the sail-plane alone rise to much higher levels relative to those generated by the body and sail-plane. This is a consequence of the observed fact that the sail-plane vortices do not undergo vortex breakdown due to the body proximity. Nevertheless, the maximum height attained by the sail-plane vortices is somewhat smaller than that attained by the vortices generated by a Delta wing ($H/b_0 = 3.6$ for the sail-plane vortices and $H/b_0 = 4.6$ for the vortices generated by a Delta wing with sharp edges). This is clearly a consequence of the effect of the wake of the sail body on the evolution of the vortices. It appears that the rise of vortices will be maximized when the wake and body-proximity effects are eliminated as in the case of Delta or rectangular wings.

D. DELTA- AND RECTANGULAR-WING GENERATED VORTICES

The Delta wings used during the first phase of the trailing-vortex studies [Ref. 1] were all sharp edged. For these models the flow visualization yielded a vortex core size of about $r_0 = 0.12b_0$. In order to determine the effect of the core size on the evolution of vortices the smaller of the two Delta wings was reconstructed and the two sharp edges were rounded with a radius of 1/16 inches (half of the model thickness). Otherwise, all dimensions of the model were kept exactly equal to that of the sharp-edged model. The new model will be referred to hereafter as 'rounded Delta 2'.

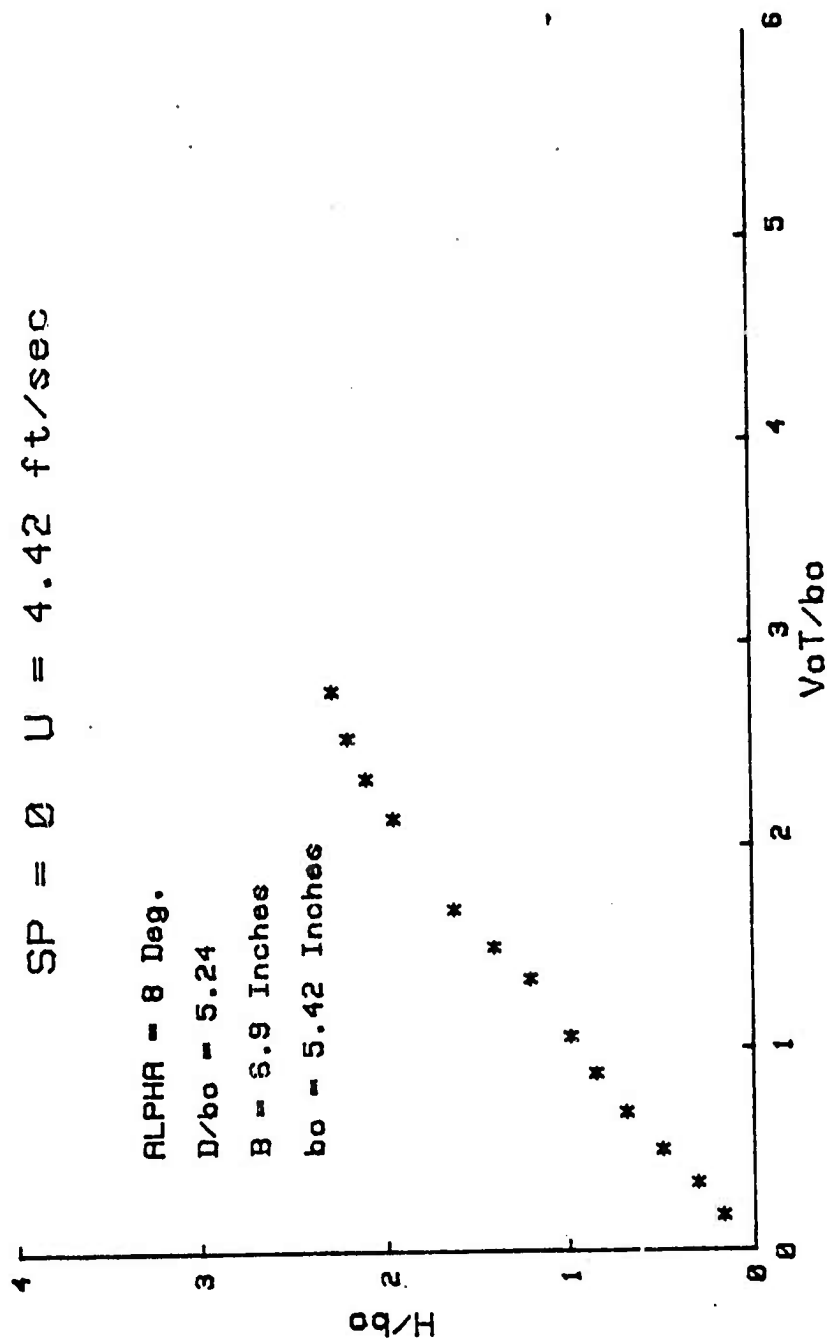


Figure 16. The Rise of Sail-Plane Generated Vortices for $\alpha = 8 \text{ deg.}$

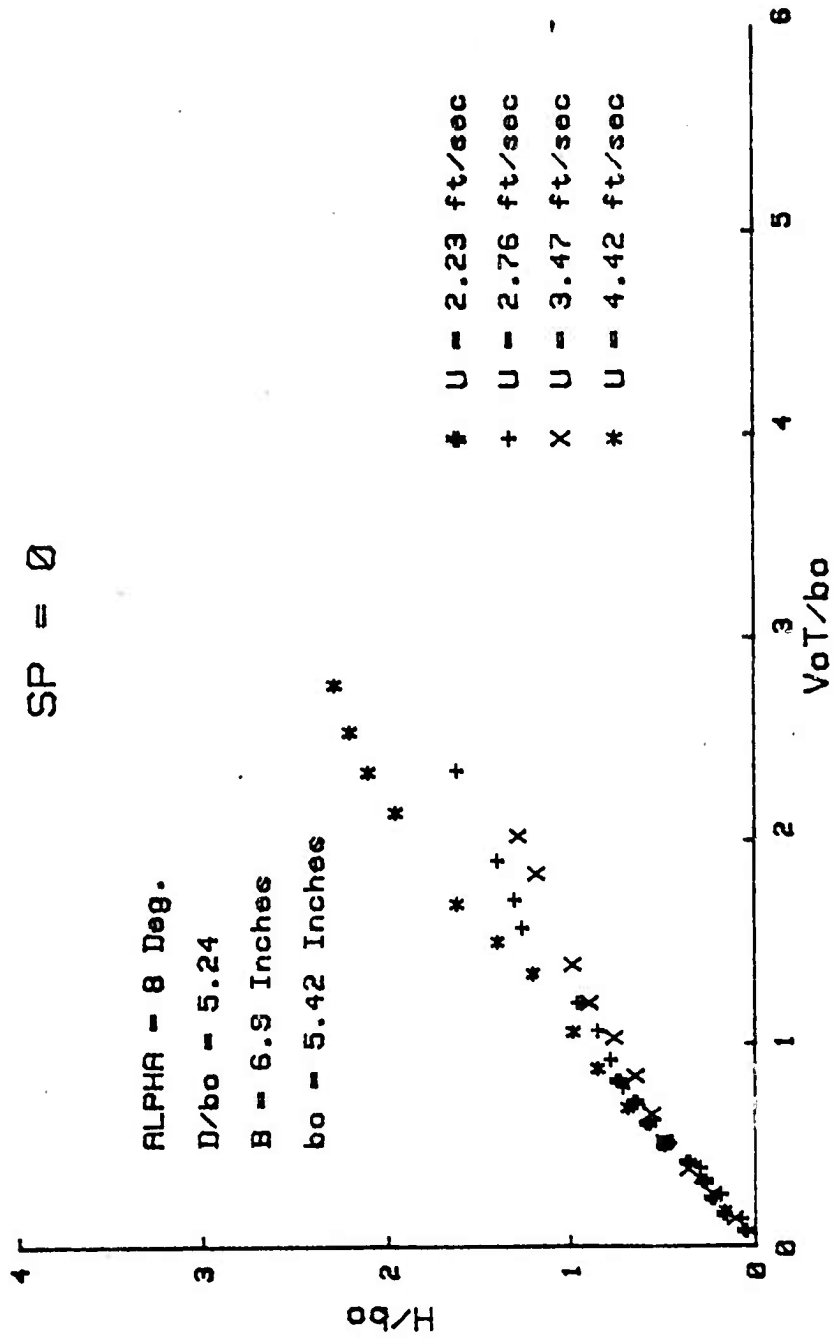


Figure 17. Comparison of the Rise of Sail-Plane Generated Vortices for $\alpha = 8$ deg.

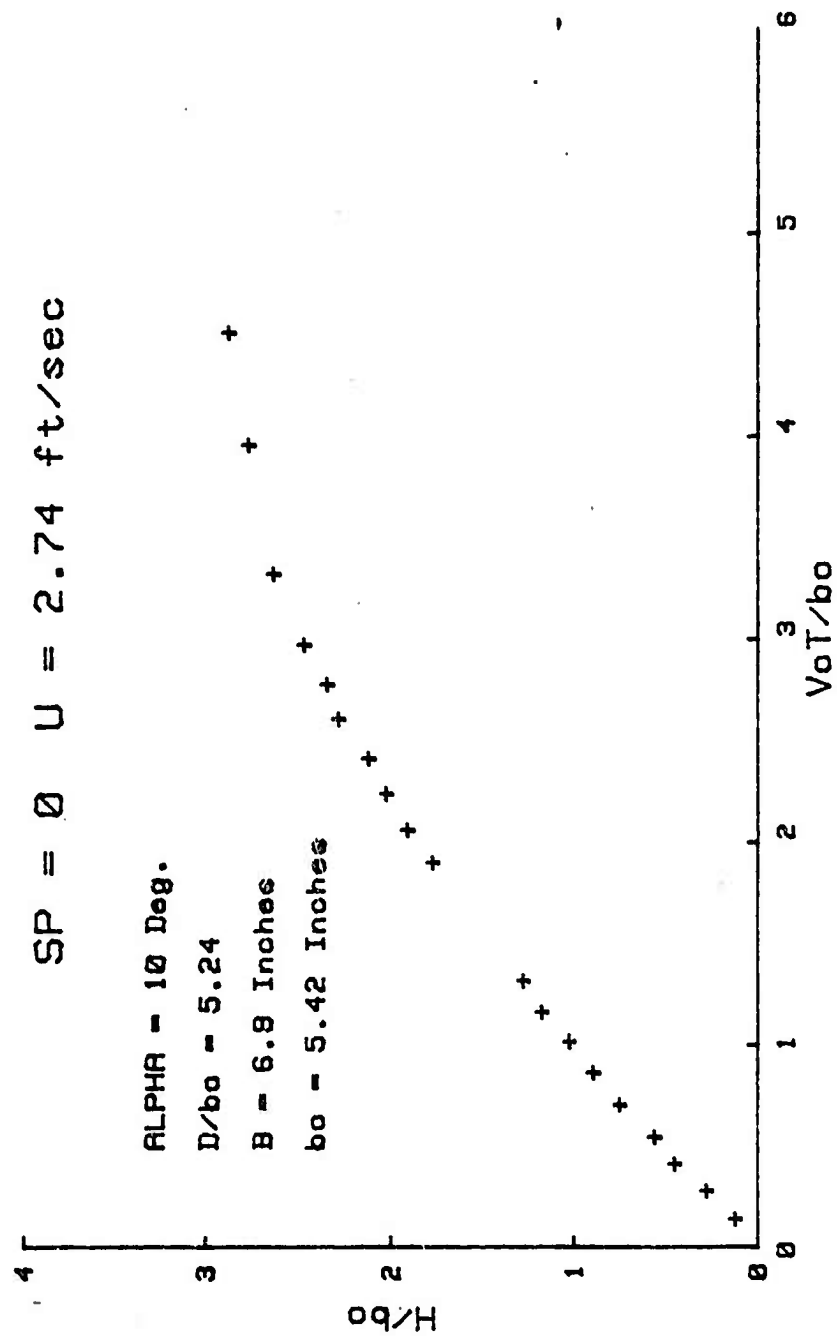


Figure 18. The Rise of Sail-Plane Generated Vortices for $\alpha = 10 \text{ deg.}$

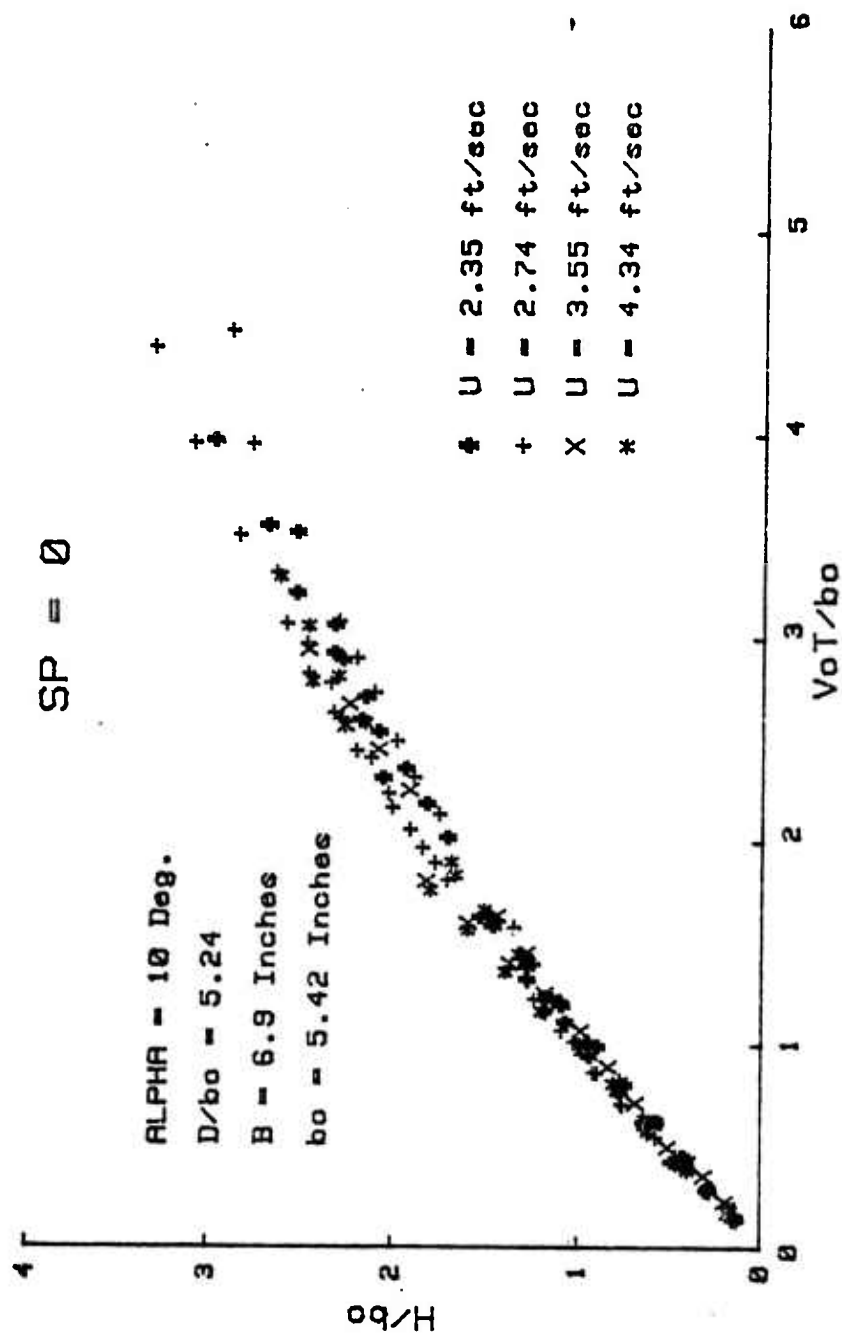


Figure 19. Comparison of the Rise of Sail-Plane
Generated Vortices for $\alpha = 10$ deg.

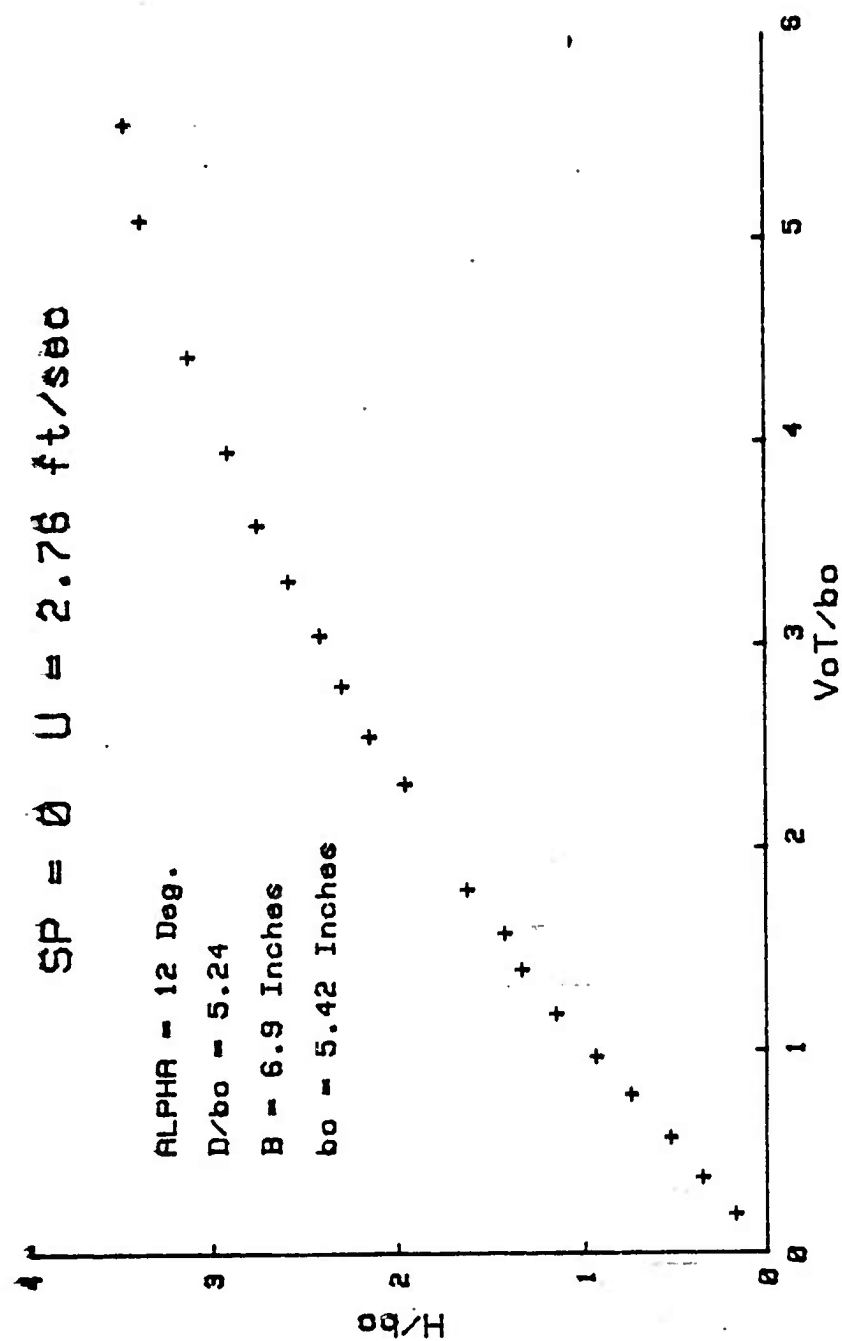


Figure 20. The Rise of the Sail-Plane
Generated Vortices for $\alpha = 12 \text{ deg.}$

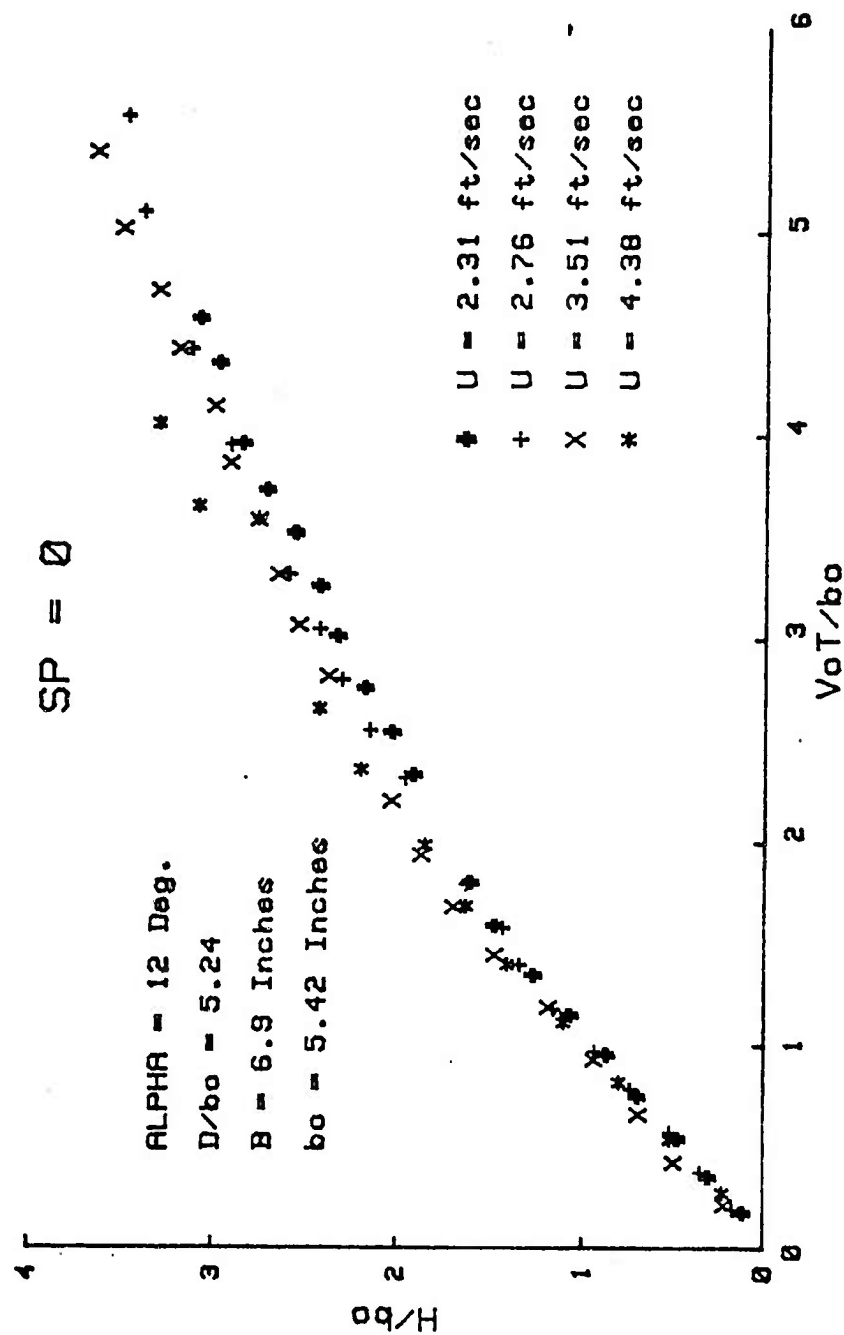


Figure 21. Comparison of the Rise of Sail-Plane Generated Vortices for $\alpha = 12$ deg.

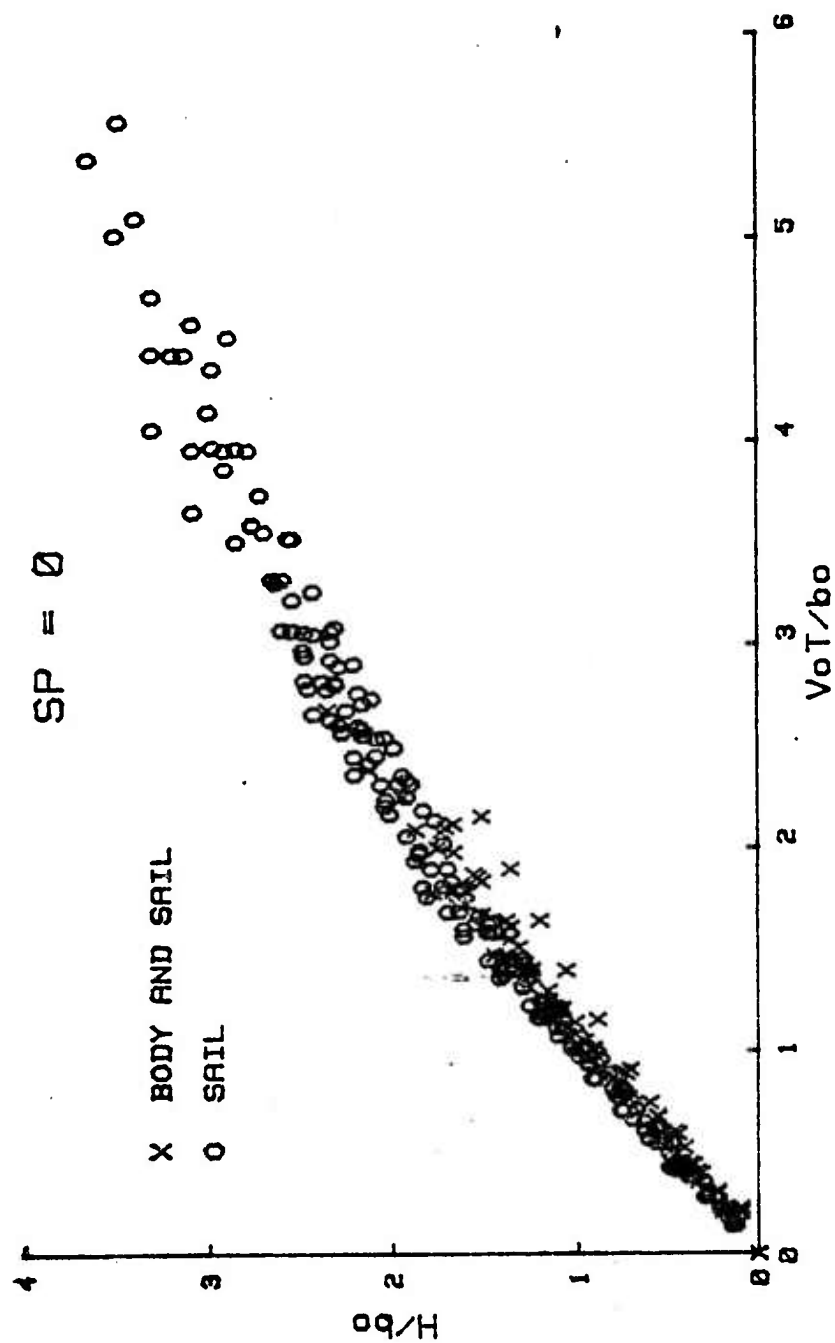


Figure 22. Comparison of the Rise of Vortices Generated by the Body-Sail-Plane Combination and the Sail-Plane.

A typical plot of H/b_0 versus $V_0 t/b_0$ is shown in Figure 23 for $U = 2.74$ ft/sec. Additional data for all other velocities used during the course of the investigation are shown in Figure 24 for an angle of attack of 8 degrees. Similar plots are shown in Figures 25 and 26 for an angle of attack of 10 degrees. Flow visualization has shown that the trailing vortices generated by the rounded Delta 2 has an initial core radius of about $r_0 = 0.07b_0$. Furthermore, the vortices appeared to be extremely smooth and parallel. In fact, these vortices approximated the ideal line vortices more closely than any other vortex observed previously. Initial observations of the rate of rise and ultimate demise of these vortices have indicated that they would rise to much greater heights relative to those generated by sharp-edged Delta wings.

Figure 27 shows a comparison of the data obtained with rounded and sharp-edged Delta wings. Clearly, the smaller the core size the larger the H/b_0 to which the vortices rise. Furthermore, the vortices with smaller core have a longer lifespan. This conclusion suggests that it is possible to accelerate the demise of the vortices by increasing their core size. This, in turn, is possible through the changes in the geometry of the trailing edges.

The rounded Delta 2 was also tested in stratified fluid with $SP = 0.375$ and $SP = 0.625$ in order to delineate the effect of core size in stratified fluid. Figure 28 shows the results obtained with the rounded Delta 2 for $SP = 0.375$. Figure 29 shows a comparison of the data obtained with sharp and rounded Delta wings. Clearly, the conclusions reached regarding the effect of the core size are valid for stratified flow also, i.e., the smaller the core size, the larger the height

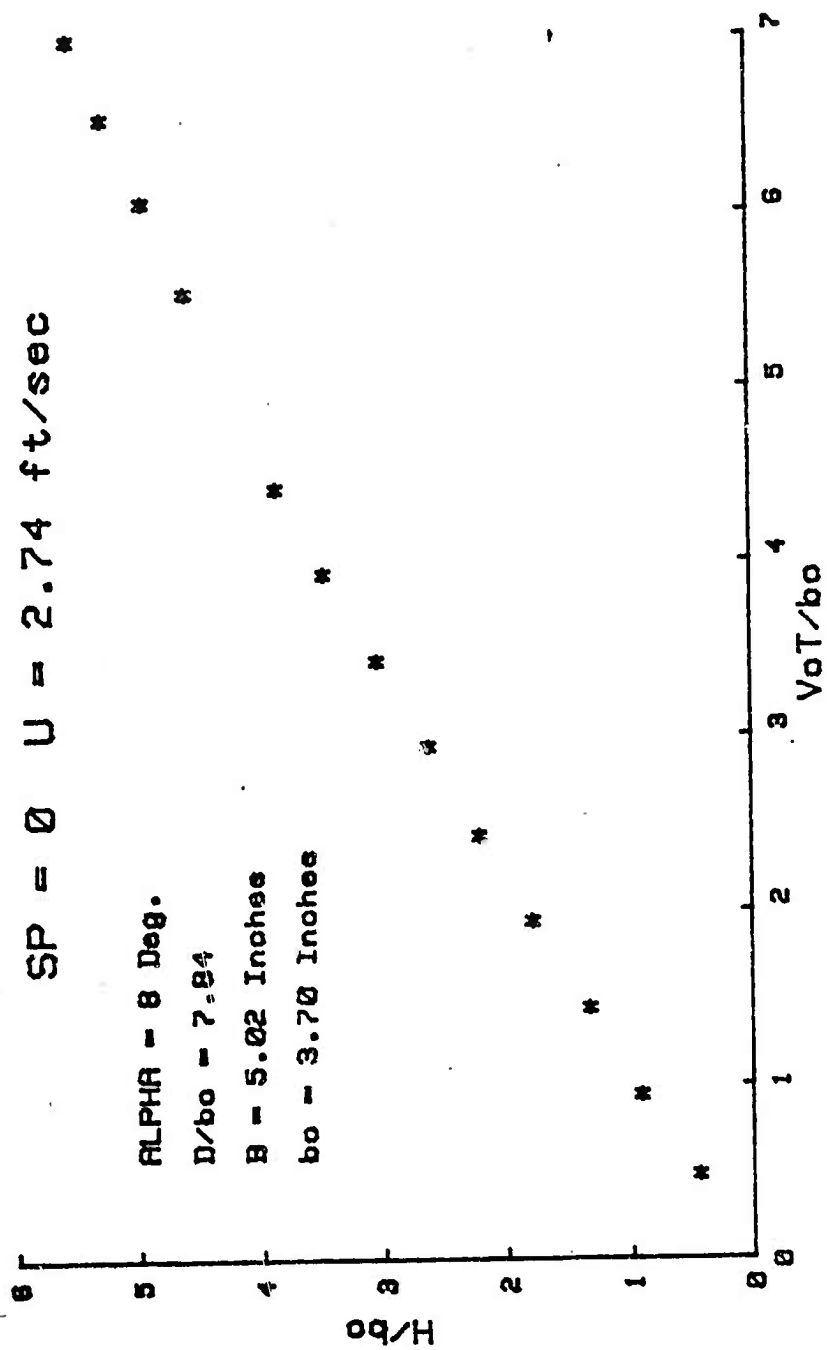


Figure 23. The Rise of Vortices Generated by the Rounded Delta 2 Model, ($\alpha = 8 \text{ deg.}$).

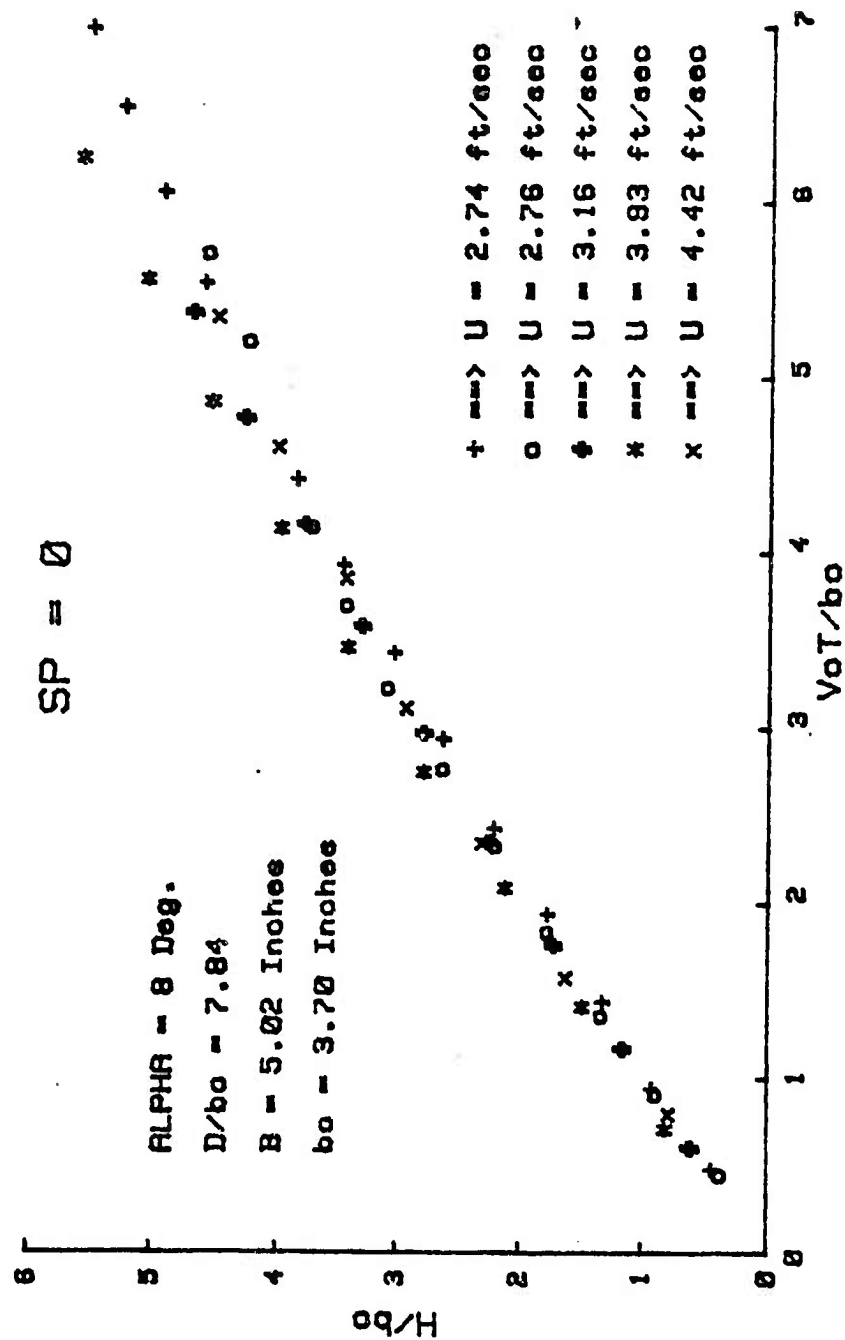


Figure 24. Comparison of the Rise of Vortices Generated by the Rounded Delta 2 Model, ($\alpha = 8$ deg.).

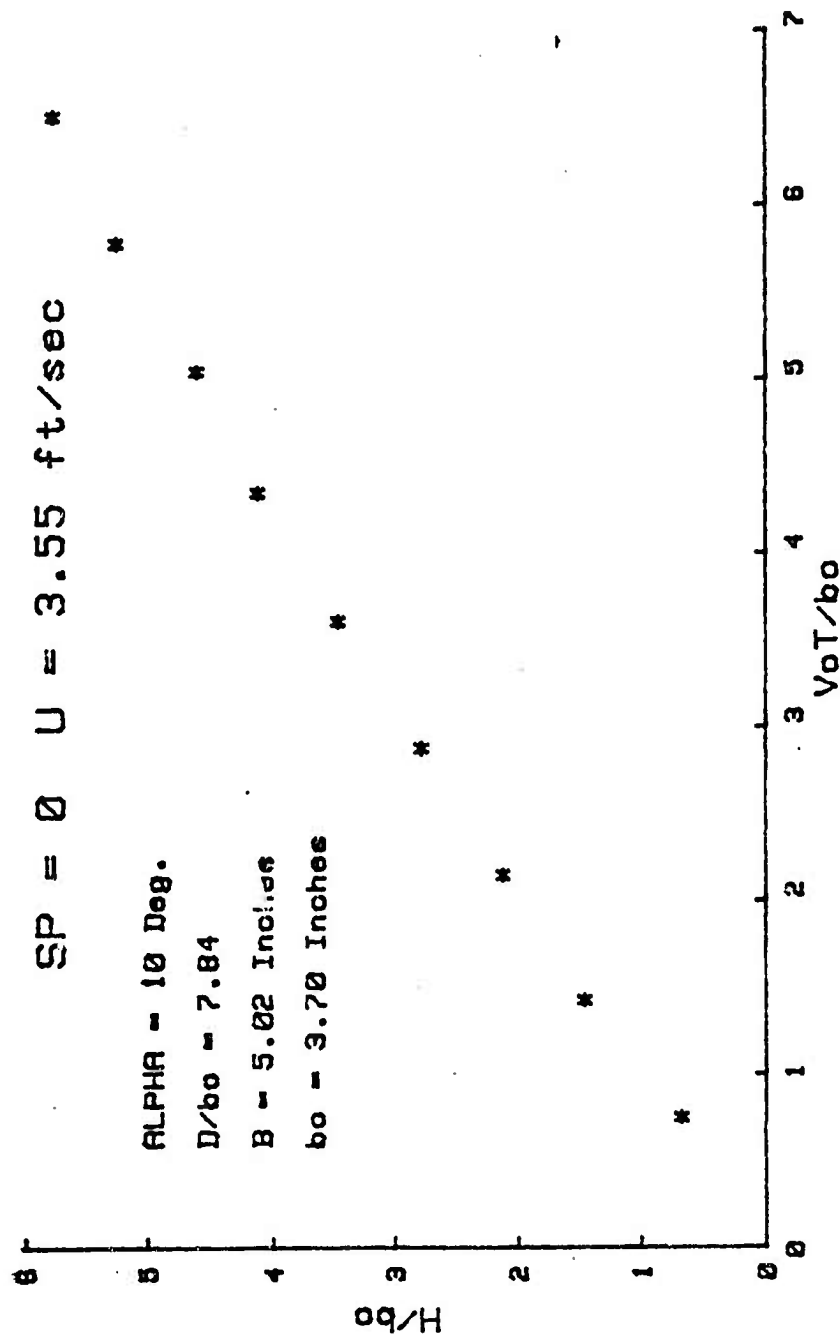


Figure 25. The Rise of Vortices Generated by the Rounded Delta 2 Model, ($\alpha = 10 \text{ deg.}$).

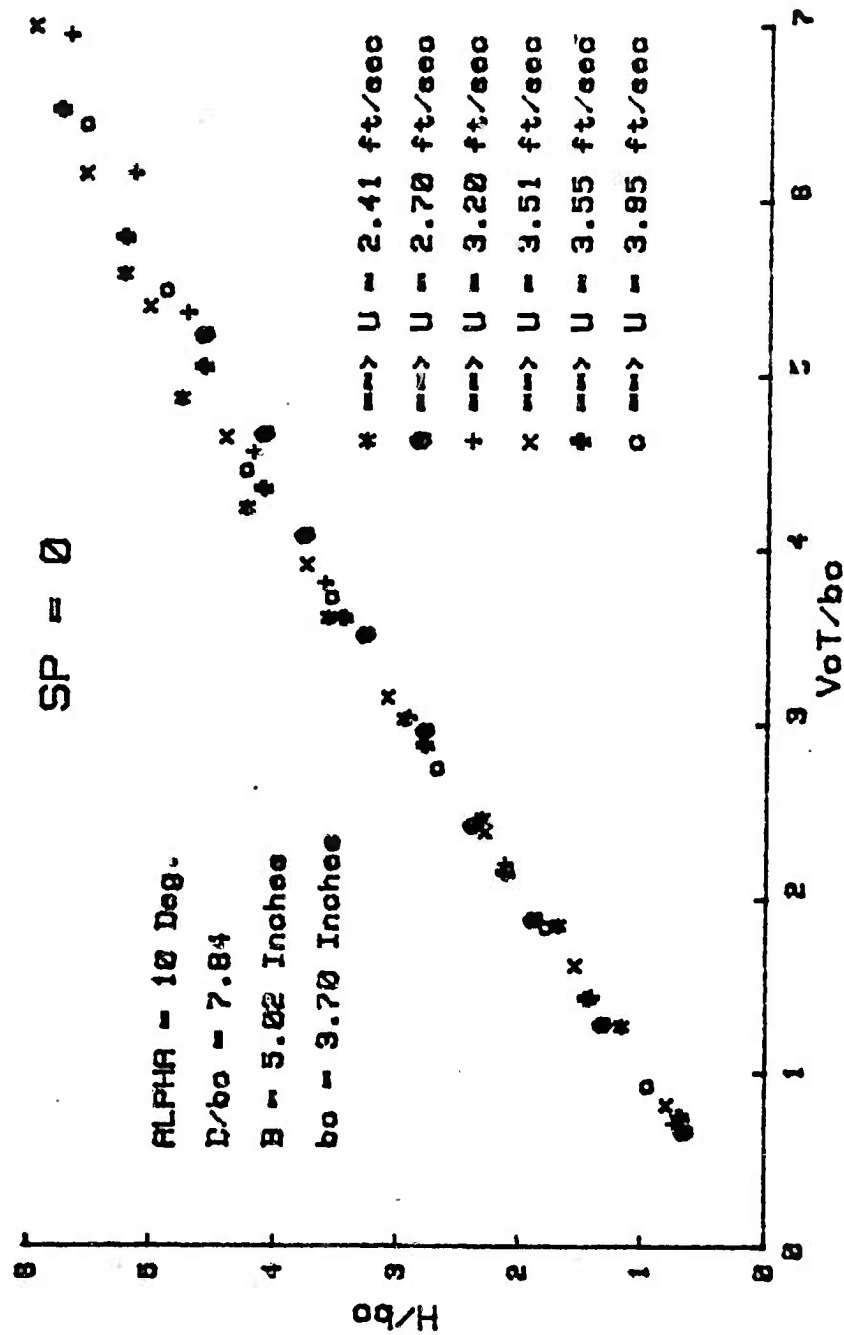


Figure 26. Comparison of the Rise of Vortices Generated by the Rounded Delta 2 Model, ($\alpha = 10$ deg.).

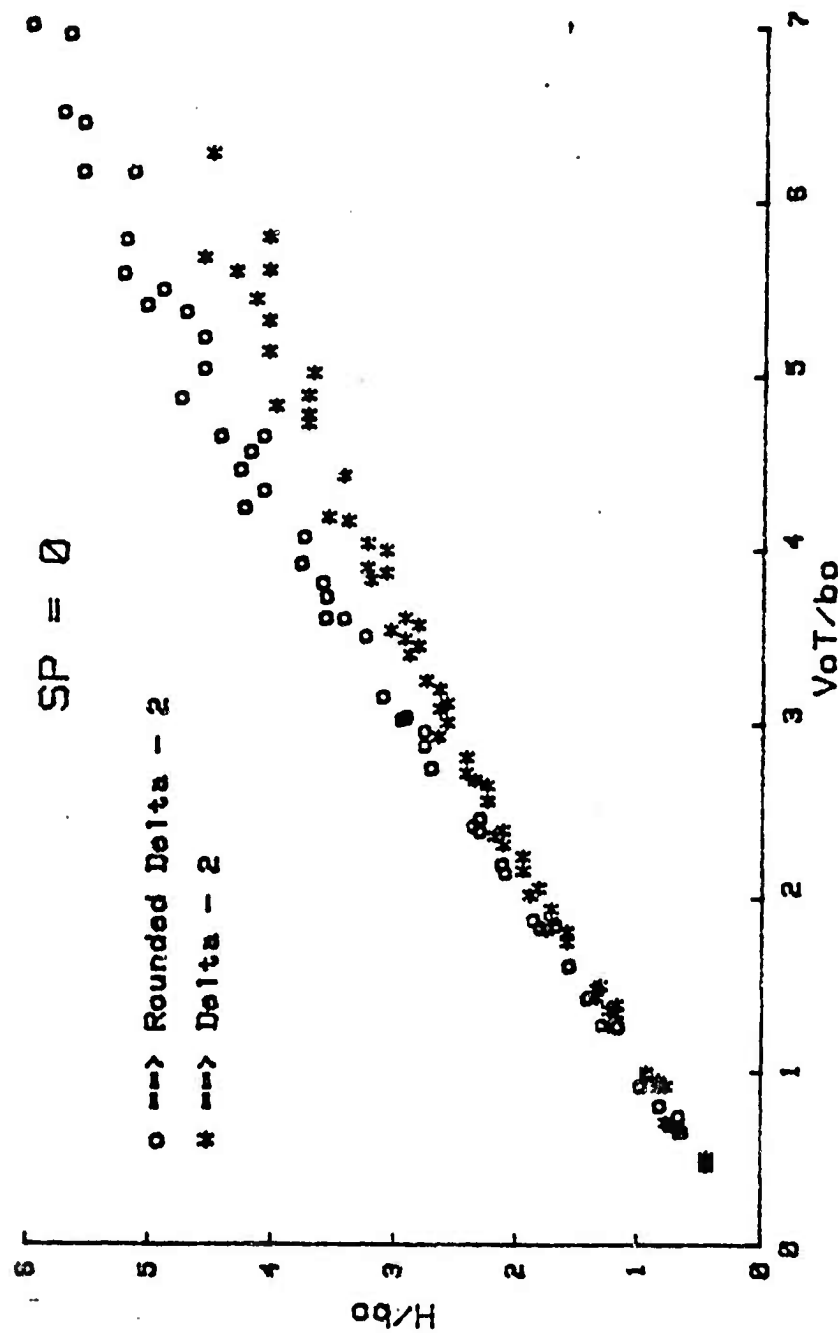


Figure 27. Comparison of the Rise of Vortices Generated by Rounded and Sharp-Edge Delta 2 Models.

attained by the vortices regardless of the degree of stratification of the ambient fluid medium. Similar conclusions may be reached from the data obtained with $Sp = 0.625$ as far as the lifespan of the vortices are concerned (see Figs. 30 and 31).

The foregoing results raised numerous new questions such as (i) can the core radius be varied systematically for a given model?; (ii) do the results depend on the aspect ratio and the shape of the model?; (iii) what are the most effective means of enhancing the demise of vortices?, etc. To answer at least partially some of these questions a rectangular wing with a cross section of NACA 0012 was constructed. The wing had an aspect ratio of $AR = 1.94$ with $B = 4.5$ inches. The wing tips of the model were carefully rounded with a radius equal to half of the local thickness. The trailing edge of the model was kept sharp as in the case of common airfoils.

Figure 32 shows sample data obtained with this wing at an angle of attack of 12 degrees for $U = 3.16$ ft/sec. Figure 33 is a composite plot of all the data obtained at the same angle of attack for various model velocities. Once again it is clear that the variation of H/b_0 with $V_0 t/b_0$ does not depend on the model velocity, within the range of velocities tested.

One is now in a position to determine as to whether the aspect ratio and the model shape have any effect on the rise of vortices for a given wing-tip shape. For this purpose, the data obtained with the rounded Delta 2 and the rectangular wing are compared in Figure 34. It is clear that there is very little difference if any between the two sets of data. Thus, one may conclude tentatively that the aspect ratio

and shape of the model do not materially affect the variation of H/b_0 with $V_0 t/b_0$. On the other hand, the rounding of the wing tips has strong influence on the rise and ultimate demise of the vortices, as noted earlier. Additional experiments with other shapes of models and wing tips are needed to put the foregoing conclusions on a firmer basis. In any case, the stratification is not expected to alter these conclusions.

The tabulated data for all models are presented in Appendices A through E.

E. NUMERICAL MODEL OF LAMINAR VORTEX PAIR

As discussed in the previous sections, the need to determine the lifespan of vortices and to understand the physics of the demise mechanisms gave rise to several approximate analyses. Numerical methods have been employed only recently using computers to attempt to incorporate the effect of turbulence in the evolution and ultimate demise of the vortex pair. It is hoped that such methods will provide not only a power of prediction of the migration of trailing vortices but also some insight as to the relationship between turbulence and the demise mechanisms. To be sure, there are, at present, no numerical methods dealing with the three-dimensional trailing vortices and the effects of vortex breakdown and Crow instability.

The most advanced numerical methods have been applied to the study of the two-dimensional, unsteady vortex pair. Hecht et al. [Ref. 3], introduced such a model which solves the mean and ensemble-averaged Reynolds stress equations of fluid motion, based on a second-order closure turbulence model. The initial distribution of vorticity was assumed to be Gaussian of the form

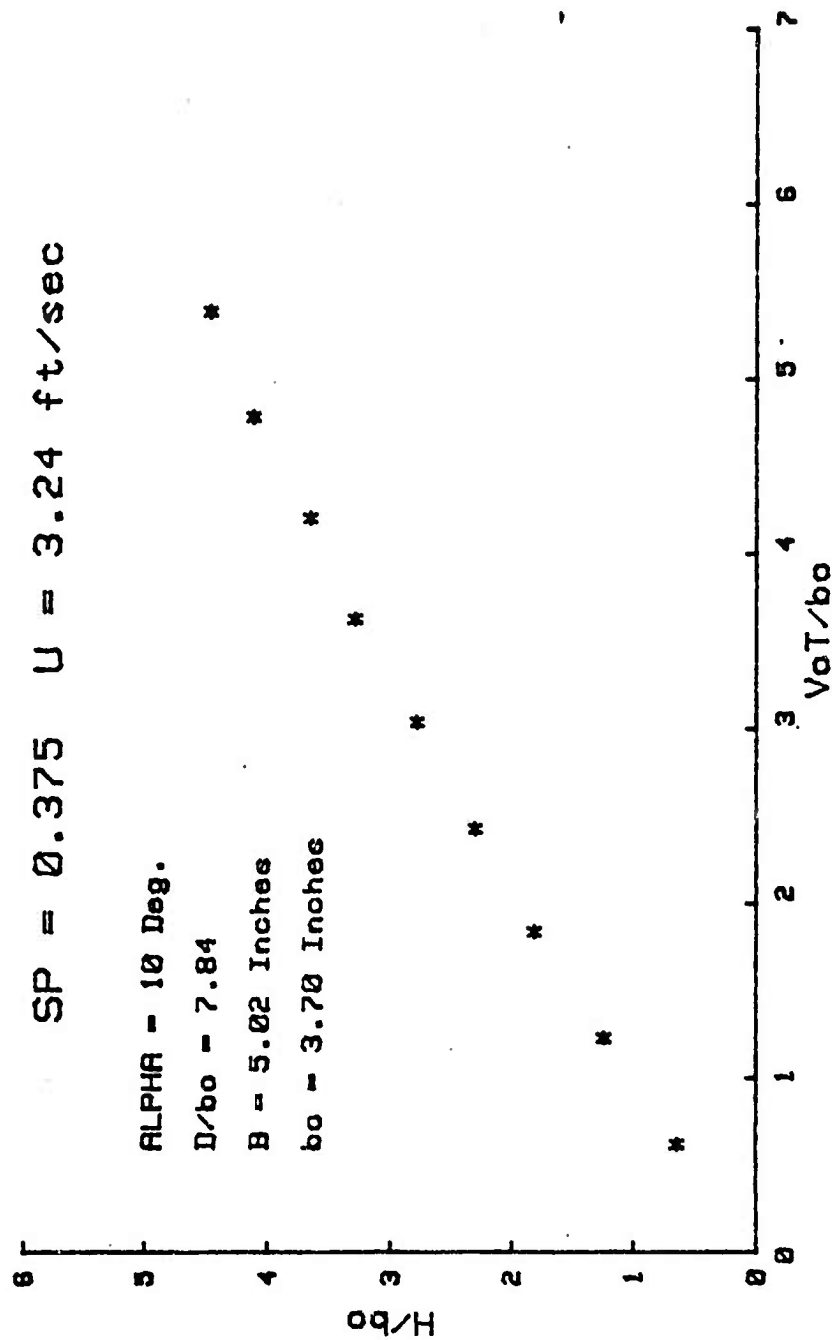


Figure 28. Effect of Stratification on the Rise of Vortices Generated by a Rounded Delta 2 Model, ($SP = 0.395$).

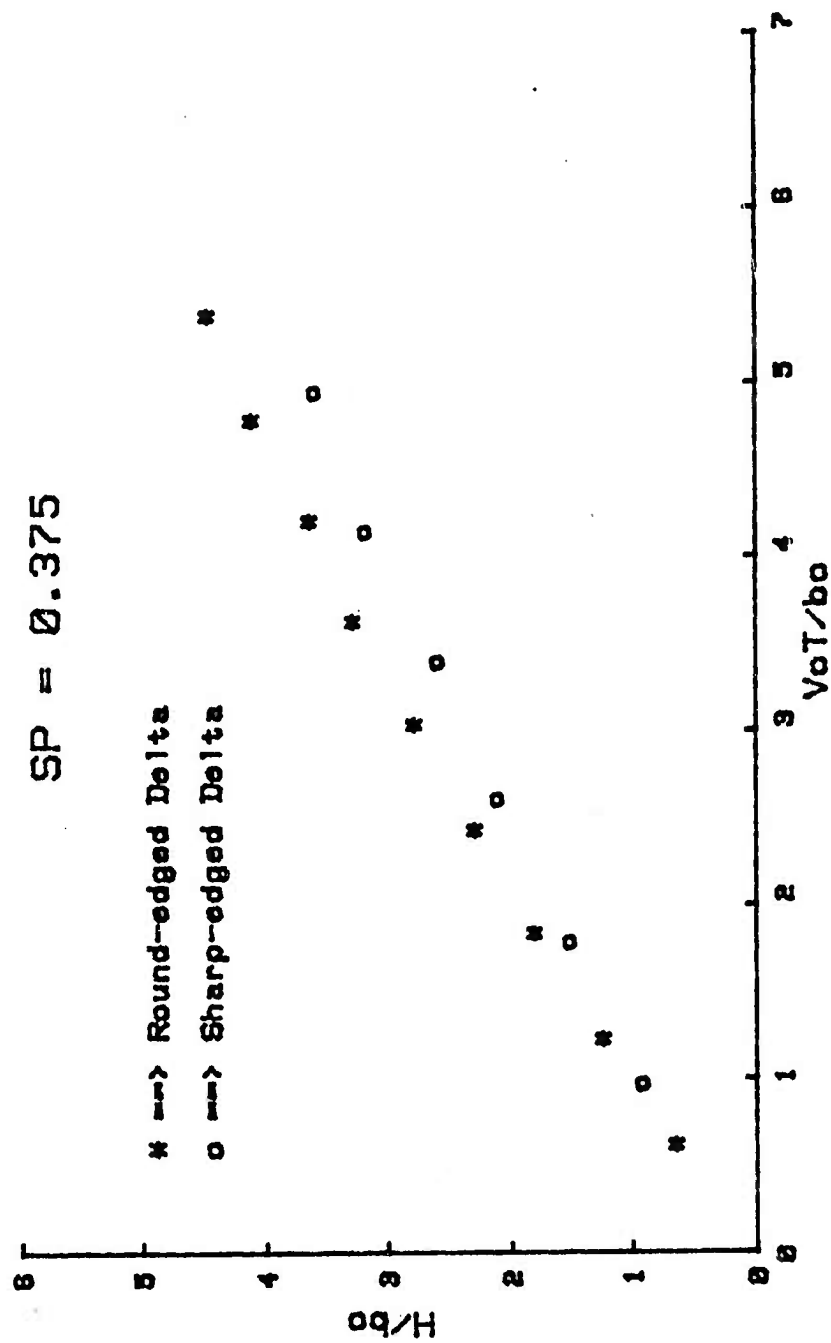


Figure 29. Comparison of the Rise of Vortices in a Stratified Fluid (Rounded Delta 2 and Sharp-Edge Delta 2, $SP = 0.375$).

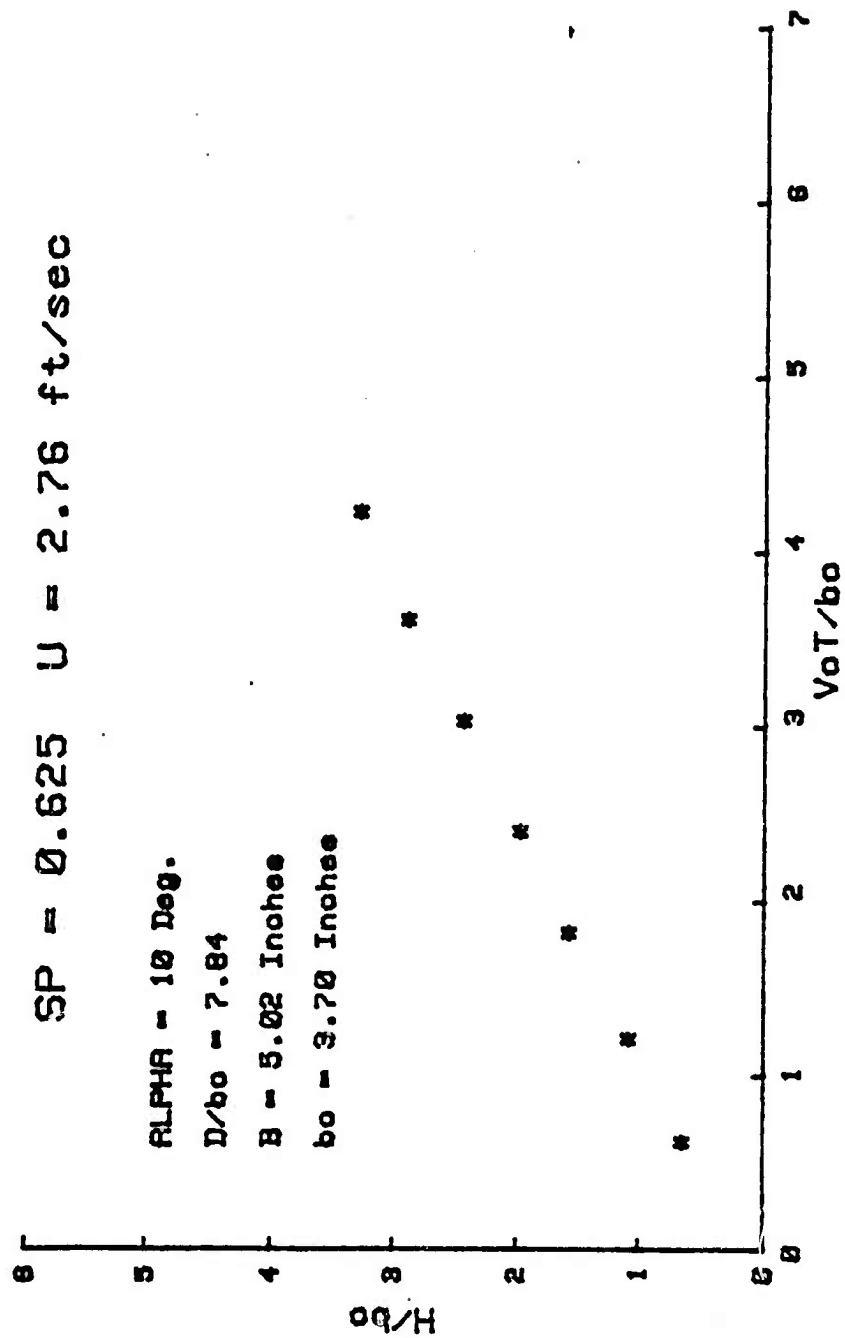


Figure 30. Effect of Stratification on the Rise of Vortices
 Generated by a Rounded Delta 2 Model, ($SP = 0.625$).

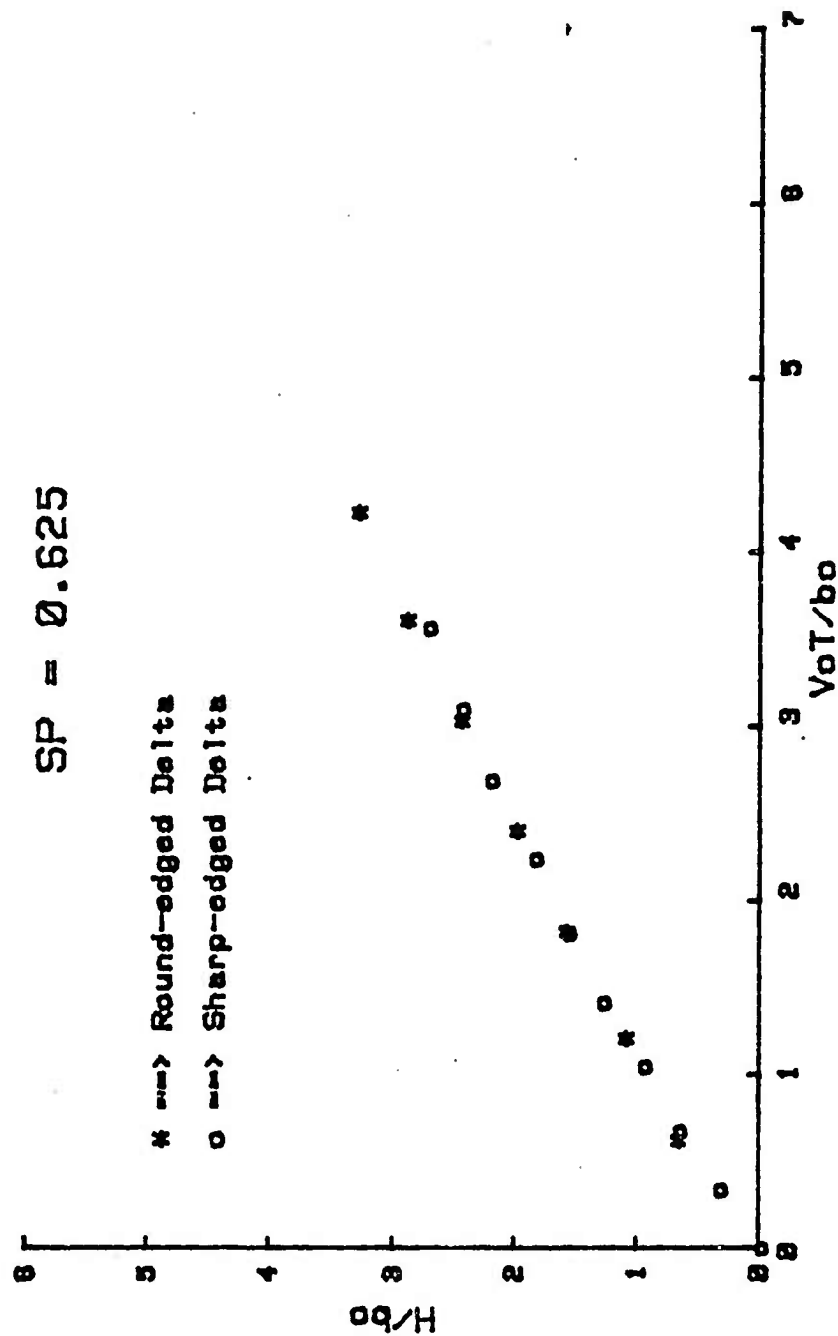


Figure 31. Comparison of the Rise of Vortices in a Stratified Fluid (Rounded Delta 2 and Sharp-Edge Delta 2, $SP = 0.625$).

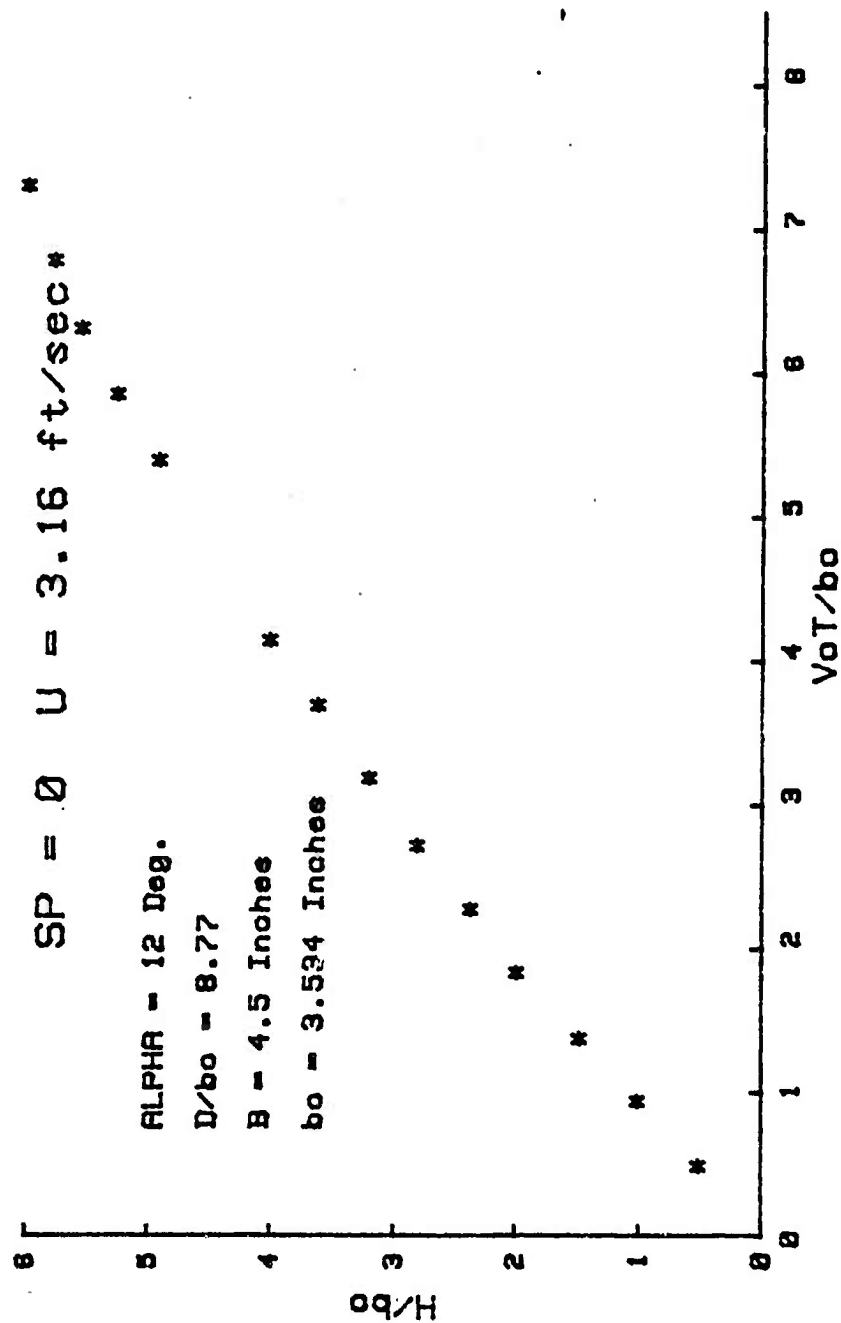


Figure 32. Rise of Vortices Generated by a Rectangular Wing ($\alpha = 12$ deg.).

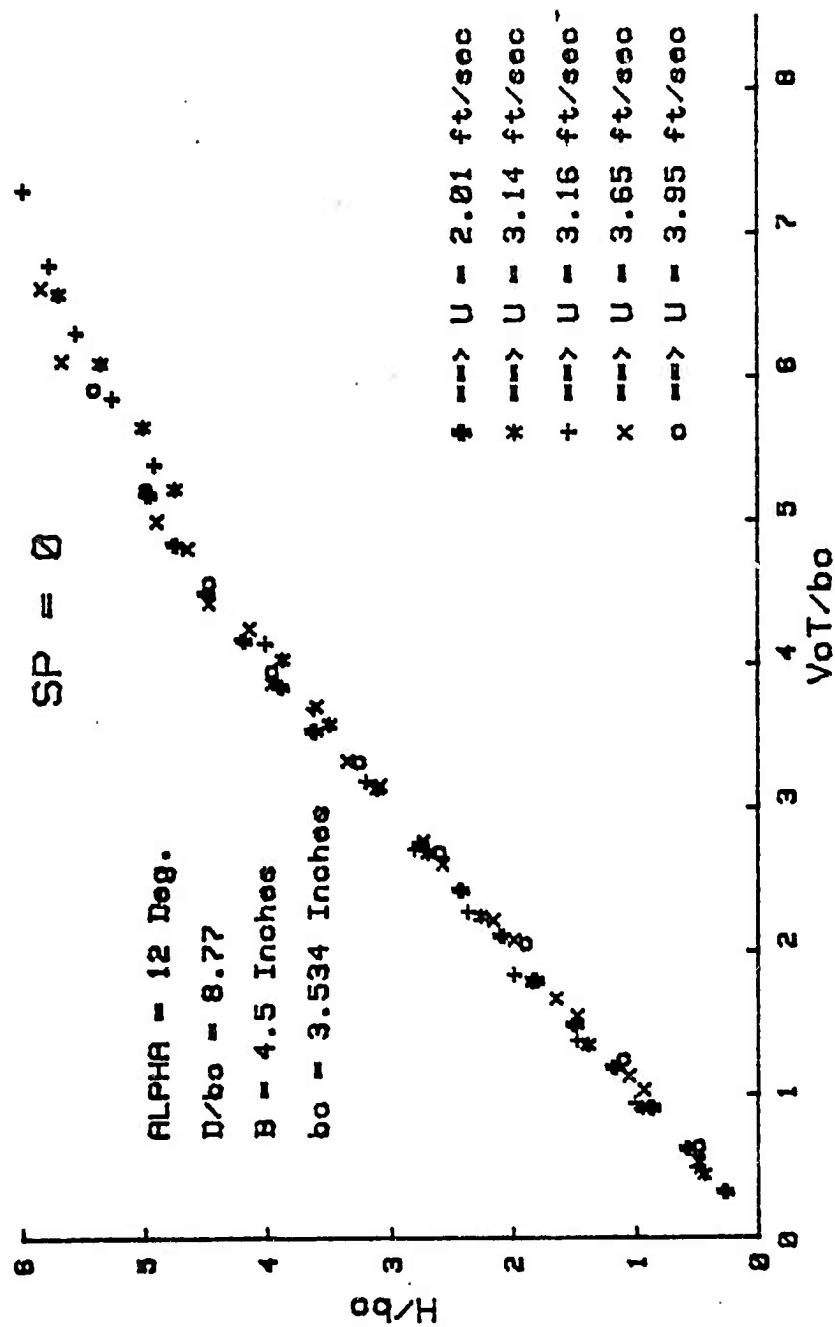


Figure 33. Comparison of the Rise of Vortices Generated by a Rectangular Wing, ($\alpha = 12$ deg.).

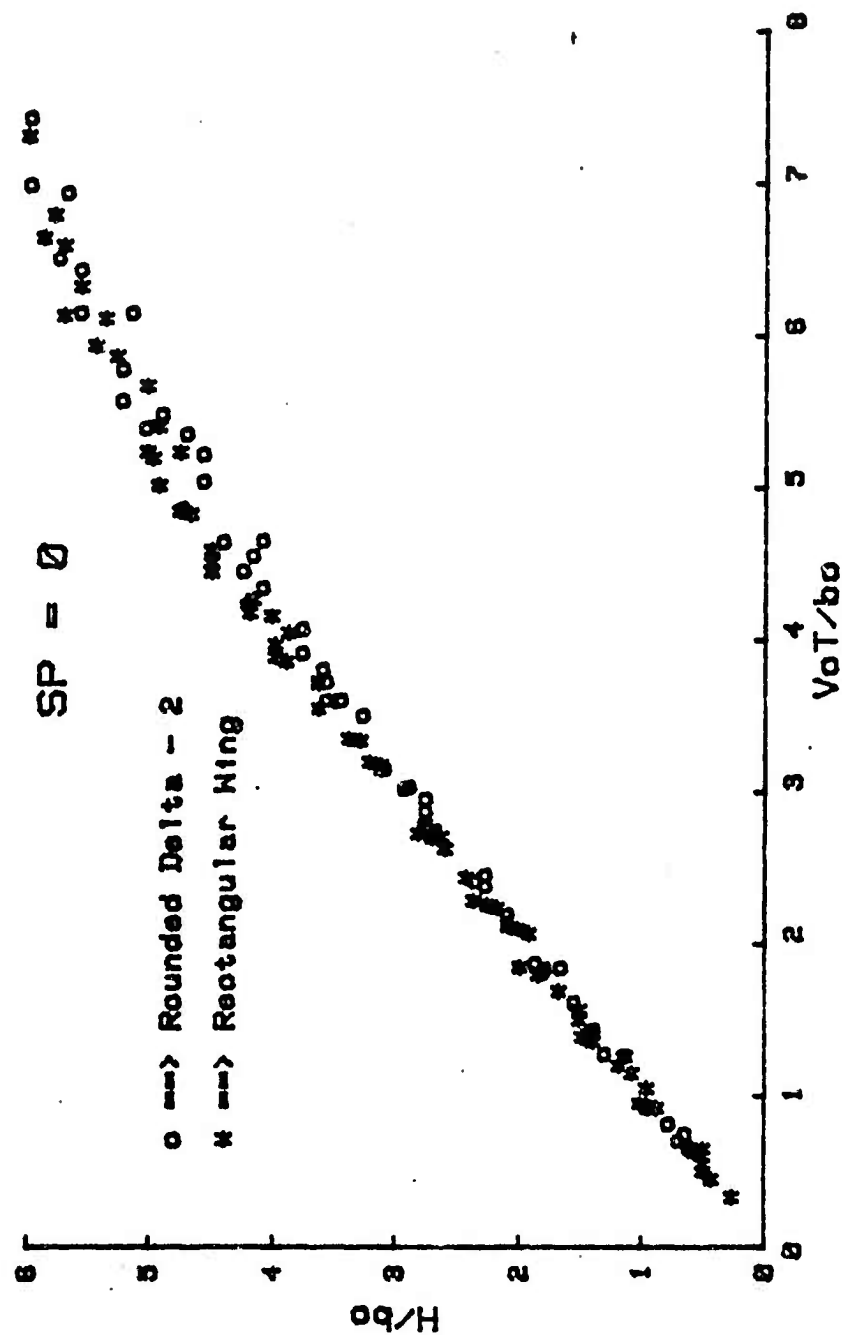


Figure 34. Comparison of the Rise of Vortices Generated by the Rounded Delta 2 and Rectangular Wing.

$$\zeta = \frac{\pm \Gamma}{\pi \sigma^2} \exp[-(r/\sigma)^2] \quad (6)$$

with $\sigma = 0.25b_0$ (this corresponds to $r_0/b_0 = 0.177$). The initial turbulence distribution was again Gaussian with a spread of $0.25b_0$, and was assumed to be isotropic with a representative integral scale. An upward velocity was employed to follow the vortex descent. A Reynolds number of $V_0 b_0 / \nu = 2 \times 10^5$ was assumed for the analysis.

The model was validated by comparing the calculated and experimentally determined trajectories of vortex rings. The results of this model for a vortex pair in atmosphere with a stratification parameter of 0.8 are compared in Figure 35 with those of the sharp-edged Delta-wings in water with a stratification parameter of 0.75. The model matched the experimental data very well, although there are no physical arguments to justify the selected integral scale for turbulence. Furthermore, the value of σ should be about half that assumed.

In a recent paper, Hecht, Bilanin, and Hirsh [Ref. 4] compared the predictions of the aforementioned model with other analytical [Refs. 5, 6, and 7] and experimental results [Ref. 8]. Initial distribution of vorticity was based on the data from Burnham et al. [Ref. 8]. The initial σ used in Eq. (6) was determined to be $0.074b_0$. The integral scale for turbulence was set to a smaller value for this analysis and a sensitivity study of the macroscale effects on vortex descent was presented. The sharp-edged results of this model for $SP = 0.67$ and $\sigma/b_0 = 0.075$

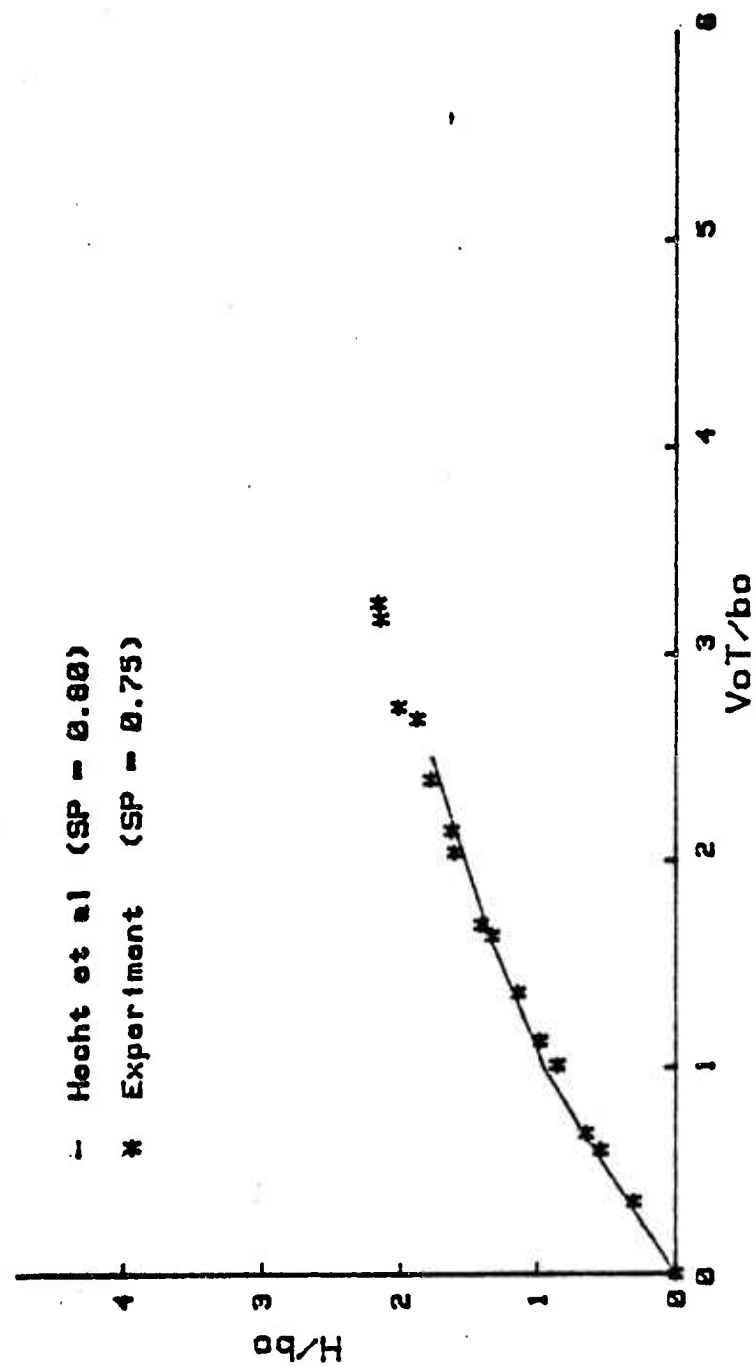


Figure 35. Comparison of Experimental Data with that Predicted by Hecht et al. [Ref. 3].

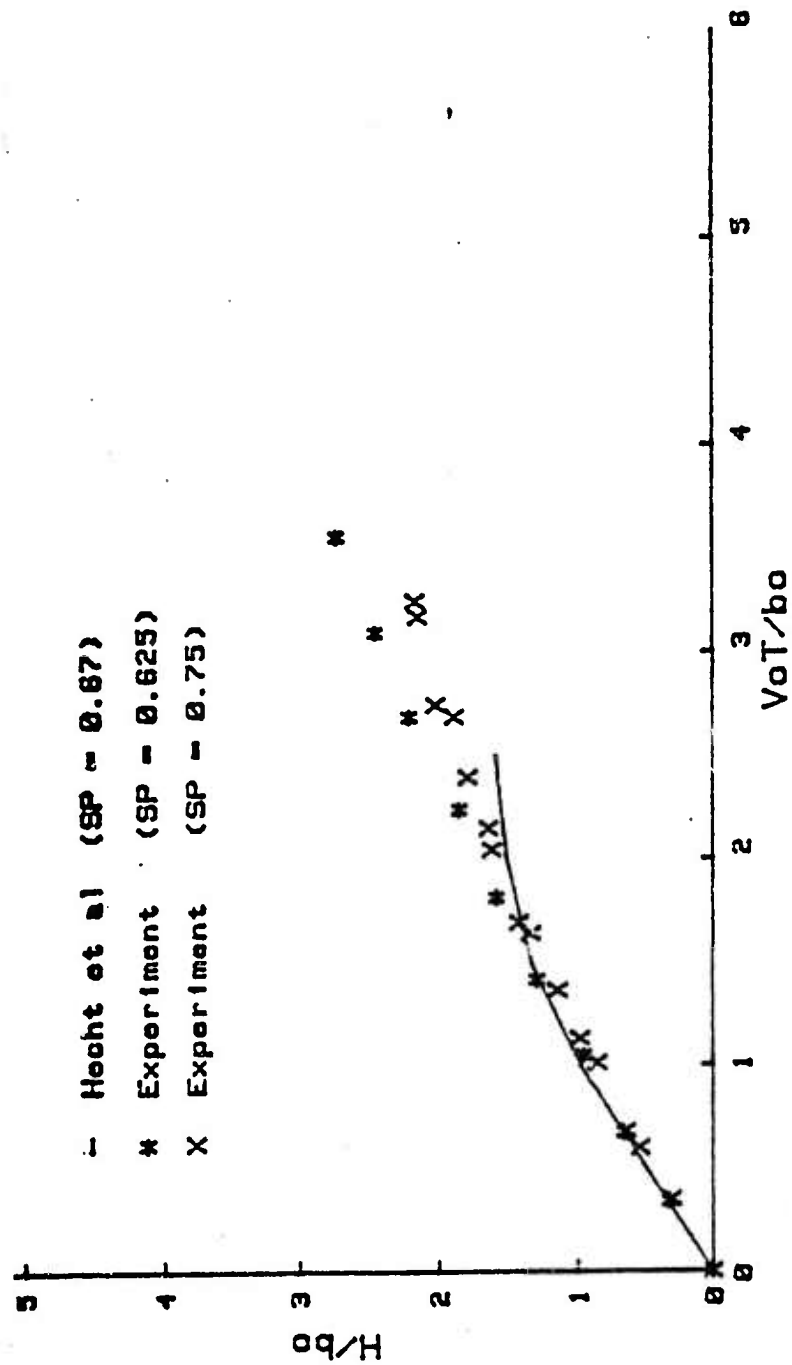


Figure 36. Comparison of Experimental Data with that Predicted by Hecht et al. [Ref. 4].

are compared with the Delta-wing results for $SP = 0.625$ and $SP = 0.75$ in Figure 36. This model does not match the data for $V_0 t/b_0$ greater than about 2.

A better match between the measured and calculated values could have been achieved with $\sigma = 0.25b_0$. But this value is larger than that in trailing vortices by a factor of about 3 relative to the observations of Burnham et al. [Ref. 8]. Of course the integral scale of turbulence could have been adjusted also to achieve more realistic results for $V_0 t/b_0$ larger than about 1.5.

While the numerical models cited above have pioneered in the study of turbulent effects in trailing vortices, the difficulties associated with the choice of free parameters (σ and the integral scale of turbulence) point out the need for additional work.

In an effort to eventually produce such a fully turbulent flow model to compare the three-dimensional trailing vortex data, gathered from the experimental models in the water basin, a two-dimensional, laminar, unsteady flow numerical model of the vortex pair was developed as part of this investigation.

For this purpose, the Navier-Stokes equations were written as

$$\frac{\partial u}{\partial t} + u \frac{\partial u}{\partial x} + v \frac{\partial u}{\partial y} = 0 - \frac{1}{\rho} \frac{\partial P}{\partial x} + \nu \nabla^2 u \quad (7)$$

$$\frac{\partial v}{\partial t} + u \frac{\partial v}{\partial x} + v \frac{\partial v}{\partial y} = g - \frac{1}{\rho} \frac{\partial P}{\partial y} + \nu \nabla^2 v \quad (8)$$

where the y-axis is assumed to be directed downwards. Eliminating the pressure between the two equations, one has

$$\begin{aligned} \frac{\partial \zeta}{\partial t} + \frac{\partial(u\zeta)}{\partial x} + \frac{\partial(v\zeta)}{\partial y} = v\nabla^2 \zeta - \frac{g}{\rho} \frac{\partial \rho}{\partial x} \\ + \left[\frac{1}{\rho} \frac{\partial \rho}{\partial y} (v\nabla^2 u - \frac{Du}{Dt}) - \frac{1}{\rho} \frac{\partial \rho}{\partial x} (v\nabla^2 v - \frac{Dv}{Dt}) \right] \end{aligned} \quad (9)$$

$$\zeta = \frac{\partial u}{\partial y} - \frac{\partial v}{\partial x} \quad (10)$$

and represents the vorticity. For flows in which the gravitational acceleration is several orders of magnitude larger than the fluid accelerations, the terms in the bracket in Eq. (9) may be neglected. This amounts to invoking the Boussinesq hypothesis. Thus, the equation of motion and the equation of continuity may be written as

$$\frac{\partial \zeta}{\partial t} + \frac{\partial(u\zeta)}{\partial x} + \frac{\partial(v\zeta)}{\partial y} = v\nabla^2 \zeta - \frac{g}{\rho_0} \frac{\partial \rho}{\partial x} \quad (11)$$

$$\frac{\partial \zeta}{\partial t} + \frac{\partial(u\rho)}{\partial x} + \frac{\partial(v\rho)}{\partial y} = v\nabla^2 \rho \quad (12)$$

The last term in Eq. (11) represents the effect of the density gradient and gives rise to opposite-signed vorticity.

The equations that were chosen to describe the motion include a Gaussian distribution of the initial vorticity given by

$$\zeta = \frac{\pm \Gamma}{2\pi r_0^2} \exp[-(r^2/2r_0^2)] \quad (13)$$

Boundary values of the u and v velocity components are determined by the Biot-Savart Integrals

$$u(x,y) = \int_A \frac{(y'-y)\zeta(x',y')}{2\pi r^2} dx' dy' \quad (14)$$

$$v(x,y) = \int_A \frac{(x-x')\zeta(x',y')}{2\pi r^2} dx' dy' \quad (15)$$

where:

$$r^2 = (x-x')^2 + (y-y')^2$$

x', y' denote the position of vorticity, and

x, y the point where the velocity components are calculated.

The stream-function values around the boundaries and velocity within the field boundaries are calculated from u and v using

$$u = \frac{\partial \psi}{\partial y} ; \quad v = - \frac{\partial \psi}{\partial x} \quad (16)$$

Field stream-function values are calculated using Poisson's equations

$$\nabla^2 \psi = - \zeta \quad (17)$$

The calculations had to be carried out in a finite numerical mesh, as in all other numerical analyses. The appropriate boundary conditions are shown on the boundaries of the quadrant in which the calculations have been performed (see Fig. 37). It should be noted that the conditions $u(0,y) = (x,0) = 0$ are satisfied automatically by evaluating the Biot-Savart equations in all four quadrants. Furthermore, the symmetry provided by the free surface (x-axis) and by the normal bisecting the vortex pair (y-axis) enable one to confine the domain of calculation to a single quadrant.

Additional details of the analysis are as follows:

- (i) The domain of calculations is prescribed;
- (ii) The vorticity distribution given by Eq. (13) is assigned to mesh points;
- (iii) A particular stratification is assigned to the density distribution;
- (iv) Boundary values of velocities are calculated using the Biot-Savart equations;
- (v) The boundary values of the stream-function are calculated;
- (vi) The flow field values of the stream-function are calculated using Poisson's equation and a successive overrelaxation scheme;
- (vii) The velocity field is calculated through the use of the stream-function values.

The foregoing marks the end of the first time step. The successive steps are sequenced as follows:

- (i) The vorticity and density fields are calculated using an upwind-differencing scheme;

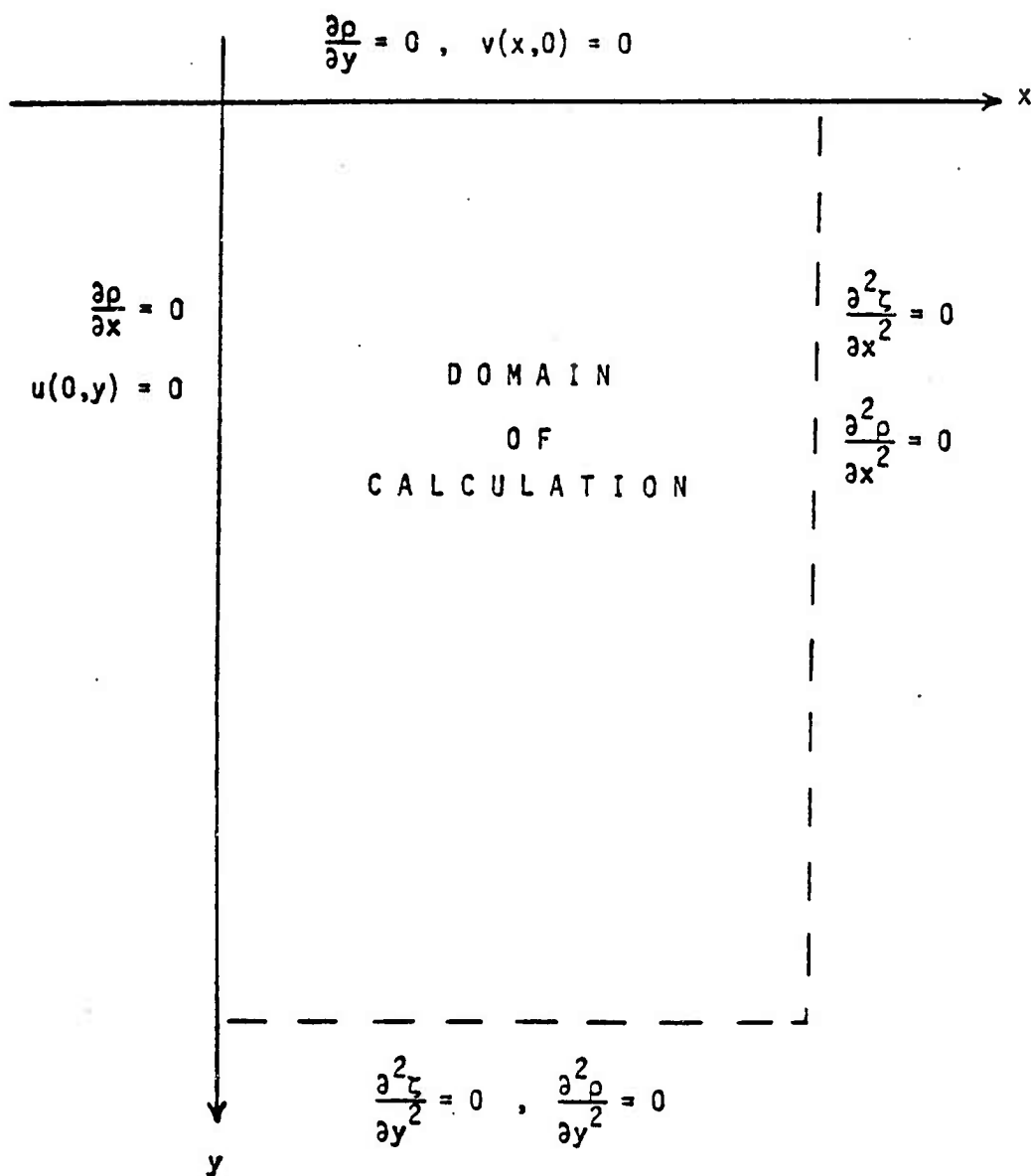


Figure 37. Computational Field and Boundary Conditions for the Numerical Model.

- (ii) The new center of vorticity is calculated using the square of vorticity as the weighing parameter;
- (iii) A vertical velocity is imposed on the field using the velocity calculated from the rate of change of the center of vorticity; and finally,
- (iv) The new points at the top of the field are initialized and the vorticity is used to calculate the boundary velocities.

The last step completes the iteration and marks the beginning of a new sequence.

The plots of the streamlines of the flow field for a simulation of the motion of the vortices generated by the rounded Delta 2 for $SP = 0$ and $r_0/b_0 = 0.09$ are shown in Figures 38 through 47. The time indicated on each plot is the normalized time $t/(b_0/V_0)$ which is of course identical to its common form $V_0 t/b_0$. In these calculations, D/b_0 was taken to be 10, and the initial value of r_0 was assumed to be $0.09b_0$. The calculated values of H/b_0 are compared with those obtained experimentally in Figure 48. The matching of the two results is surprising in view of the fact that neither turbulence nor any other demise mechanism in conjunction with turbulence was taken into consideration. The surprising agreement between the two results may be attributed to numerical diffusion and to the relative stability of the trailing vortices in unstratified fluids.

It should be emphasized that the foregoing was only an exploratory numerical investigation of the evolution of a laminar vortex pair. It served to confirm the need for the development of a comprehensive numerical model which is not only true to the underlying physics of the

phenomena but also devoid of floating parameters whose values are arbitrarily chosen (e.g., initial vorticity diffusion, r_0/b_0 , mesh size, size of calculation domain, etc.). The results also show that turbulence plays an extremely important role in the diffusion of vorticity and thus in the entire life of vortices from their inception to their ultimate demise.

Even when such a comprehensive model is developed it does not now appear that it would be too easy to surmount the difficulties associated with the modeling of the consequences of the Crow instability, vortex breakdown, and the entrainment and detrainment of the recirculation cell. Of course it is not too surprising that such an investigation should require a better understanding of turbulence itself through measurements and calculations of vortical flows.

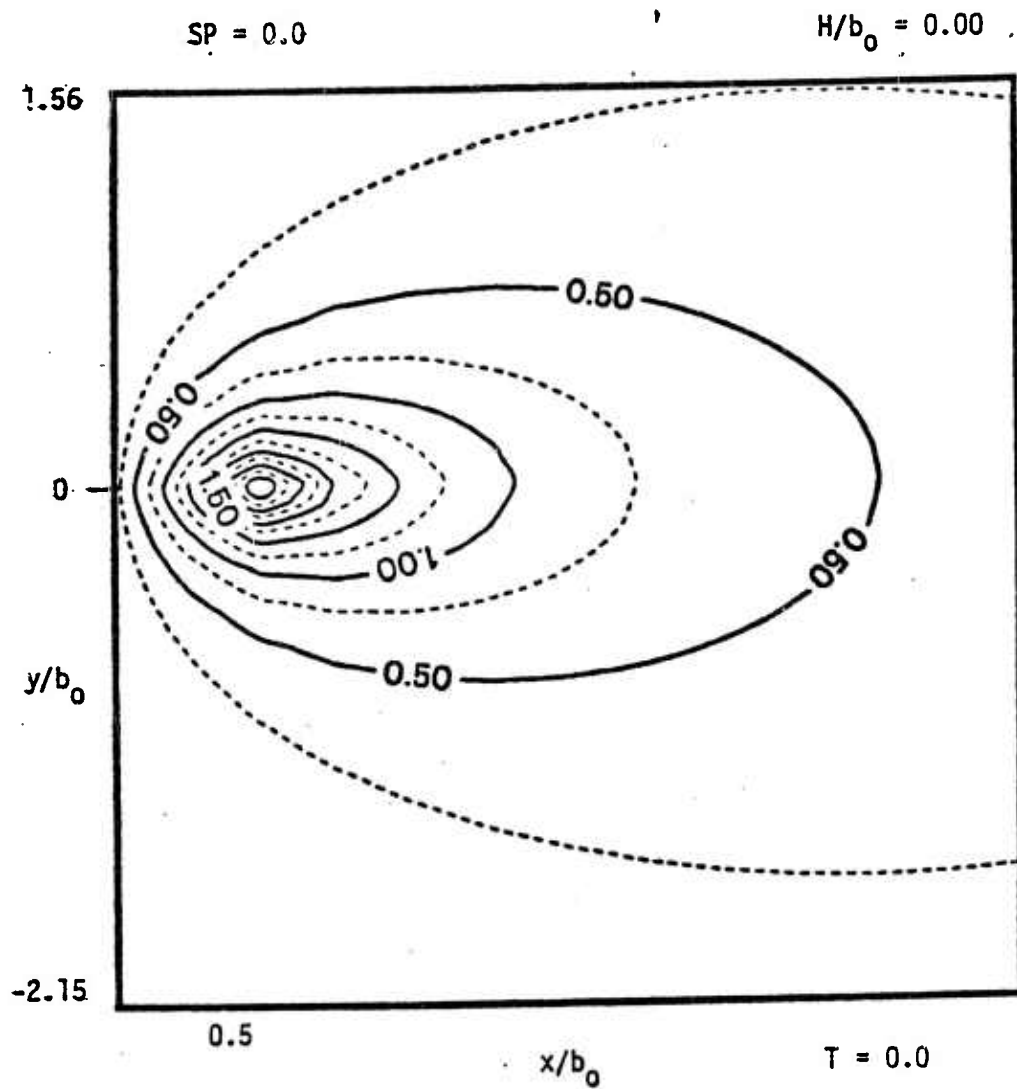


Figure 38. Streamlines of the Numerical Model for $H/b_0 = 0.00$.

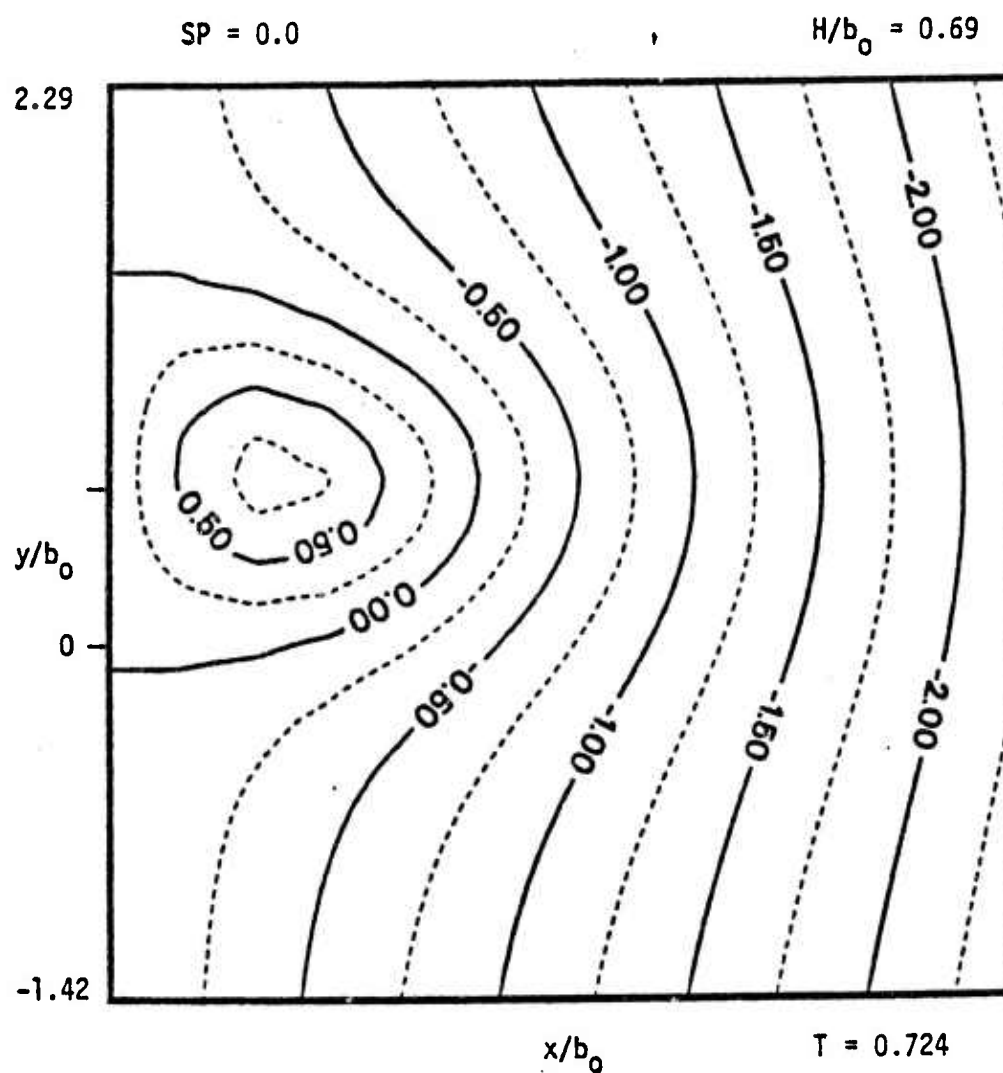


Figure 39. Streamlines of the Numerical Model for the $H/b_0 = 0.69$.

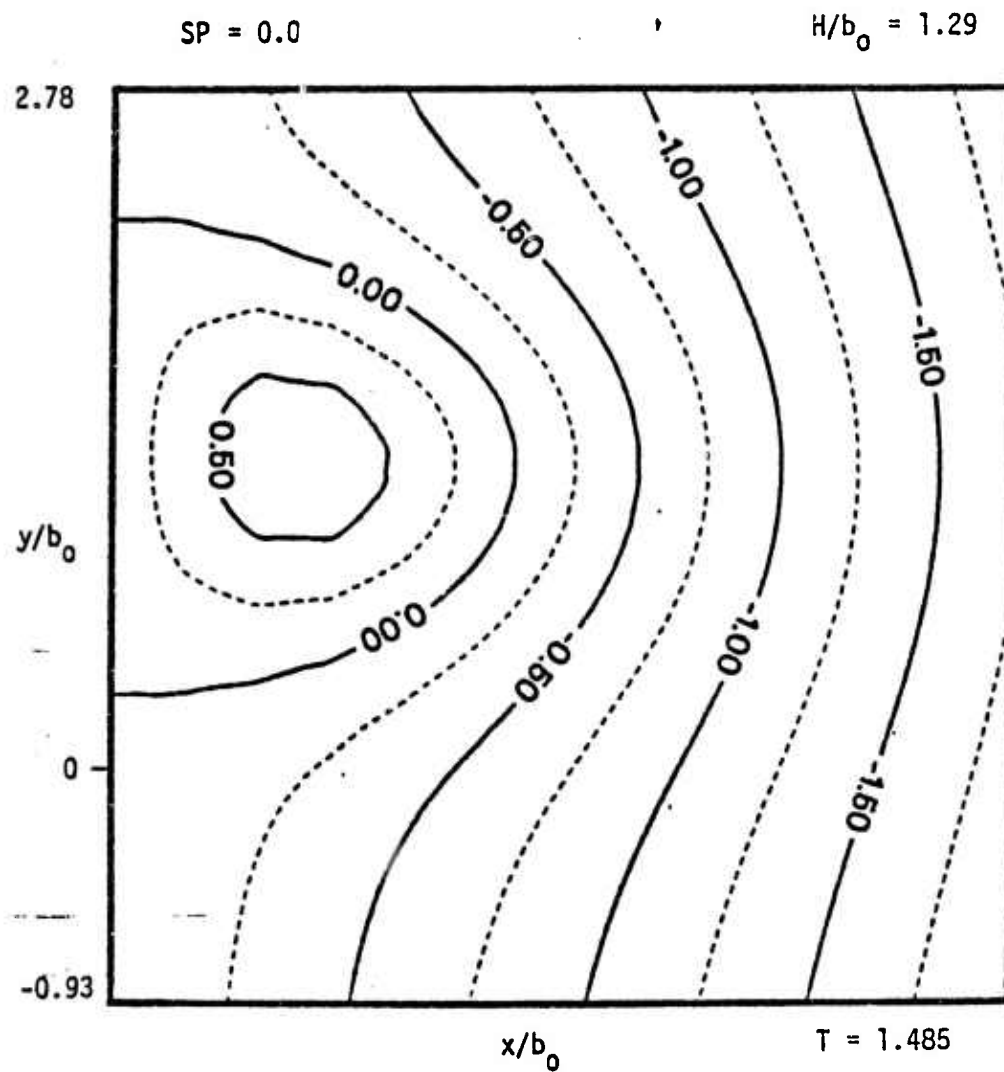


Figure 40. Streamlines of the Numerical Model for $H/b_0 = 1.29$.

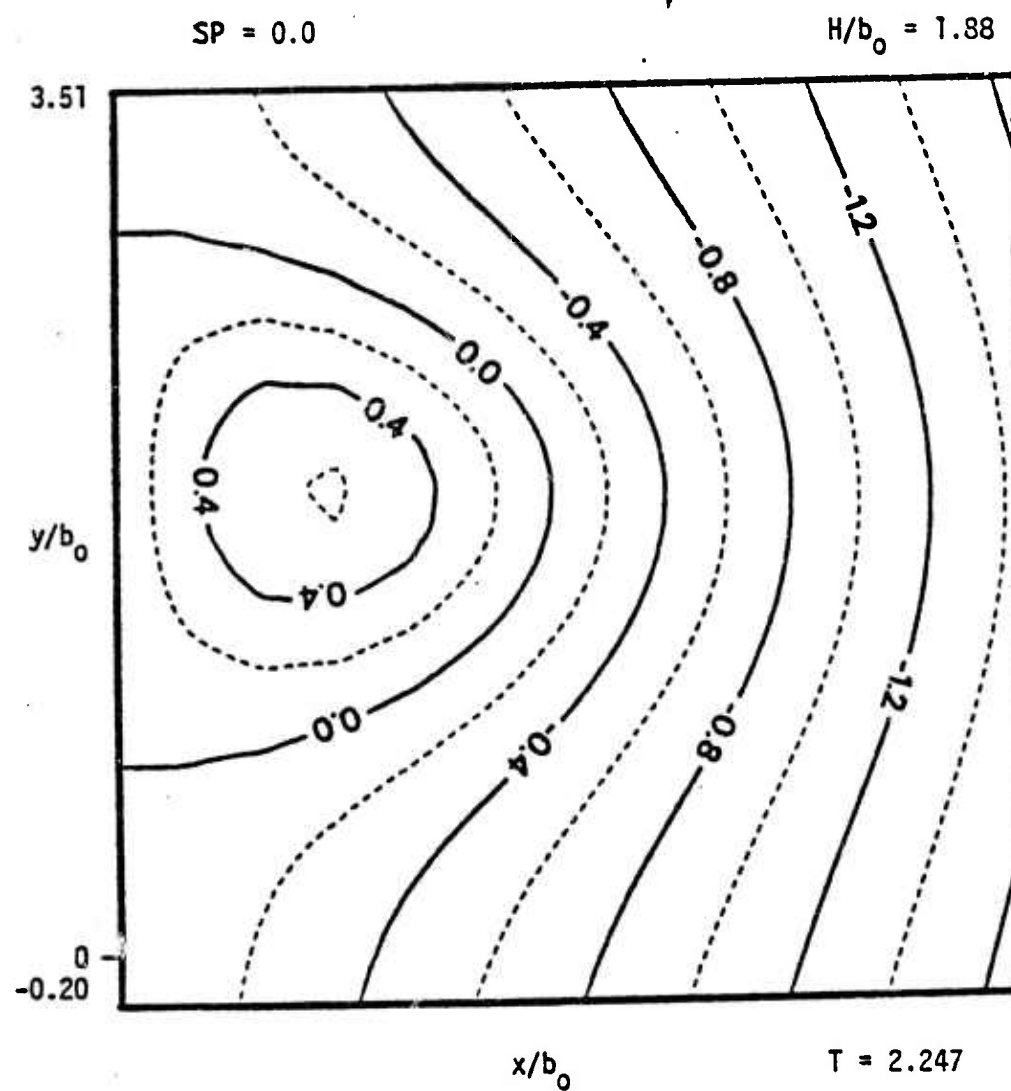


Figure 41. Streamlines of the Numerical Model for $H/b_0 = 1.88$.

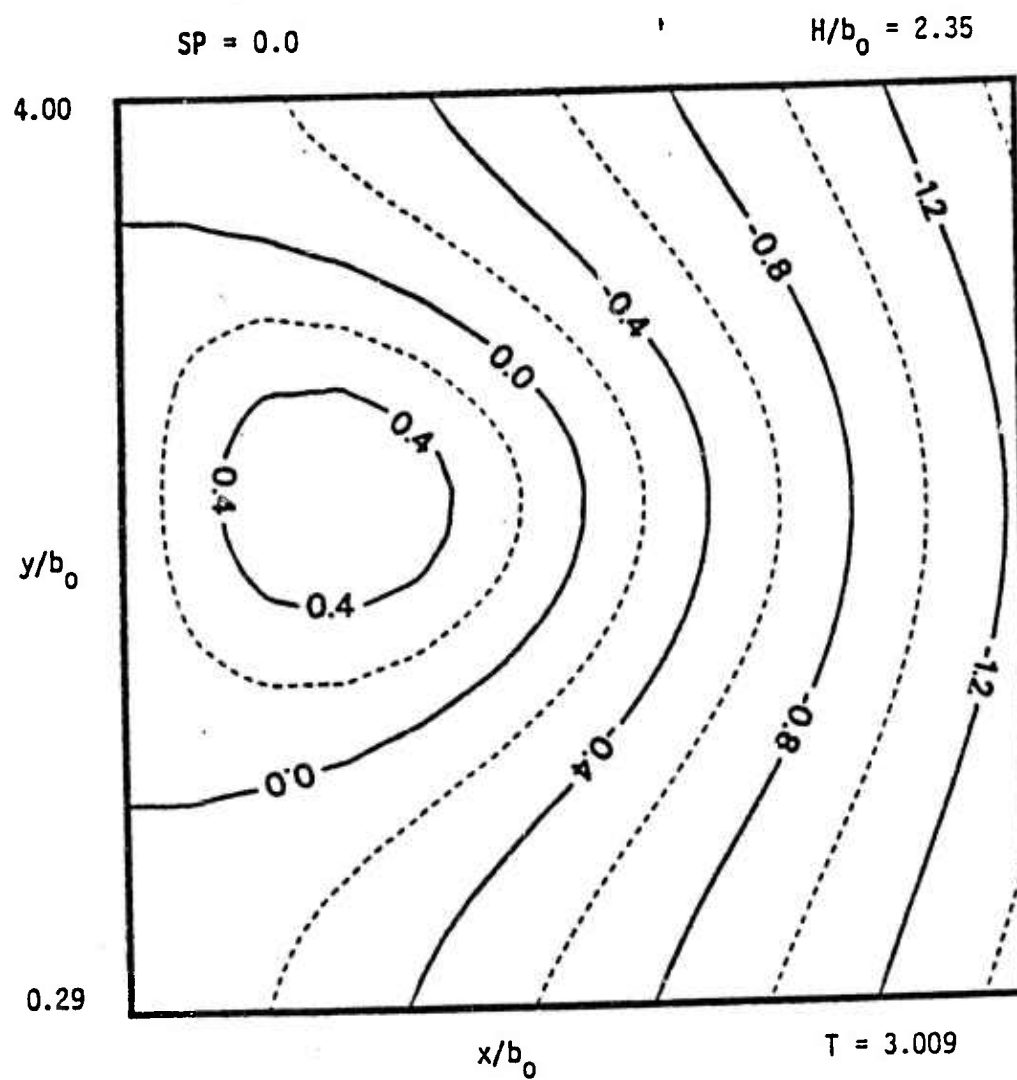


Figure 42. Streamlines of the Numerical Model for $H/b_0 = 2.35$.

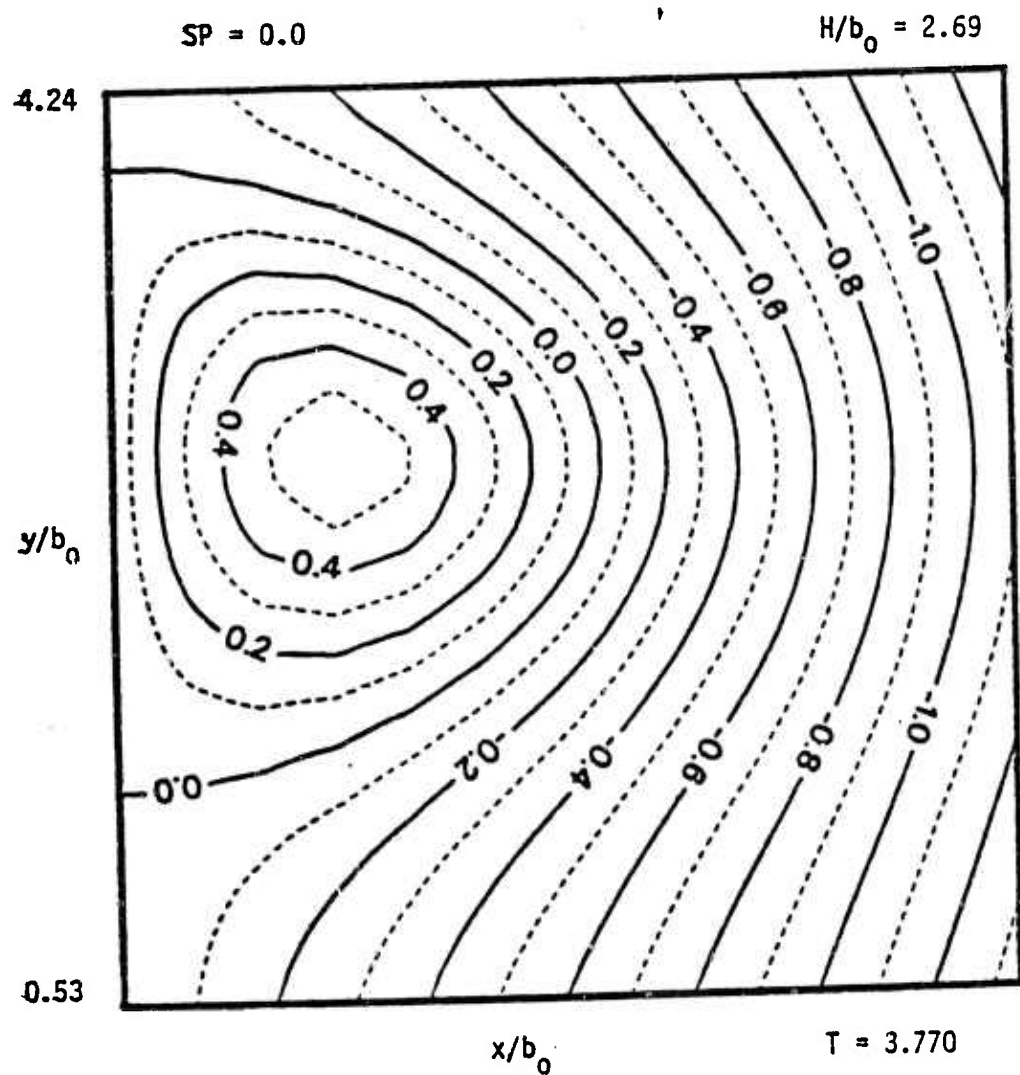


Figure 43. Streamlines of the Numerical Model for $H/b_0 = 2.69$.

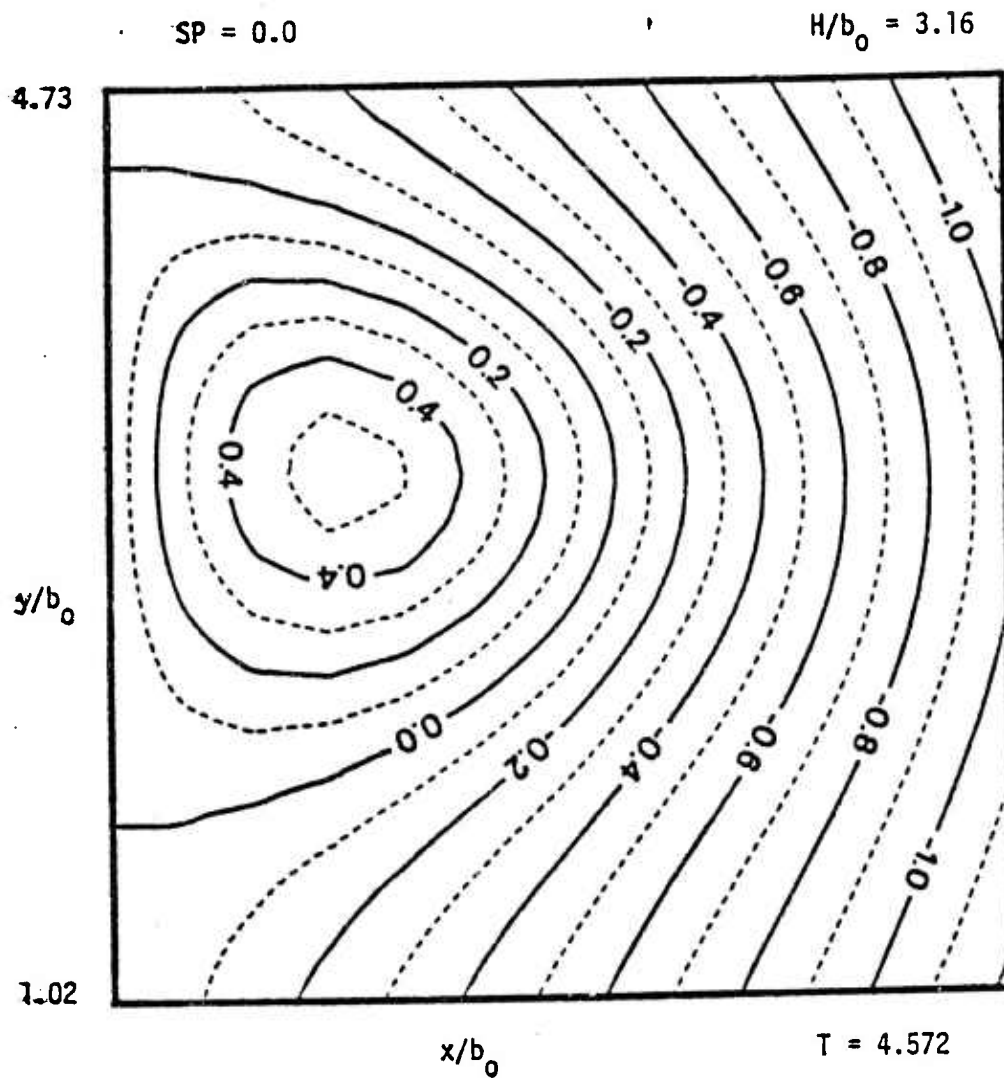


Figure 44. Streamlines of the Numerical Model for $H/b_0 = 3.16$.

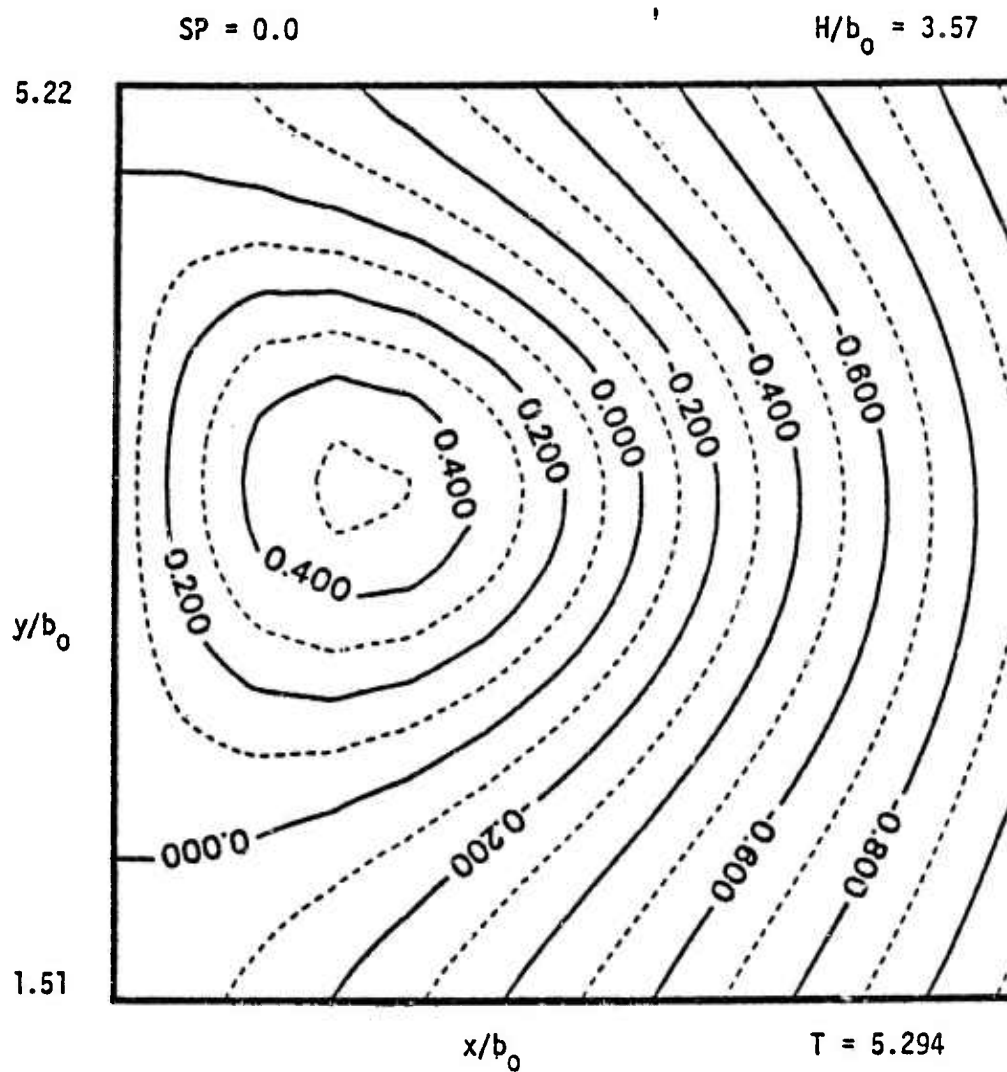


Figure 45. Streamlines of the Numerical Model for $H/b_0 = 3.57$.

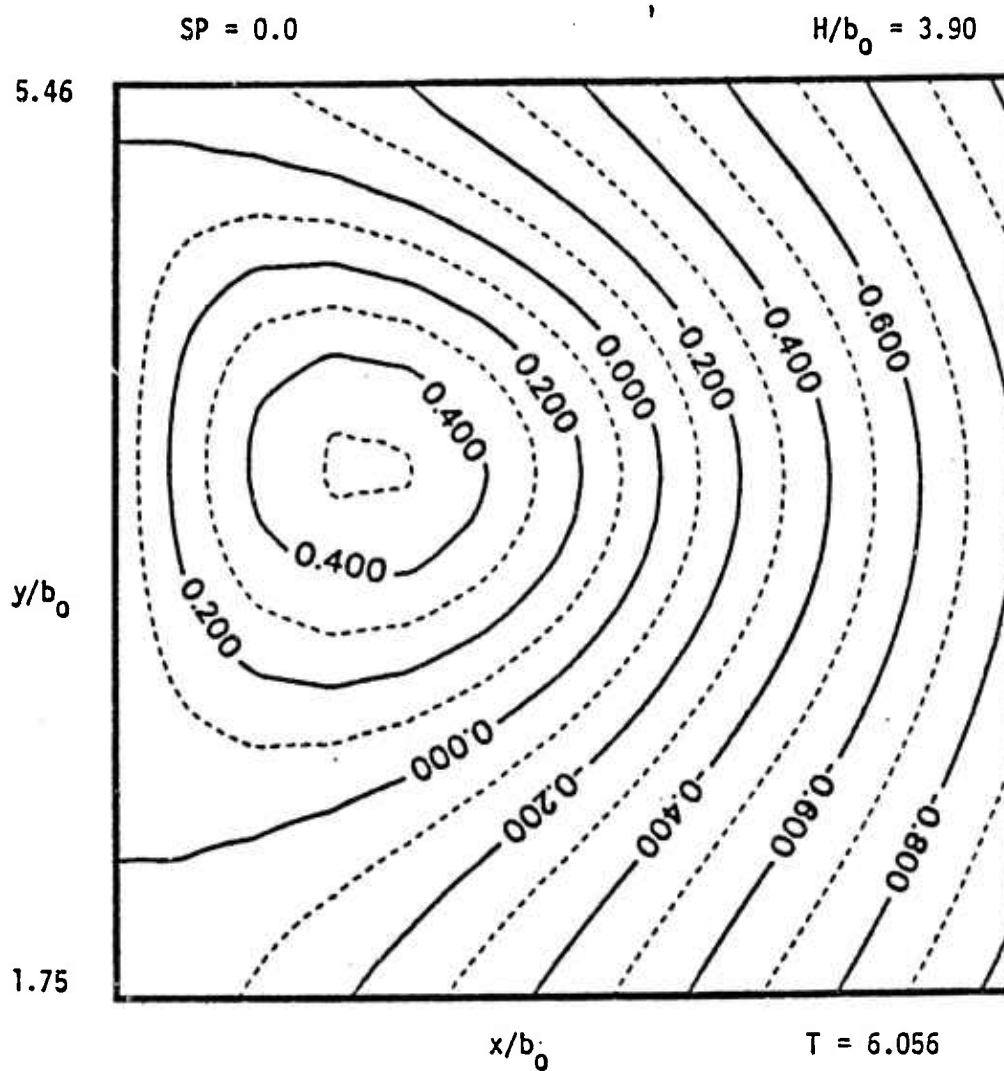


Figure 46. Streamlines of the Numerical Model for $H/b_0 = 3.90$.

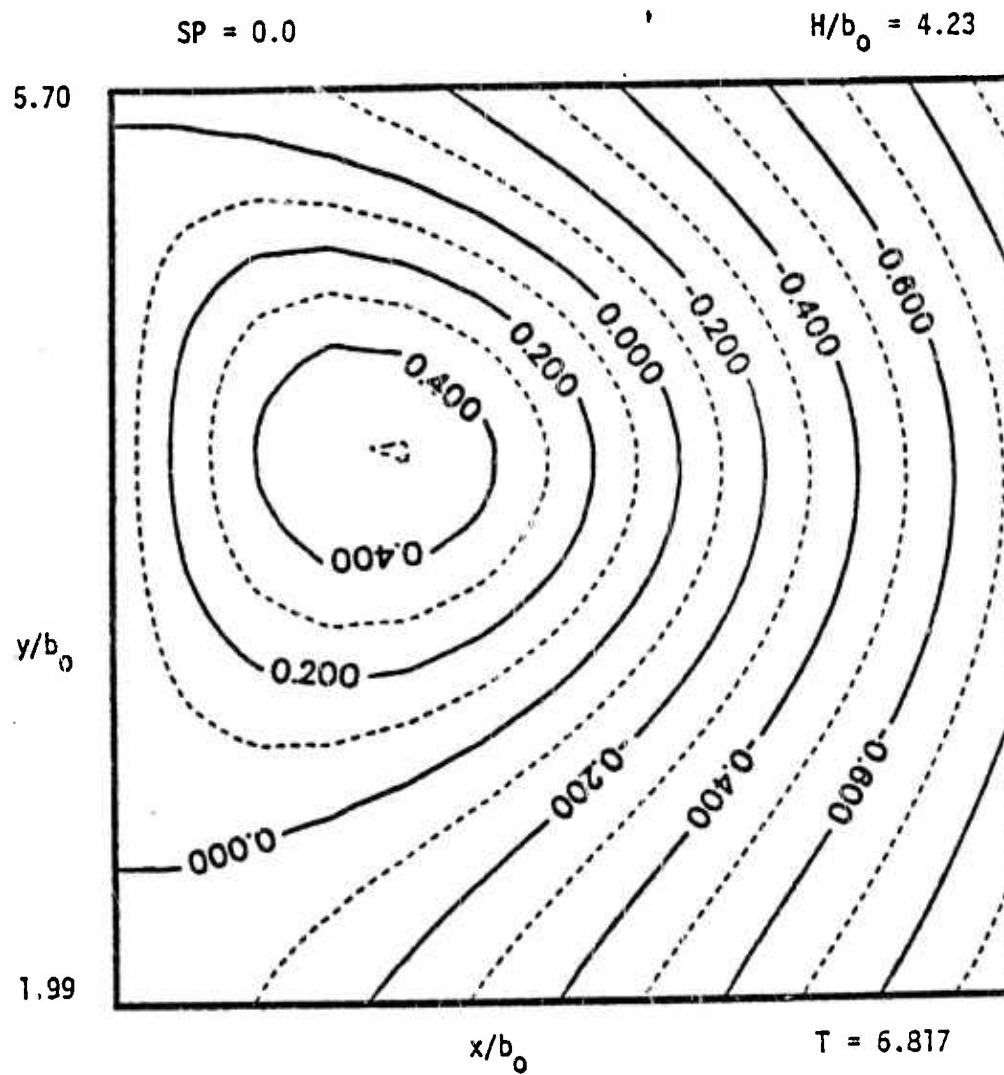


Figure 47. Streamlines of the Numerical Model for $H/b_0 = 4.23$.

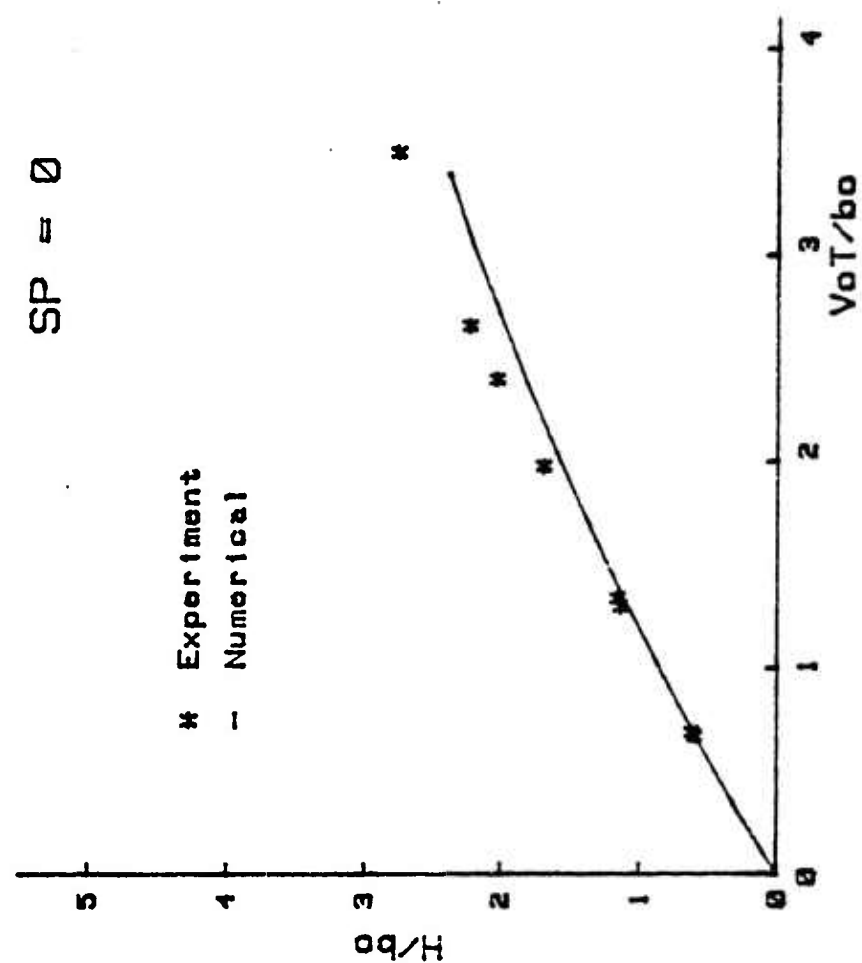


Figure 48. Comparison of Experimental Data with the Predictions of the Numerical Model for $SP = 0$.

IV. CONCLUSIONS

The investigation reported herein warranted the following conclusions:

1. In unstratified fluid, the trailing vortices generated by a lifting surface moving at a negative angle of attack rise with time and dissipate at a finite height.
2. The rate of rise of vortices is always smaller than that predicted theoretically through the use of the inviscid line vortices.
3. The rise of vortices is governed by $V_0 t/b_0$, D/b_0 , Nb_0/V_0 , and r_0/b_0 for a given body moving in a linearly stratified fluid with no background turbulence.
4. The effect of stratification is to reduce the rate of rise of vortices and the maximum height attained by them. In fact, the larger the stratification, the smaller the maximum height attained by the vortices.
5. The demise of the vortices is brought about by turbulent diffusion, Crow instability, and vortex breakdown. The vortex breakdown is particularly prominent for trailing vortices near a body.
6. Various analyses were considered and all were deemed to be inadequate. None of the approximate models yielded satisfactory results and none considered the effects of the demise mechanisms.
7. The real fluid effects on the rise and demise of the trailing vortices in a stratified fluid must be accounted for by considering the combined contributions of turbulence, sinusoidal instability, vortex breakdown, vortex-core size, and the ambient turbulence.

LIST OF REFERENCES

1. Sarpkaya, T. and Johnson, K. S., Trailing Vortices in Stratified Fluids, NPS-69-82-003, June 1982, Monterey, CA.
2. Elle, B. J., An Investigation at Low Speed of the Flow near the Apex of Thin Delta Wings with Sharp Leading Edges, A. R. C. Reports and Memoranda No. 3176, January 1958.
3. Hecht, A. M., Bilanin, A. J., Hirsh, J. E., and Snedeker, R. S., "Turbulent Vortices in Stratified Fluids," AIAA Journal, Vol. 18, 1979, pp. 738-746.
4. Hecht, A. M., Bilanin, A. J., Hirst, J. E., "Turbulent Trailing Vortices in Stratified Fluids," AIAA Journal, Vol. 19, 1981, pp. 691-698.
5. Saffman, P. G., "The Motion of a Vortex Pair in Stratified Atmosphere," Studies in Applied Mathematics, Vol. II, No. 2, June 1972, pp. 107-119.
6. Crow, S. C., Motion of Vortex Pair in a Stably Stratified Fluid, Poseidon Research Report No. 1, May 1974.
7. Tombach, I. H., Transport of a Vortex Wake in a Stably Stratified Atmosphere, Aircraft Wake Turbulence and its Detection, Edited by J. H. Olsen et al., Plenum Press, New York, 1971, pp. 41-57.
8. Burnham, D. C., Hallock, J. N., Tombach, I. H., Brashears, M. R., and Barger, M. R., Ground Based Measurements of a B-747 Aircraft in Various Configurations, U.S. Dept. of Transportation Report FAA-RD-78-146, December 1978.

APPENDIX A: BODY AND SAIL-PLANE TABULATED DATA

BODY AND SAIL $D/b_o = 4.45$ $B = 6.9$ inches
 $b_o = 5.42$ inches $ALPHA = 10$ DEG

$U = 3.59$ ft/s	$U = 2.84$ ft/s	$U = 3.59$ ft/s
$V_o/U = 0.021$	$V_o/U = 0.017$	$V_o/U = 0.018$
$N_{bo}/V_o = 0.0$	$N_{bo}/V_o = 0.0$	$N_{bo}/V_o = 0.0$

<u>V_oT/b_o</u>	<u>H/b_o</u>	<u>V_oT/b_o</u>	<u>H/b_o</u>	<u>V_oT/b_o</u>	<u>H/b_o</u>
0.000	0.000	0.000	0.000	0.000	0.000
.262	.116	.169	.144	.229	.092
.537	.376	.355	.332	.448	.376
.810	.620	.524	.406	.748	.598
1.082	.980	.781	.664	.974	.886
1.340	1.273	.887	.819	1.192	1.125
1.620	1.680	1.080	1.054	1.432	1.273
1.894	2.000	1.274	1.192	1.647	1.369
2.187	2.230	1.475	1.435	1.876	1.546
2.485	2.450	1.723	1.635	2.107	1.701

$U = 4.064$ ft/s	$U = 3.59$ ft/s
$V_o/U = 0.019$	$V_o/U = 0.018$
$N_{bo}/V_o = 0.0$	$N_{bo}/V_o = 0.0$

<u>V_oT/b_o</u>	<u>H/b_o</u>	<u>V_oT/b_o</u>	<u>H/b_o</u>
0.000	0.000	0.000	0.000
.256	.221	.229	.173
.504	.487	.455	.421
.769	.720	.675	.554
1.039	1.006	.913	.708
1.298	1.148	1.159	.886
1.556	1.347	1.402	1.054
1.838	1.502	1.648	1.192
2.120	1.657	1.903	1.347
		2.160	1.502

BODY AND SAIL

$D/b_o = 4.45$

$B = 6.9$ inches

$b_o = 5.42$ inches $ALPHA = 12$ DEG

$U = 3.57$ ft/s

$U = 3.69$ ft/s

$U = 2.84$ ft/s

$V_o/U = 0.023$

$V_o/U = 0.023$

$V_o/U = 0.0205$

$N_{b_o}/V_o = 0.0$

$N_{b_o}/V_o = 0.0$

$N_{b_o}/V_o = 0.0$

V_oT/b_o

H/b_o

V_oT/b_o

H/b_o

V_oT/b_o

H/b_o

0.000 0.000

0.000 0.000

0.000 0.000

.305 .221

.301 .221

.206 .197

.586 .531

.605 .465

.405 .376

.891 .731

.902 .753

.621 .554

1.174 1.125

1.184 1.125

.840 .775

1.469 1.391

1.481 1.369

1.054 .958

1.727 1.590

1.785 1.768

1.255 1.148

2.003 1.745

1.457 1.347

2.252 1.934

2.563 2.140

$U = 3.65$ ft/s

$U = 2.80$ ft/s

$V_o/U = 0.023$

$V_o/U = 0.0205$

$N_{b_o}/V_o = 0.0$

$N_{b_o}/V_o = 0.0$

V_oT/b_o

H/b_o

V_oT/b_o

H/b_o

0.000 0.000

0.000 0.000

.312 .221

.205 .162

.604 .531

.408 .332

.870 .797

.602 .554

1.212 1.077

.799 .753

1.515 1.303

1.014 .910

1.792 1.590

1.233 1.170

2.093 1.862

1.456 1.368

2.390 2.118

1.678 1.502

2.682 2.339

1.983 1.657

APPENDIX B: SAIL-PLANE TABULATED DATA

SAIL $D/b_o = 5.24$ $B = 6.9$ inches
 $b_o = 5.42$ inches $\alpha = 10$ DEG

$U = 4.34$ ft/s $U = 4.34$ ft/s $U = 2.37$ ft/s
 $V_o/U = 0.0134$ $V_o/U = 0.0134$ $V_o/U = 0.0155$
 $N_{bo}/V_o = 0$ $N_{bo}/V_o = 0$ $N_{bo}/V_o = 0$

$V_o T/b_o$	H/b_o	$V_o T/b_o$	H/b_o	$V_o T/b_o$	H/b_o
0.00	0.00	0.00	0.00	0.00	0.00
.21	.17	.20	.17	.14	.14
.40	.38	.40	.38	.28	.28
.61	.63	.60	.63	.43	.47
.80	.78	.81	.80	.62	.63
1.01	.98	1.01	.98	.77	.78
1.23	1.14	1.24	1.18	.95	.94
1.43	1.28	1.45	1.33	1.11	1.07
1.63	1.47	1.67	1.51	1.33	1.28
1.84	1.67	1.88	1.68	1.63	1.54
2.58	2.15			2.32	2.05
2.81	2.30			2.60	2.17
3.06	2.46			2.93	2.32
3.30	2.62			3.23	2.53
				3.58	2.68
				3.88	2.87

SAIL

$D/b_o = 5.24$

$B = 6.9$ inches

$b_o = 5.42$ inches

$\text{ALPHA} = 10$ DEG

$U = 3.55$ ft/s

$V_o/U = 0.015$

$N_{b_o}/V_o = 0$

$U = 3.55$ ft/s

$V_o/U = 0.015$

$N_{b_o}/V_o = 0$

$U = 4.34$ ft/s

$V_o/U = 0.0134$

$N_{b_o}/V_o = 0$

$V_o T/b_o$	H/b_o	$V_o T/b_o$	H/b_o	$V_o T/b_o$	H/b_o
0.00	0.00	0.00	0.00	0.00	0.00
.23	.18	.18	.17	.19	.17
.42	.38	.35	.30	.38	.39
.82	.57	.50	.49	.57	.81
.81	.76	.71	.67	.78	.78
1.01	.88	.89	.83	.87	.88
1.20	1.18	1.07	.98	1.17	1.20
1.40	1.38	1.23	1.18	1.36	1.40
1.60	1.60	1.46	1.28	1.57	1.60
1.81	1.82	1.84	1.45	1.76	1.80
2.58	2.26	2.26	1.81	2.57	2.26
2.85	2.46	2.46	2.08	2.78	2.44
		2.68	2.24		

SAIL

$D/b_o = 5.24$

$B = 6.9$ inches

$b_o = 5.42$ inches $\text{ALPHA} = 10$ DEG

$U = 2.35$ ft/s

$V_o/U = 0.0156$

$N_{b_o}/V_o = 0$

$U = 2.74$ ft/s

$V_o/U = 0.0146$

$N_{b_o}/V_o = 0$

$U = 2.74$ ft/s

$V_o/U = 0.0146$

$N_{b_o}/V_o = 0$

<u>$V_o T/b_o$</u>	<u>H/b_o</u>	<u>$V_o T/b_o$</u>	<u>H/b_o</u>	<u>$V_o T/b_o$</u>	<u>H/b_o</u>
0.00	0.00	0.00	0.00	0.00	0.00
.15	.13	.14	.12	.14	.14
.20	.20	.20	.20	.20	.30
.40	.41	.41	.45	.43	.43
.60	.58	.55	.56	.57	.61
.81	.74	.71	.75	.71	.76
1.00	.88	.86	.89	.87	.82
1.20	1.00	1.02	1.03	1.07	1.00
1.30	1.20	1.16	1.18	1.23	1.24
1.50	1.47	1.32	1.29	1.30	1.30
2.02	1.71	1.80	1.78	1.82	1.71
2.10	1.82	2.06	1.91	1.97	1.85
2.30	1.93	2.24	2.02	2.17	2.00
2.54	2.08	2.42	2.12	2.45	2.20
2.72	2.15	2.61	2.20	2.64	2.32
2.80	2.20	2.70	2.34	2.83	2.46
3.07	2.32	2.88	2.47	3.00	2.50
3.53	2.53	3.33	2.64	3.51	2.84
		3.86	2.77	3.86	3.00
		4.52	2.88	4.44	3.30

SAIL

 $D/b_o = 5.24$ $B = 6.9$ inches $b_o = 5.42$ inches

ALPHA = 12 DEG

 $U = 2.31$ ft/s $V_o/U = 0.0198$ $N_{b_o}/V_o = 0$ $U = 2.76$ ft/s $V_o/U = 0.01875$ $N_{b_o}/V_o = 0$ $U = 3.51$ ft/s $V_o/U = 0.0178$ $N_{b_o}/V_o = 0$

$V_o T/b_o$	H/b_o	$V_o T/b_o$	H/b_o	$V_o T/b_o$	H/b_o
0.00	0.00	0.00	0.00	0.00	0.00
.18	.11	.19	.17	.21	.21
.35	.30	.37	.34	.43	.48
.54	.47	.57	.52	.66	.69
.75	.70	.78	.74	.83	.84
.88	.87	.87	.84	1.18	1.18
1.15	1.07	1.18	1.16	1.45	1.47
1.35	1.28	1.40	1.33	1.69	1.69
1.59	1.47	1.58	1.42	1.84	1.87
1.81	1.60	1.80	1.62	2.21	2.03
2.34	1.81	2.32	1.86	2.82	2.37
2.54	2.03	2.55	2.15	3.07	2.53
2.76	2.17	2.80	2.30	3.32	2.64
3.02	2.32	3.05	2.42	3.58	2.75
3.26	2.42	3.32	2.58	3.87	2.88
3.52	2.53	3.59	2.75	4.15	2.98
3.74	2.71	3.86	2.88	4.43	3.19
3.96	2.84	4.43	3.13	4.72	3.30
4.36	2.87	5.18	3.38	5.02	3.58
4.58	3.08	5.57	3.48	5.39	3.64

SAIL

$D/b_o = 5.24$

$B = 6.9$ inches

$b_o = 5.42$ inches

ALPHA = 8 DEG

$U = 2.23$ ft/s

$V_o/U = 0.0101$

$N_{b_o}/V_o = 0$

$U = 2.76$ ft/s

$V_o/U = 0.0127$

$N_{b_o}/V_o = 0$

$U = 3.47$ ft/s

$V_o/U = 0.01$

$N_{b_o}/V_o = 0$

$V_o T/b_o$	H/b_o	$V_o T/b_o$	H/b_o	$V_o T/b_o$	H/b_o
0.00	0.00	0.00	0.00	0.00	0.00
.08	.08	.13	.08	.14	.11
.16	.17	.26	.18	.26	.23
.24	.23	.39	.30	.36	.37
.32	.28	.52	.47	.52	.48
.42	.37	.63	.57	.65	.58
.51	.48	.78	.72	.84	.65
.61	.58	.82	.78	1.03	.76
.71	.65	1.07	.85	1.21	.88
.82	.74	1.21	.96	1.39	.88
		1.58	1.26	1.84	1.18
		1.72	1.31	2.03	1.28
		1.81	1.40		
		2.35	1.62		

APPENDIX C: RECTANGULAR PLATE TABULATED DATA

R. PLATE SP = 0 B = 6.8 inches

bo = 5.34 inches ALPHA = 12 DEG

U = 3.55 ft/s	U = 1.99 ft/s	U = 2.74 ft/s
Vo/U = 0.0266	Vo/U = 0.0283	Vo/U = 0.0265
D/bo = 5.45	D/bo = 5.45	D/bo = 5.45

<u>VoT/bo</u>	<u>H/bo</u>	<u>VoT/bo</u>	<u>H/bo</u>	<u>VoT/bo</u>	<u>H/bo</u>
0.00	0.00	0.00	0.00	0.00	0.00
.38	.41	.26	.19	.27	.23
.75	.77	.48	.41	.53	.52
1.15	1.17	.72	.68	.88	.82
1.55	1.55	.97	.83	1.08	1.04
1.98	1.91	1.21	1.16	1.33	1.33
2.38	2.28	1.46	1.37	1.61	1.58
2.78	2.48	1.70	1.61	1.91	1.88
3.18	2.76	1.95	1.84	2.19	2.16
3.58	3.03	2.73	2.54	2.48	2.48
		2.96	2.74	3.18	2.88
		3.20	3.03	3.44	3.18
		3.43	3.15	3.71	3.42
		3.70	3.35	3.98	3.60
		3.85	3.48	4.24	3.83
		4.24	3.62	4.51	4.04
		4.47	3.83	4.80	4.18
		4.84	4.02	5.11	4.27
		5.12	4.18	5.41	4.38
				6.10	4.51

R. PLATE

SP = 0

B = 6.8 inches

bo = 5.34 inches

ALPHA = 8 DEG

U = 2.78 ft/s

Vo/U = 0.0177

D/bo = 5.45

U = 3.61 ft/s

Vo/U = 0.0192

D/bo = 5.45

U = 2.73 ft/s

Vo/U = 0.0212

D/bo = 4.31

<u>VoT/bo</u>	<u>H/bo</u>	<u>VoT/bo</u>	<u>H/bo</u>	<u>VoT/bo</u>	<u>H/bo</u>
0.00	0.00	0.00	0.00	0.00	0.00
.20	.19	.31	.30	.23	.13
.39	.38	.59	.58	.45	.38
.58	.58	.84	.82	.67	.60
.78	.77	1.10	1.10	.80	.82
.84	.84	1.38	1.35	1.13	1.05
1.12	1.10	1.61	1.62	1.38	1.27
1.30	1.31	1.88	1.88	1.61	1.48
1.48	1.48	2.15	2.14	1.84	1.72
1.68	1.67	2.42	2.42	2.07	1.85
2.14	2.12	3.27	3.15	2.55	2.42
2.32	2.30	3.54	3.37	2.78	2.64
2.50	2.48	3.79	3.62	3.02	2.83
2.71	2.70	4.07	3.83	3.24	3.03
2.80	2.87	4.34	4.04	3.47	3.20
3.12	3.09	4.63	4.27	3.71	3.37
3.33	3.28	4.85	4.38	4.07	3.54
3.53	3.48	5.30	4.48	4.67	3.65
3.74	3.60	5.74	4.51	5.00	3.60
3.88	3.81			5.52	3.54

R. PLATE

SP = 0

S = 6.8 inches

bo = 5.34 inches

ALPHA = 8 DEG

U = 3.20 ft/s
Vo/U = 0.0205
D/bo = 4.31

U = 2.78 ft/s
Vo/U = 0.0197
D/bo = 3.24

U = 3.57 ft/s
Vo/U = 0.0192
D/bo = 3.24

<u>VoT/bo</u>	<u>H/bo</u>	<u>VoT/bo</u>	<u>H/bo</u>	<u>VoT/bo</u>	<u>H/bo</u>
0.00	0.00	0.00	0.00	0.00	0.00
.26	.18	.21	.18	.26	.18
.51	.41	.41	.41	.52	.47
.76	.68	.61	.63	.77	.77
1.01	.84	.83	.82	1.02	.88
1.30	1.22	1.03	.88	1.28	1.28
1.58	1.50	1.26	1.22	1.53	1.48
1.88	1.78	1.48	1.38	1.78	1.72
2.17	2.06	1.71	1.58	2.08	1.88
2.46	2.36	1.93	1.88	2.34	2.24
3.21	2.87	2.62	2.38	2.88	2.47
3.51	3.08	2.87	2.48	3.17	2.58
3.77	3.26	3.08	2.52	3.42	2.58
4.07	3.37	3.34	2.58	3.67	2.58
4.34	3.43	3.65	2.58	3.87	2.58
4.64	3.48				
4.88	3.48				
5.22	3.48				
5.52	3.48				
5.88	3.37				

R. PLATE

SP = 0

B = 6.8 inches

bo = 5.34 inches

ALPHA = 8 DEG

U = 2.76 ft/s

U = 3.59 ft/s

U = 2.80 ft/s

Vo/U = 0.0201

Vo/U = 0.0196

Vo/U = 0.0199

D/bo = 2.70

D/bo = 2.70

D/bo = 2.15

<u>VoT/bo</u>	<u>H/bo</u>	<u>VoT/bo</u>	<u>H/bo</u>	<u>VoT/bo</u>	<u>H/bo</u>
0.00	0.00	0.00	0.00	0.00	0.00
.23	.19	.26	.19	.20	.14
.45	.41	.52	.47	.40	.36
.67	.66	.79	.77	.61	.57
.91	.88	1.06	1.05	.82	.77
1.15	1.18	1.36	1.33	1.03	.97
1.38	1.36	1.61	1.55	1.29	1.19
1.60	1.55	1.84	1.76	1.48	1.33
1.83	1.70	2.09	1.88	1.69	1.43
2.07	1.89	2.32	1.98	1.90	1.53
2.54	2.00	2.98	2.03	2.30	1.55
2.79	2.00	3.27	2.03	2.61	1.55
3.03	2.00	3.55	2.03	2.83	1.55
3.29	2.00	3.82	2.03	3.08	1.55
3.53	2.00	4.11	2.03	3.58	1.55

R. PLATE

B = 6.8 inches

bo = 5.34 inches ALPHA = 8 DEG

U = 3.60 ft/s
 Vo/U = 0.0193
 D/bo = 4.5
 SP = 0.625

U = 3.59 ft/s
 Vo/U = 0.0192
 D/bo = 5.43
 SP = 0.75

<u>VoT/bo</u>	<u>H/bo</u>	<u>VoT/bo</u>	<u>H/bo</u>
0.00	0.00	0.00	0.00
.25	.24	.25	.18
.48	.50	.48	.48
.72	.71	.72	.71
.88	.84	.87	.84
1.20	1.17	1.22	1.17
1.45	1.43	1.48	1.43
1.60	1.67	1.76	1.67
1.82	1.89	2.02	1.88
2.17	2.12	2.27	2.07
2.76	2.70	2.79	2.48
3.01	2.92	3.08	2.70
3.28	3.15	3.32	2.80
3.50	3.31	3.58	3.06
3.74	3.57	3.88	3.21
4.00	3.69	4.13	3.37
4.34	3.83		
4.51	3.85		
4.77	3.95		
5.38	3.95		

APPENDIX D: ROUNDED DELTA 2 TABULATED DATA

DELTA - 2R. $D/b_o = 7.84$ $B = 5.02$ inches

$b_o = 3.70$ inches ALPHA = 10 DEG

U = 2.70 ft/s $U = 3.55$ ft/s $U = 2.41$ ft/s
 $V_o/U = 0.0422$ $V_o/U = 0.0394$ $V_o/U = 0.0422$
 $N_{bo}/V_o = 0$ $N_{bo}/V_o = 0$ $N_{bo}/V_o = 0$

<u>V_oT/b_o</u>	<u>H/b_o</u>	<u>V_oT/b_o</u>	<u>H/b_o</u>	<u>V_oT/b_o</u>	<u>H/b_o</u>
0.00	0.00	0.00	0.00	0.00	0.00
.68	.65	.75	.68	.67	.65
1.20	1.32	1.43	1.45	1.27	1.16
1.80	1.80	2.15	2.12	1.85	1.60
2.42	2.30	2.80	2.70	2.40	2.30
2.88	2.70	3.01	3.40	3.03	2.85
3.51	3.20	4.35	4.11	3.61	3.50
4.00	3.70	5.05	4.50	4.24	4.24
4.60	4.11	5.70	5.24	4.87	4.76
5.23	4.50	6.52	5.70	5.50	5.24

U = 3.51 ft/s $U = 3.85$ ft/s
 $V_o/U = 0.044$ $V_o/U = 0.042$
 $N_{bo}/V_o = 0$ $N_{bo}/V_o = 0$

<u>V_oT/b_o</u>	<u>H/b_o</u>	<u>V_oT/b_o</u>	<u>H/b_o</u>
0.00	0.00	0.00	0.00
.82	.81	.93	.87
1.62	1.57	1.84	1.81
2.30	2.30	2.75	2.70
3.16	3.11	3.73	3.50
3.82	3.70	4.40	4.27
4.60	4.40	5.40	4.82
5.40	5.00	6.44	5.50
6.10	5.50	7.44	6.00
7.00	6.00		

DELTA - 2R.

D/bo = 7.84

B = 5.02 inches

bo = 3.70 inches ALPHA = 8 DEG

U = 3.93 ft/s

Vo/U = 0.0345

Nbo/Vo = 0

U = 3.16 ft/s

Vo/U = 0.034

Nbo/Vo = 0

U = 4.42 ft/s

Vo/U = 0.034

Nbo/Vo = 0

<u>VoT/bo</u>	<u>H/bo</u>	<u>VoT/bo</u>	<u>H/bo</u>	<u>VoT/bo</u>	<u>H/bo</u>
0.00	0.00	0.00	0.00	0.00	0.00
.71	.81	.60	.62	.80	.81
1.41	1.49	1.17	1.16	1.50	1.65
2.00	2.12	1.76	1.73	2.35	2.33
2.75	2.70	2.35	2.25	3.12	2.85
3.40	3.42	2.87	2.78	3.86	3.46
4.14	3.88	3.50	3.30	4.61	4.03
4.86	4.53	4.18	3.78	5.35	4.51
5.56	5.05	4.77	4.27		
6.25	5.50	5.37	4.68		
		7.17	5.86		
		7.60	6.05		
		8.27	6.31		
		8.88	6.57		

DELTA - 2R.

$D/b_0 = 7.84$

$B = 5.02 \text{ inches}$

$b_0 = 3.70 \text{ inches}$

$\text{ALPHA} = 8 \text{ DEG}$

$U = 2.76 \text{ ft/s}$

$V_0/U = 0.033$

$N_{b_0}/V_0 = 0$

$U = 2.74 \text{ ft/s}$

$V_0/U = 0.033$

$N_{b_0}/V_0 = 0$

<u>$V_0 T/b_0$</u>	<u>H/b_0</u>	<u>$V_0 T/b_0$</u>	<u>H/b_0</u>
0.00	0.00	0.00	0.00
.45	.41	.48	.45
.81	.82	.84	.82
1.36	1.36	1.44	1.32
1.84	1.81	1.84	1.78
2.33	2.23	2.43	2.21
2.77	2.65	2.84	2.62
3.23	3.11	3.43	3.03
3.70	3.46	3.83	3.46
4.15	3.75	4.42	3.85
5.21	4.27	5.54	4.58
5.71	4.58	6.08	4.82
		6.54	5.24
		6.88	5.51

DELTA - 2R.

$D/b_0 = 7.84$

$B = 5.02 \text{ inches}$

$b_0 = 3.70 \text{ inches}$ $\text{ALPHA} = 10 \text{ DEG}$

$U = 3.24 \text{ ft/s}$

$V_0/U = 0.037$

$SP = 0.375$

$U = 2.76 \text{ ft/s}$

$V_0/U = 0.0422$

$SP = 0.625$

<u>V_0T/b_0</u>	<u>H/b_0</u>	<u>V_0T/b_0</u>	<u>H/b_0</u>
0.00	0.00	0.00	0.00
.62	.65	.62	.65
1.23	1.24	1.21	1.08
1.84	1.81	1.82	1.57
2.43	2.30	2.40	1.97
3.04	2.78	3.03	2.43
3.63	3.28	3.61	2.88
4.21	3.64	4.23	3.28
4.78	4.11		
5.38	4.46		

APPENDIX E: SMALL RECTANGULAR PLATE TABULATED DATA

R. PLATE - 2 $D/b_o = 8.77$ $B = 4.58$ inches
 $b_o = 3.534$ inches $\text{ALPHA} = 12$ DEG

$U = 2.01$ ft/s	$U = 3.14$ ft/s	$U = 3.18$ ft/s
$V_o/U = 0.0277$	$V_o/U = 0.0265$	$V_o/U = 0.0265$
$N_{bo}/V_o = 0$	$N_{bo}/V_o = 0$	$N_{bo}/V_o = 0$

<u>V_oT/b_o</u>	<u>H/b_o</u>	<u>V_oT/b_o</u>	<u>H/b_o</u>	<u>V_oT/b_o</u>	<u>H/b_o</u>
0.00	0.00	0.00	0.00	0.00	0.00
.32	.27	.44	.44	.49	.51
.62	.59	.91	.85	.84	1.01
.81	.88	1.35	1.39	1.39	1.43
1.19	1.18	1.79	1.84	1.84	1.89
1.49	1.58	2.25	2.28	2.28	2.37
1.88	1.82	2.69	2.70	2.72	2.81
2.11	2.09	3.14	3.11	3.19	3.20
2.43	2.43	3.59	3.48	3.70	3.62
2.75	2.76	4.04	3.87	4.15	4.01
3.54	3.82	5.23	4.75	5.48	4.82
3.85	3.88	5.66	5.01	5.88	5.26
4.17	4.19	6.11	5.35	6.32	5.55
4.50	4.50	6.59	5.69	6.78	5.77
4.84	4.75			7.21	5.89
5.19	4.87				

R. PLATE - 2

D/b₀ = 8.77

B = 4.50 inches

b₀ = 3.534 inches ALPHA = 12 DEG

U = 3.85 ft/s

V₀/U = 0.0285

N_{b0}/V₀ = 0

U = 3.65 ft/s

V₀/U = 0.0285

N_{b0}/V₀ = 0

U = 3.95 ft/s

V₀/U = 0.0316

N_{b0}/V₀ = 0

V₀T/b₀

H/b₀

V₀T/b₀

H/b₀

V₀T/b₀

H/b₀

0.00

0.00

0.00

0.00

0.00

0.00

.54

.51

.58

.51

.64

.51

1.04

.96

1.14

1.08

1.25

1.13

1.56

1.50

1.68

1.67

2.06

1.82

2.08

2.01

2.23

2.18

2.70

2.63

2.62

2.60

2.78

2.76

3.33

3.28

3.17

3.11

3.34

3.37

3.86

3.88

3.72

3.62

3.98

3.88

4.58

4.50

4.26

4.16

4.44

4.50

5.23

5.01

4.82

4.67

5.81

4.82

5.83

5.43

5.13

5.88

5.64

5.88

INITIAL DISTRIBUTION LIST

	<u>No. Copies</u>
Dr. Arthur J. Bruckheim DARPA/TTO 1400 Wilson Blvd. Arlington, VA 22209	1
Chief of Naval Operations OP-95T, Room 5D616 The Pentagon Washington, DC 20350 Attn: Dr. Jack Breedlove Attn: Dr. A. Andreassen	1 1
Commander Department of the Navy Strategic Systems Project Office Washington, DC 20376 Attn: Dr. Philip Selwyn (SP2023)	1
Chief of Naval Operations OP-021, Room 4D544 The Pentagon Washington, DC 20350 Attn: Dr. Ed Harper	1 1
Dr. Irwin E. Alber Arete Associates P.O. Box 350 Encino, CA 91316	1
Dr. Steve Crow Poseidon Research 1299 Ocean Avenue Suite 821 Santa Monica, CA 90401	1
Dr. Wasył Wasyłkiwskyj Physical Dynamics, Inc. Suite 1620 1300 N. 17th Street Arlington, VA 22209	1
Dr. Richard Hoglund ORI, Inc. 1400 Spring Street Silver Spring, MD 70910	1

Dr. Denny Ko
Dynamics Technology, Inc.
22939 Hawthorne Blvd.
Suite 200
Torrance, CA 90505

1

Dr. C. D. Donaldson
Aeronautical Research Associates of Princeton, Inc.
1800 Old Meadow Road
Suite 114
McLean, VA 22102

1

Applied Physics Laboratory
The John Hopkins University
Johns Hopkins Road
Laurel, MD 20810

Attn: Dr. L. Crawford
Attn: Dr. H. Gilreath
Attn: Dr. G. Merritt
Attn: Dr. Gary Smith
Attn: Dr. Tom Taylor
Attn: Dr. D. Wenstrand

1

1

1

1

1

1

1

Dr. Dennis Holliday
R&D Associates
4640 Admiralty Way
Marina del Rey, CA 90291

1

Dr. Don LeVine
JASON Program Office
The MITRE Corporation
1820 Dolley Madison Blvd.
McLean, VA 22102

1

Flow Research
21414 68th Ave. South
Kent, WA 98031
Attn: Peter Liu

1

Continuum Dynamics
P. O. Box 3073
32 Nassau St.
Princeton, NJ 08540
Attn: Alan Bilanin

1

Defense Technical Information Center
Attn: DTK-DDA-2
Building 5
Cameron Station
Alexandria, VA 22314

2

Dr. T. Sarpkaya Code 69SL Mechanical Engineering Naval Postgraduate School Monterey, CA 93940	10
Office of Research Administration Code 012A Naval Postgraduate School Monterey, CA 93940	1
Library, Code 0142 Naval Postgraduate School Monterey, CA 93940	4
Chairman, Mechanical Engineering Code 69 Naval Postgraduate School Monterey, CA 93940	1